NASA Contractor Report 172540

NASA-CR-172540
19850017663

Development of Algorithms for Using Satellite and Meteorological Data Sets to Study Global Transport of Stratospheric Aerosols and Ozone

Pi-Huan Wang and Adarsh Deepak

SCIENCE AND TECHNOLOGY CORPORATION
Hampton, VA 23666-1340

Contract NAS1-16362

March 1985

National Aeronautics and
Space Administration

Langley Research Center
Hampton, Virginia 23665

FOREWORD

Science and Technology Corporation is pleased to submit this technical report No. 2017 entitled, "Development of Algorithms for Using Satellite and Meteorological Data Sets to Study Global Transport of Stratospheric Aerosols and Ozone," as the Final Report of this work performed under NASA contract NAS1-16362. It is a pleasure to acknowledge the valuable discussions held with L. R. McMaster and M. P. McCormick of NASA Langley Research Center in connection with this work.

ABSTRACT

This report presents results of the development of algorithms for using satellite and meteorological data sets to study global-scale transport of stratospheric aerosol and ozone and to understand the behavior of their global distribution. The main objective of the work reported has been to investigate the global-scale behavior of stratospheric aerosol and ozone during the January-February 1979 stratospheric sudden warming by using SAGE I and SAM II measurements. In particular, the discussions presented in this report are focused on the relationship between zonal mean aerosol and temperature, and on the ozone controlling mechanisms. Especially the ozone transport effect of planetary waves during the late February 1979 stratospheric warming has been investigated in detail.

The main conclusions drawn from the study are:

1. SAGE data set has been used for determining the correlation coefficients (R) between the ozone mixing ratio and temperature. The results indicate that they show strong negative correlation in the upper stratosphere and significant positive correlation in the lower stratosphere. These two different regions correspond to the ozone photochemical and dynamical control, respectively, in agreement with the ozone theory.

2. Between the regions of significant positive and negative correlation between ozone and temperature, there is a region in which only small values of R ($|R| \geqslant 0.5$) are showing. This is a region in which the

effects of ozone photochemistry and dynamics are about equal, and can be regarded as a transition region between the regions of ozone photochemical and dynamical control. The feature of this transition region derived in this analysis is in good agreement with the numerical results of Cunnold et al. (1980) and the report by Gille et al. (1980).

3. The results from an analysis of the relationship between zonal mean aerosol extinction ratio and mean temperature during the January-February 1979 stratospheric warming using SAM II aerosol measurements, indicate that dynamics may play an important role in determining the aerosol distribution during stratospheric warmings.

4. The calculated results for the period from February 23 to March 2, 1979, using SAGE I data set indicates an intense poleward eddy ozone transport in the middle stratosphere between approximately altitudes 24 and 38 km near 55° N, and equatorward eddy ozone transports exist below 24 and above 38 km near 55° N.

5. The computed ozone solar heating associated with planetary waves using SAGE ozone measurements is found to accelerate the damping rate due to infrared cooling alone in the upper stratoshere in agreement with the theoretical analysis and earlier report based on observations.

TABLE OF CONTENTS

LIST OF TABLES

LIST OF FIGURES

1. INTRODUCTION

The stratospheric aerosols and ozone are two important constituents of the atmosphere and have been receiving wide attention in recent years. Due to the fact that they both interact strongly with the solar and terrestrial radiations, perturbations of their concentration may result in change of the weather and climate pattern. In addition, stratospheric aerosols are the source of high-altitude cloud condensation nuclei. Therefore, they can affect indirectly the radiation budget of the earth-atmospheric system by modifying the cloud characteristics. For example, it is believed that the eruption of the volcano Tumbora in the Dutch East Indies in 1815 had a significant impact on global weather patterns (Stommel and Stommel, 1979; Toon and Pollack, 1976). Newell (1970) has shown that the eruption of Mt. Agung in Bali in March, 1963 increased the stratospheric temperature temporarily by about $5^{o}C$ over more than one quarter of the globe, while the tropical tropospheric temperature dropped by about $.5^{o}C$ (Newell and Weare, 1976). More recently, the effect of the El Chichon eruption in late March and early April 1982 on the atmospheric temperature has been shown by Labitzke et al. (1983). Between July and October 1982, the temperature at the 30 mb level at $10^{o}N$ is $3\text{-}4^{o}C$ warmer than the mean values for the same months in preceeding years. It should also be noted that the intense enhancement of stratospheric aerosols due to volcanic eruptions can affect the radiance measurements from satellite instruments. It has been reported that the El Chichon cloud has resulted in negative bias to the satellite derived sea surface temperature of greater than $2^{o}C$ (Bandeen and Fraser, 1982). In the case of stratospheric ozone, it absorbs strongly the

incoming solar radiation at ultraviolet wavelengths. Thus, it not only generates a major source of heating in the atmosphere which is important to the circulation, but also shields the biosphere from this harmful radiation.

The distributions of stratospheric aerosols and ozone are strongly influenced by atmospheric dynamics. Dynamical processes not only directly transport the aerosol particles and ozone themselves, but also affect the distribution of many important minor gases which engage in the formation and growth of the stratospheric aerosols through processes of photochemistry and microphysics and involve in catalytic reactions with stratospheric ozone. It should be noted that the motions that produce the transport are, in turn, driven in large measure by the radiative forcing, of which the ozone absorption of solar radiation is a principal component.

For the purpose of understanding the global behavior of stratospheric aerosols and ozone, NASA has developed two programs, i.e., the Stratospheric Aerosol and Gas Experiment (SAGE), and Stratospheric Aerosol Measurements II (SAM II). The SAM II instrument measures aerosol at 1.0 μm, and SAGE I at 0.45 and 1.0 μm. The ozone channel of SAGE I is centered at 0.65 μm. The aerosol and ozone measurements from the SAM II and SAGE I provide unique data set for studying their global behavior. The main emphasis of the work presented in this final report is on the analysis of the global transport effect of stratospheric planetary waves on the ozone flux and the zonal mean field of the aerosol extinction ratio during the winter 1978-1979. In addition, the calculation is also made for the correlation coefficient between ozone and temperature for understanding the stratospheric ozone controlling mechanism. The general information of the SAGE I and SAM II data sets relevant to this reported analysis is given in Chapter 2.

Chapter 3 is devoted to an analysis of the relationship between stratospheric ozone and temperature in terms of their correlation coefficients. The discussion of the relationship between zonally-averaged stratospheric aerosol and temperature is given in Chapter 4. Chapter 5 is devoted to a discussion of the ozone transport effect of planetary waves during the late February stratospheric warming. The radiative damping rate of planetary waves due to ozone solar heating in the stratosphere is discussed in Chapter 6. The summary and concluding remarks are presented in Chapter 7.

2. SAM II, SAGE I, AND CORRELATIVE DATA SETS

For the purpose of monitoring stratospheric aerosol and gases, NASA has developed two satellite experiments, namely, the Stratospheric Aerosol Measurement II (SAM II), and the Stratospheric Aerosol and Gas Experiment (SAGE I). The SAM II instrument, which is mounted on the Nimbus-7 satellite launched October 23, 1978, consists of a single channel sun photometer, centered at 1.0 μm wavelength. Aerosol extinction profiles, with 1 km vertical resolution and an accuracy better than 10%, are being obtained from this experiment. The SAGE I instrument is aboard a dedicated AEM-B satellite which was launched on February 18, 1979. The instrument is a sun photometer consisting of four channels centered at 0.385, 0.45, 0.60, and 1.0 μm wavelengths. Intensity measurements from these channels can be inverted to obtain profiles of aerosol extinction as well as extinction profiles that can be interpreted to give concentrations of ozone, nitrogen dioxide (Chu and McCormick, 1979). The ozone concentration profiles are deduced from the measurements at the 0.6 μm channel of the SAGE instrument which is centered at the peak of the ozone Chappius absorption band. The vertical resolution is 1 km from 10 to 35 km altitudes, and 5 km above 35 km altitude. The uncertainties (random errors) associated with the SAGE ozone profile are typically 10% for the above vertical resolution with better accuracy at the 10 mb height level. Good agreement has been found between SAGE ozone profiles and ground based measurements (Reiter et al., 1982; McCormick et al., 1984). The SAGE nitrogen dioxide profile can be inverted to an accuracy of about 25% in the 25-38 km altitude range.

Sampling opportunities of both SAM II and SAGE I instruments occur twice per orbit during sunrise and sunset encountered by the satellite. Since the satellite period is approximately 1.5 hours, there are about 15 sunrise and 15 sunset measurements per day. Due to the orbital characteristics of the Nimbus-7 satellite, the SAM II aerosol extinction measurements are confined to latitude bands ranging from 64^{o}S to 81^{o}S for sunrise events and from 65^{o}N to 85^{o}N for sunset events. The latitudinal shift of the measurement location is only 2^{o} or less per week. It takes approximately 13 weeks for the measurement location to cross the latitude bands. In contrast, the highly processing orbit of the AEM-B satellite allows the SAGE-I measurements covering latitudes between about 79^{o}S and 79^{o}N (depending on the season). The satellite sunrise or sunset measuring events shift from one extreme in latitude to the other in about a month. As a result of the slow latitudinal movement of the measurement location in high latitudes, it allows more sampling opportunities in these regions than in low latitudes. The detailed aspects of the SAM II and SAGE programs have been described by McCormick et al. (1979).

Figure 2.1 shows the latitudinal coverage of the SAM II and SAGE 1 measurements. An example of the SAGE sampling locations of the sunrise event on February 25, 1979 is given in Figure 2.2

Accompanying each profile of the SAM II and SAGE I measurement there are meteorological information including temperature and height data at 18 standard pressure levels[1] provided by NOAA's National Meteorological Center based on the routine operational analyses (Gelman et al., 1981; Hamilton, 1982). These meteorological data, in conjunction with the SAM II and SAGE I measurements are being used in the analysis presented in this final report.

[1]The standard pressure levels are 1000, 850, 700, 500, 400, 300, 250, 200, 150, 100, 70, 50, 30, 10, 5, 2, 1, 0.4 mb.

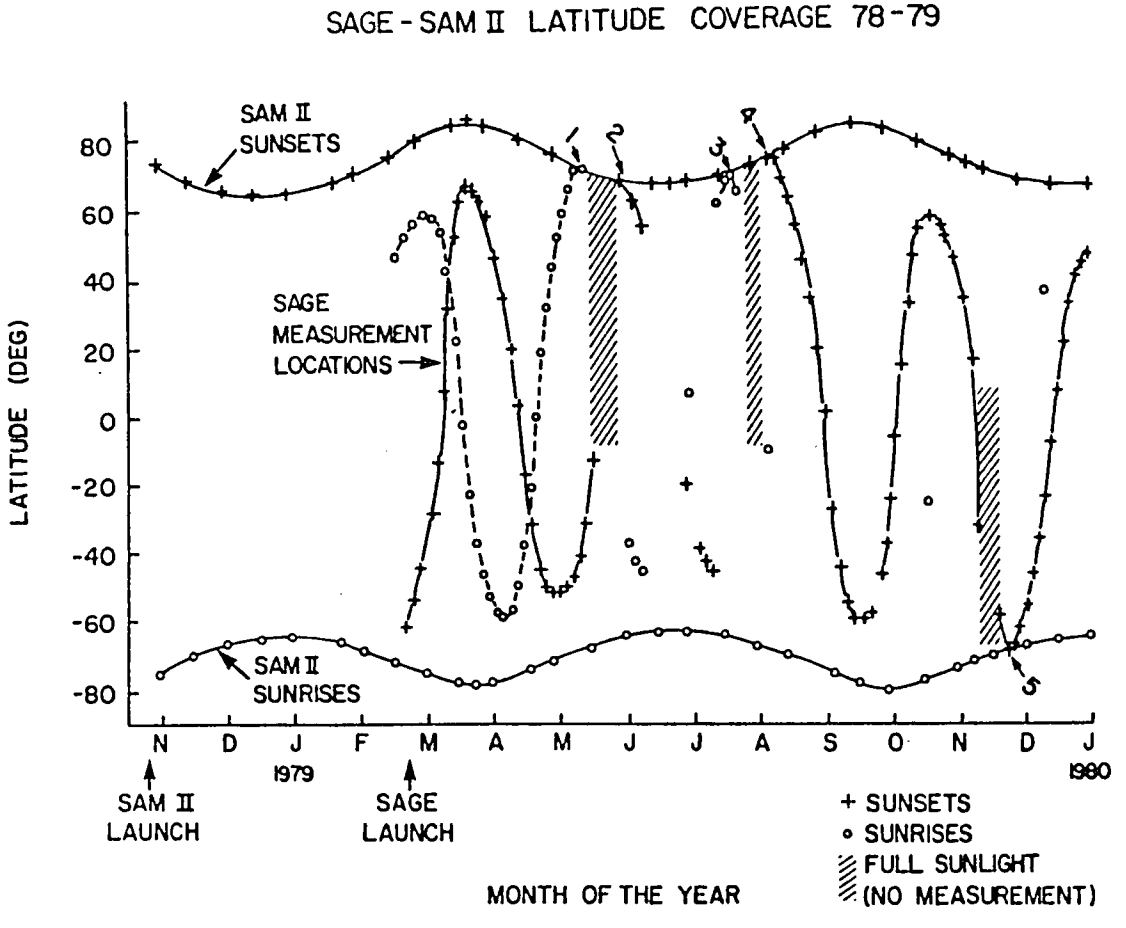

FIG. 2.1: SAGE and SAM II latitudinal coverage during 1979.

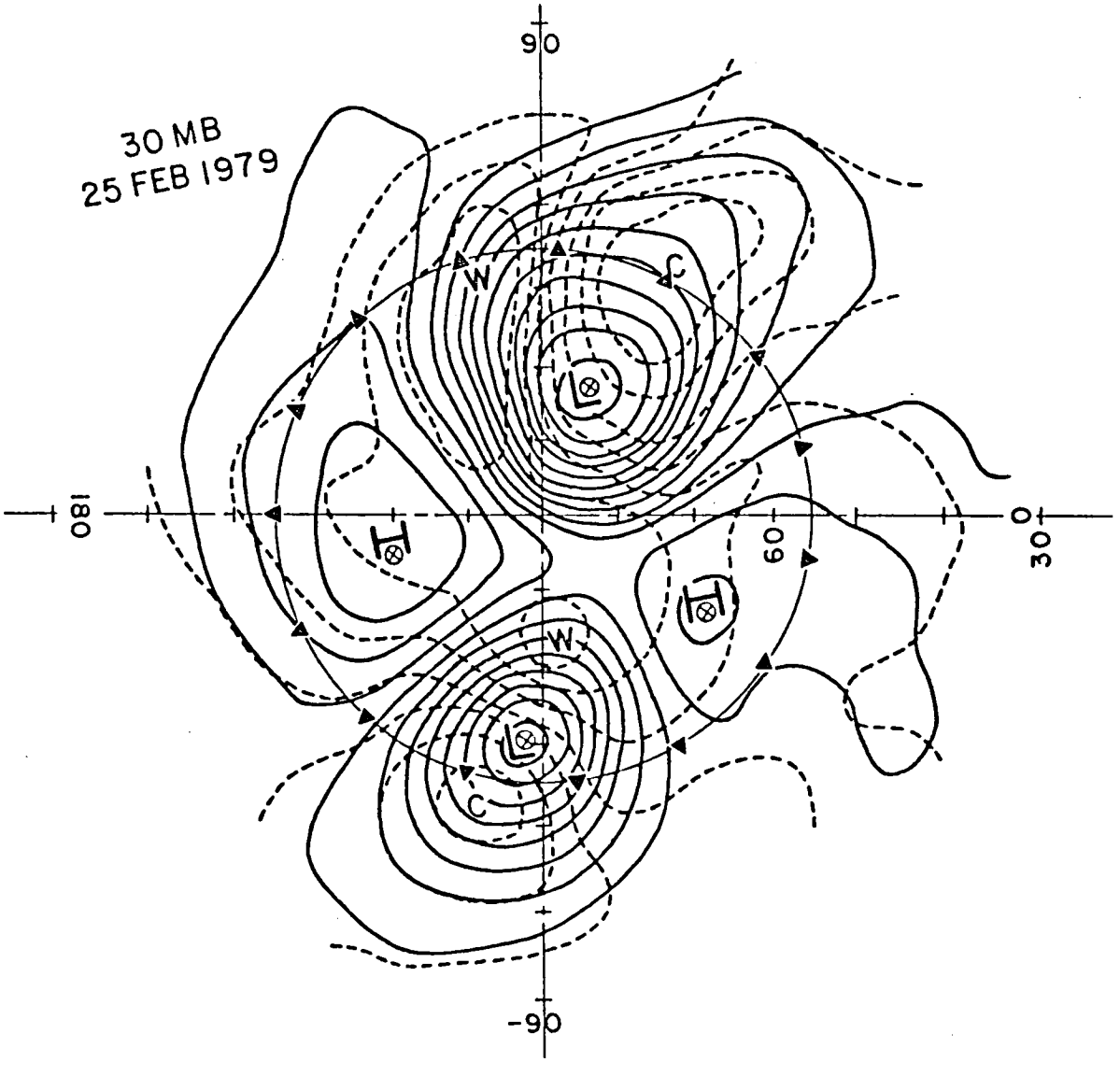

FIG. 2.2: The 30 mb height contour map and the approximate sampling locations of SAGE measurements on February 25, 1979.

3. THE RELATIONSHIP BETWEEN OZONE AND TEMPERATURE IN THE STRATOSPHERE

3.1 BACKGROUND

Generally, in the midlatitude below about 25 km (15 to 25 mb) the ozone distribution is mainly controlled by dynamical processes (Dutsch, 1969), while photochemical reactions play a decisive role in determining ozone concentrations above 35 km (Blake and Lindzan, 1973). The relative importance of the dynamical and photochemical processes in determining ozone concentration can be simply estimated based on their relaxation effects on the ozone perturbations. In terms of the relaxation concept, any introduced departure of ozone concentrations from its local equilibrium in the dynamically controlled region will be smoothed out through mainly transport processes, and by ozone photochemical production or lose in the ozone photochemically controlled region. Thus, the effect of dynamical processes on the ozone perturbations depends critically on the distribution of ozone concentration, and on the velocity field. As for the ozone photochemical production and loss processes, their effects on ozone perturbations are strongly temperature dependent. Due to the fact that ozone production/loss rate changes negatively/positively with respect to the temperature changes (Hartmann, 1978), it is expected that ozone and temperature perturbations will show an out-of-phase relationship in the photochemically controlled region in response to the temperature disturbances. This out-of-phase relationship implies a negative correlation between ozone and temperature in the photochemically controlled region. In contrast, in the dynamically controlled region (below altitude 25 km), they would be expected to show an in-phase relationship, i.e., a positive correlation. This is because ozone is now acting as an inert gas. Thus, like the temperature perturbations ($\delta_T \sim \delta\theta$, the deviation of potential temperature), it is conservative. In addition, the ozone mixing ratio and temperature show a similar meridional

distribution in the lower stratosphere. In the analysis presented in this chapter, it is intended to show the dominance of the dynamical and photochemical processes in determining ozone distribution in different regions in the stratosphere based on SAGE I ozone measurements and meteorological information. The approach is to compute the correlation coefficients between ozone (O_3) and temperature (T). Since O_3 concentration in the upper stratosphere depends much on T through ozone photochemical reactions, and on the dynamical processes in the lower stratosphere, study on the correlation coefficients between O_3 and T would help us to assess the relative importance of chemistry against dynamics in different regions in the stratosphere. As will be shown later, the results of this analysis agree very well with the earlier findings using limited observed data and with the predictions generated from a numerical model.

3.2 METHOD OF APPROACH

The characteristics of the SAGE ozone measurements and the meteorological data have been described in Chapter 2. These data, in the months of March and August, 1979, were used for determining the correlation coefficients R between ozone mixing ratio and temperature. These data were first grouped on a 5 km by altitude and 5 degrees by latitude grid area. Due to the fact that the vertical reference of the SAGE I ozone data is measured in kilometers, whereas the meteorological data are given at fixed pressure levels, an interpolation scheme is used to transfer the temperature data to the same vertical frame as that of ozone mixing ratio. Then, computations of correlation coefficient were applied to each data group. The calculated results of R values are plotted in a meridional cross-section. Table 3.1 indicates the number of data pair of ozone mixing ratios and temperature used in this analysis.

TABLE 3.1: Number of data points used in computation of the correlation coefficient between ozone mixing ratio and temperature

Latitude (Deg.)	MARCH 1979	AUGUST 1979	Latitude (Deg.)	MARCH 1979	AUGUST 1979
65.	150	150	- 5.	70	55
60.	150	115	-10.	70	45
55.	150	115	-15.	35	--
50.	70	5	-20.	45	--
45.	45	10	-25.	60	--
40.	70	70	-30.	70	--
35.	70	70	-35.	150	--
30.	70	70	-40.	150	--
25.	55	40	-45.	65	--
20.	15	20	-50.	150	--
15.	40	20	-55.	150	--
10.	60	55			
5.	30	45			
0.	70	45			

3.3 RESULTS AND DISCUSSION

Figure 3.1 shows the meridional cross-section of the calculated correlation coefficients between ozone mixing ratio and temperature for the month of March 1979. The correlation coefficients are clearly shown to be negative in the upper stratosphere and positive in the lower stratosphere. A zero line of the correlation coefficients, which separates the regions of negative values from that of the positive values, takes place at an altitude of about 32 km at the equator and rises to about 37 km at the midlatitude. This zero line of the correlation coefficients can be regarded as the center of a transition layer (region) within which the effect of both the dynamical and photochemical processes are about equal. Above this layer, photochemistry plays the significant roles in determining the ozone distribution, while dynamics is important in the region below. If we take the values of the correlation coefficient between -.5 and +.5 as the condition for the transition region. It is found from Fig. 3.2 that the vertical extent of this transition layer is about 3. km in the tropics and increases to more than 7 km at the midlatitudes. The calculated results for the month of August 1979 is given in Fig. 3.2. The latitudinal coverage is from -10^{o}S to 65^{o}N. Figure 3.2 shows rather similar features to Fig. 3.1. The distinct common features are: (1) the negative-positive regions of the correlation coefficients are well defined; (2) the zero line of the correlation coefficient, i.e., the center of the transition region, is generally tilted in such a manner that its altitude increases with the latitude; and (3) the vertical extension of this transition region increases with the latitude. Based on a somewhat different definition for the boundaries between the photochemical and dynamical regions, Cunnold et al. (1980) have derived a transition

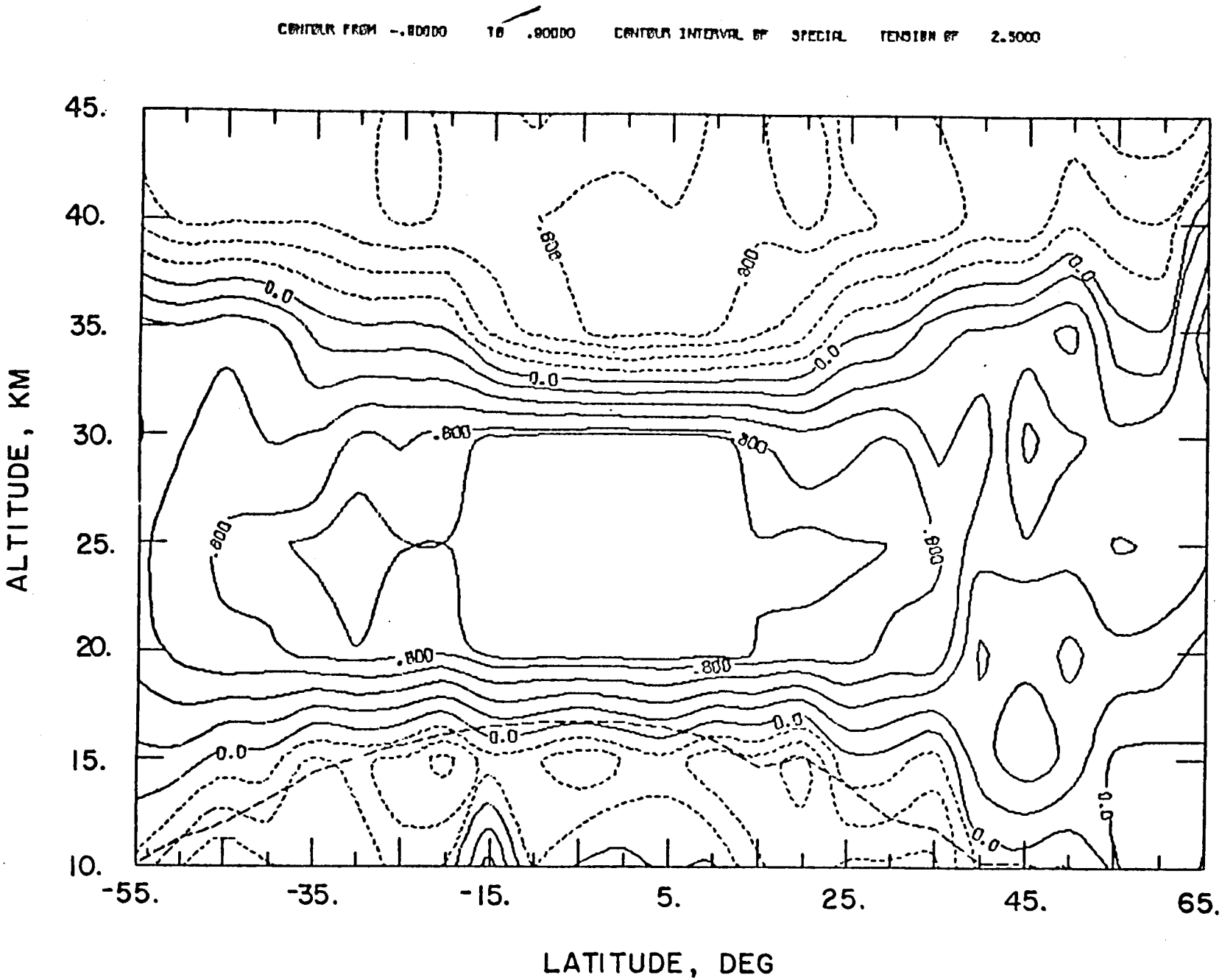

FIG. 3.1: CORRELATION BETWEEN OZONE MIXING RATIO AND TEMP, MARCH 1979.

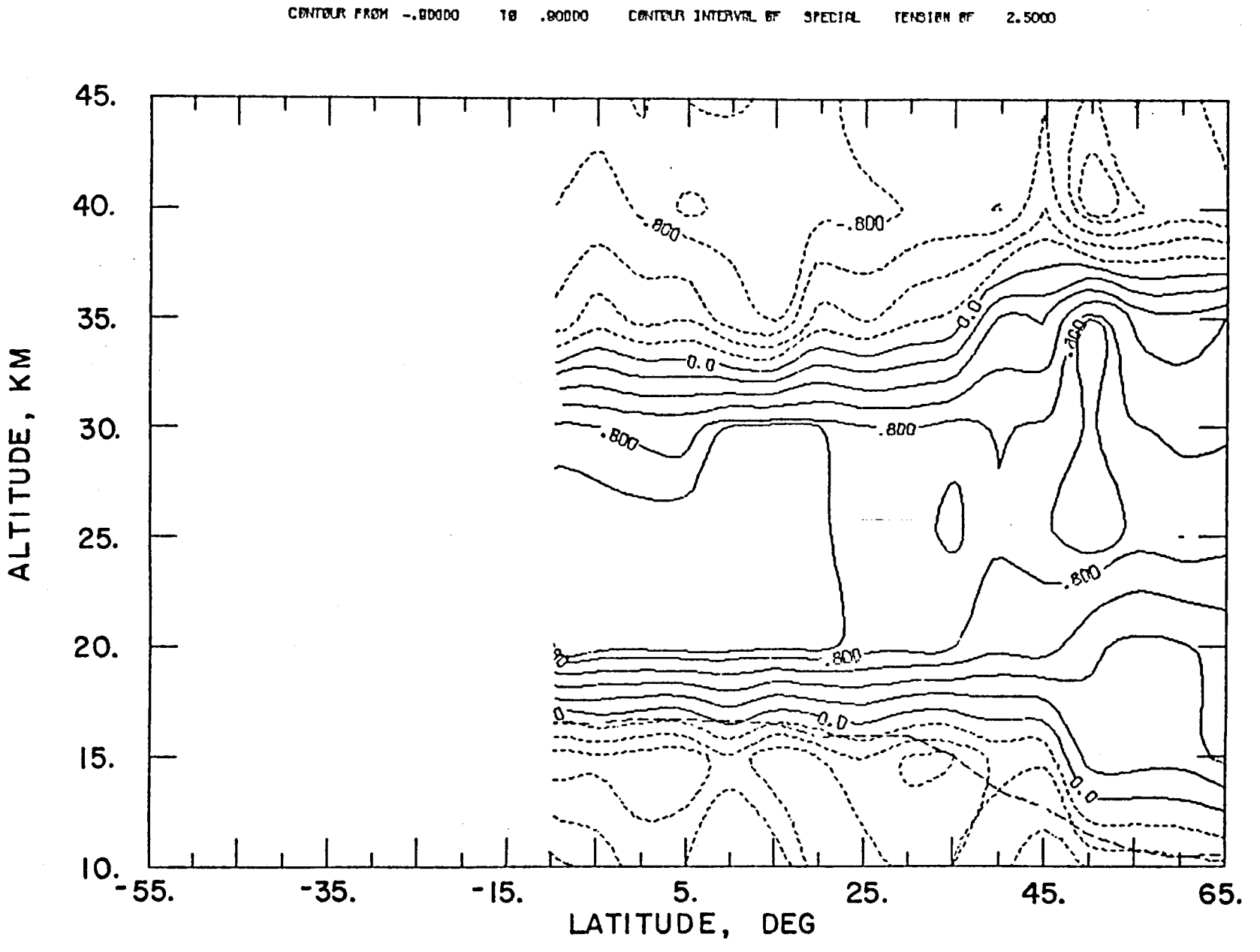

FIG. 3.2: CORRELATION BETWEEN OZONE MIXING RATIO AND TEMP, AUGUST 1979.

region using their spectral 3-D photochemical-dynamical model. Their definition is given in terms of the contribution of the advection and the chemical production and loss to the ozone tendency. Their results are reproduced in Fig. 3.3. The upper dashed line (Fig. 3.3) represents where effect of advection is roughly equal 0.1 times that of the smaller of chemical production and loss. Similarly, the lower dashed line represents where the effect of advection roughly equals 10 times that of the smaller of chemical production and loss. Although their model results show a slightly lower location of the transition region, the general pattern of the layer is in good agreement with the results derived from this correlation coefficient computation using observed information.

By using LRIR measurements during November and December 1975, Gille et al. (1980) have examined the transition region in terms of the phase relationship between ozone, temperature, and geopotential height waves (wavenumber 1). The region in which the phase difference is 90° or less between height and ozone waves is defined as the dynamically controlled region, while the region in which the phase difference between ozone and temperature waves is at least 135° is considered to be under photochemical control. The layer in between is the transition region. Their results are reproduced in Fig. 3.4. It exhibits a very strong latitudinal dependence. In addition, Fig. 3.4 shows that the dynamical and photochemical boundaries merge in the polar darkness. In comparison with Gille et al.'s (1980) results (Fig. 3.4), Figures 3.1 and 3.2 show generally a similar behavior of the transition region as in Fig. 3.4 at the same latitudes, despite the difference in the months of the data used in the analysis.

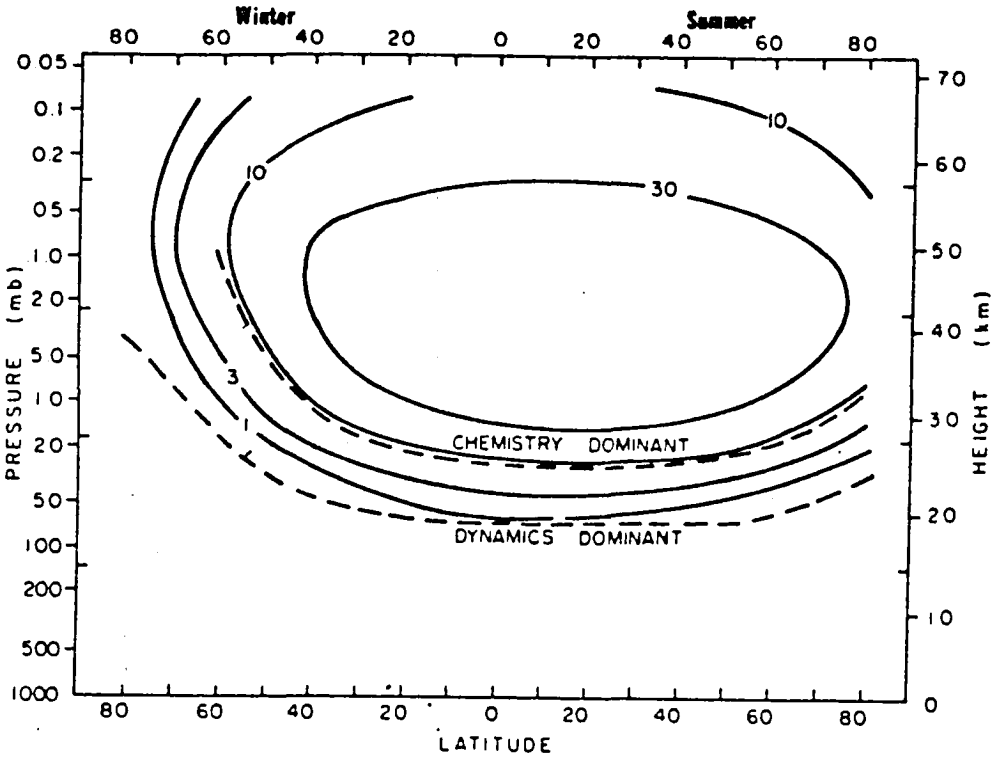

FIG. 3.4: The calculated daily-averaged photodissociation rate for molecular oxygen during the solsticial seasons. Values have been weighted by the volume 10° latitude by 360° longitude by approximately 2.8 km (ΔZ = 0.40574), and are expressed in tons/sec. The dashed lines indicate the boundary of the transition region (Cunnold et al., 1980).

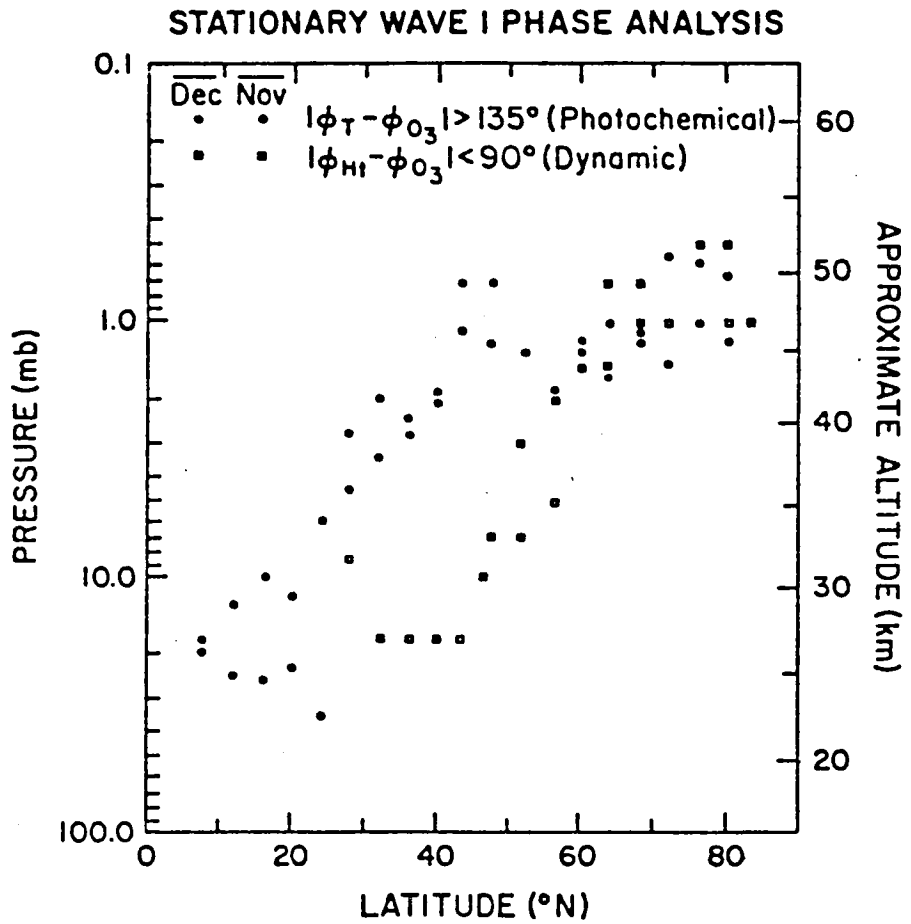

FIG. 3.5: Latitudinal dependence of the lower boundary of the photochemically controlled region (circles) and the upper boundary of the dynamically controlled region (squares) for November and December, 1975 (Gille et al., 1980).

4. ZONAL MEAN STRATOSPHERIC AEROSOL, JANUARY - FEBRUARY, 1979

4.1 BACKGROUND

Since its discovery about 20 years ago (Junge et al., 1961), the stratospheric aerosol layer has been a subject of considerable interest to atmospheric scientists and climatologists. It is recognized that this aerosol layer consists mainly of sulfate particles (Rosen, 1971; Arnold et al., 1981). Kessee and Castleman (1982), Yue and Deepak (1982), Yue (1981), Hamill et al. (1977), and Hidy et al. (1978), etc., have examined theoretically the formation and growth of stratospheric aerosols. There is no doubt that the behavior of stratospheric aerosols is intimately related to the air temperature. It should be noted that the distribution of stratospheric aerosols is also strongly influenced by atmospheric dynamics. Dynamic processes not only directly transport the particles themselves but also affect the distribution of precursor gases and vapors which engage in the formation and growth of the stratospheric aerosols through processes of photochemistry and microphysics. The effect of dynamic processes on stratospheric aerosols injected from volcanic eruptions has been reported by many investigators (Cadel et al., 1976; Cadel et al., 1977; Newell and Deepak, 1982). The transport effect has been incorporated in a one-dimensional model study and is simulated in terms of the eddy diffusion coefficient (Turco, et al., 1979; see also Turco, 1982). It is well known that, in the winter northern hemisphere, the meteorological condition of the stratosphere in high latitudes is characterized by stratospheric warming associated with large scale disturbances - the so-called planetary waves. These long wave activities

are generally accompanied by distinct changes in the zonal mean thermal structure and mean flow pattern. Therefore, it is of interest to examine the behavior of the zonal mean aerosol and to study its relationship with the zonal mean temperature in the high latitude stratosphere during winter season. In the work presented in this chapter, we have chosen the winter of January-February 1979 as the period for the analysis since the meteorological behavior of the stratosphere during this period has been extensively investigated by Quiroz (1979) and Labitzke (1981).

4.2 DATA AND METHOD OF ANALYSIS

The data set used in this study consists of the aerosol extinction ratio obtained from the SAM II satellite experiment and the meteorological information provided by the Climate Analysis Center of NOAA. The meteorological information includes temperature and height data from their gridded analysis at 18 standard pressure levels interpolated to the tangent locations where SAM II measurements were made. The general features of the SAM II aerosol data and the meteorological information have been described in Chapter 2. Since the vertical reference of the aerosol extinction ratio is measured in kilometers, whereas the meteorological data are given at fixed pressure levels, an interpolation scheme is used to transfer the temperature data to the same vertical frame as that of aerosol extinction ratio. In this study, we have used the vertical grid points in the altitude range from 14 km to 28 km with 2 km vertical increments. A typical altitude-longitude distribution of the aerosol extinction ratio and temperature is displayed in Fig. 4.1a and Fig. 4.1b, respectively. The tickmarks on the abscissae denote the longitudes where SAM II made the measurements on that particular day. Table 4.1 gives the number of profiles and the average latitude of the SAM II daily

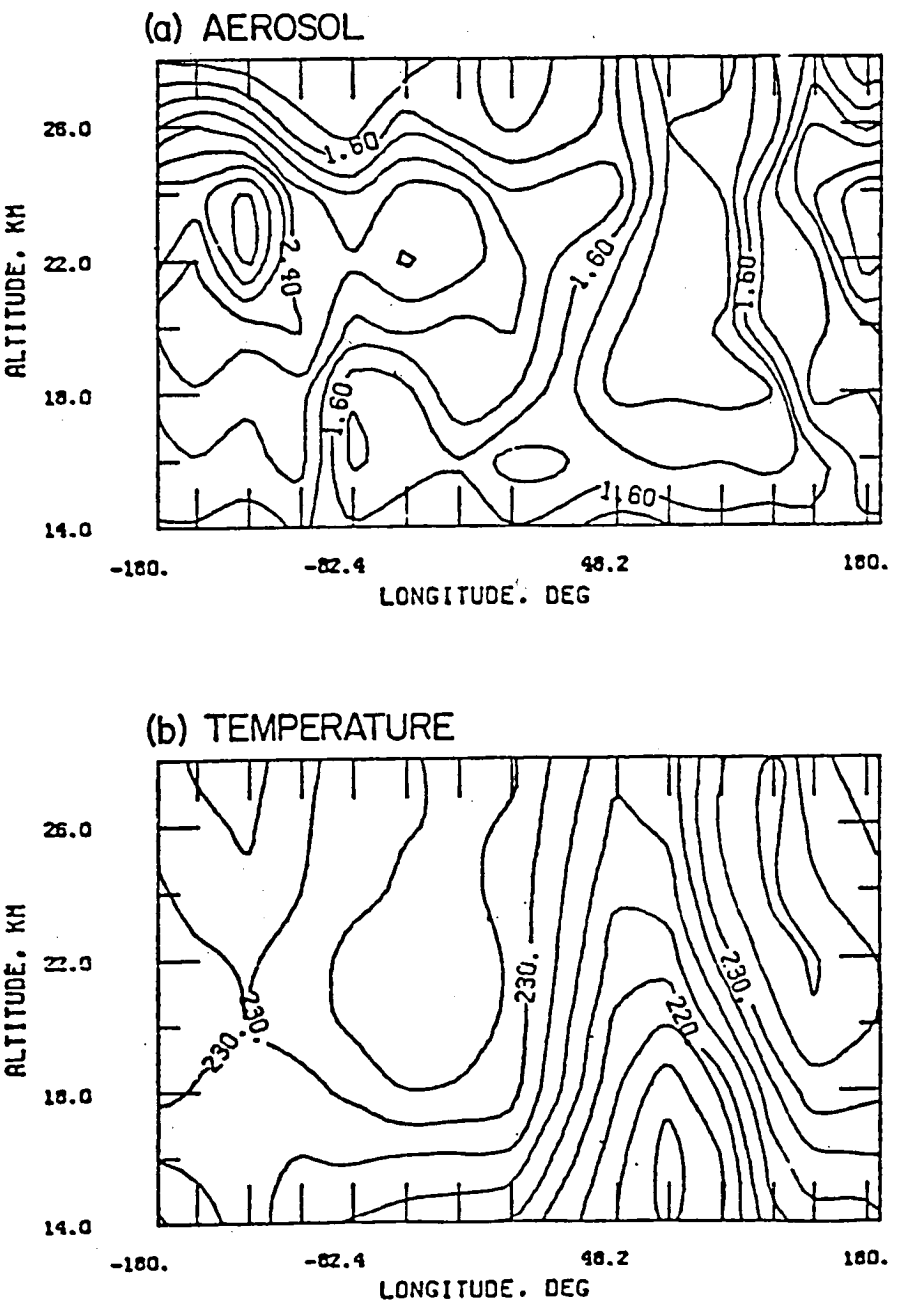

FIG. 4.1: Typical height-longitude distribution (~75°N) of (a) aerosol extinction ratio (1. μm) contour interval .2; and (b) temperature (°K) for February 24, 1979, contour interval 2.5°C.

TABLE 4.1: The number of profiles and average latitude of SAM II observations from January 24 to March 5, 1979

Date	Number of Profiles	Average Latitude (°N)	Date	Number of Profiles	Average Latitude (°N)
Jan. 24	11	68.95	Feb. 14	10	74.69
25	12	69.18	15	11	75.02
26	14	69.42	16	13	75.32
27	11	69.67	17	12	75.65
28	13	69.91	18	12	75.97
29	12	70.16	19	11	76.28
30	10	70.43	20	11	76.57
31	10	70.70	21	12	76.87
Feb. 1	12	70.96	22	12	77.21
2	12	71.23	23	11	77.51
3	12	71.49	24	13	77.84
4	12	71.75	25	12	78.13
5	12	72.06	26	9	78.38
6	13	72.34	27	10	78.71
7	11	72.65	28	13	79.01
8	12	72.94	Mar. 1	10	79.29
9	12	73.21	2	12	79.60
10	11	73.50	3	13	79.87
11	12	73.81	4	12	80.15
12	11	74.10	5	13	80.41
13	11	74.41			

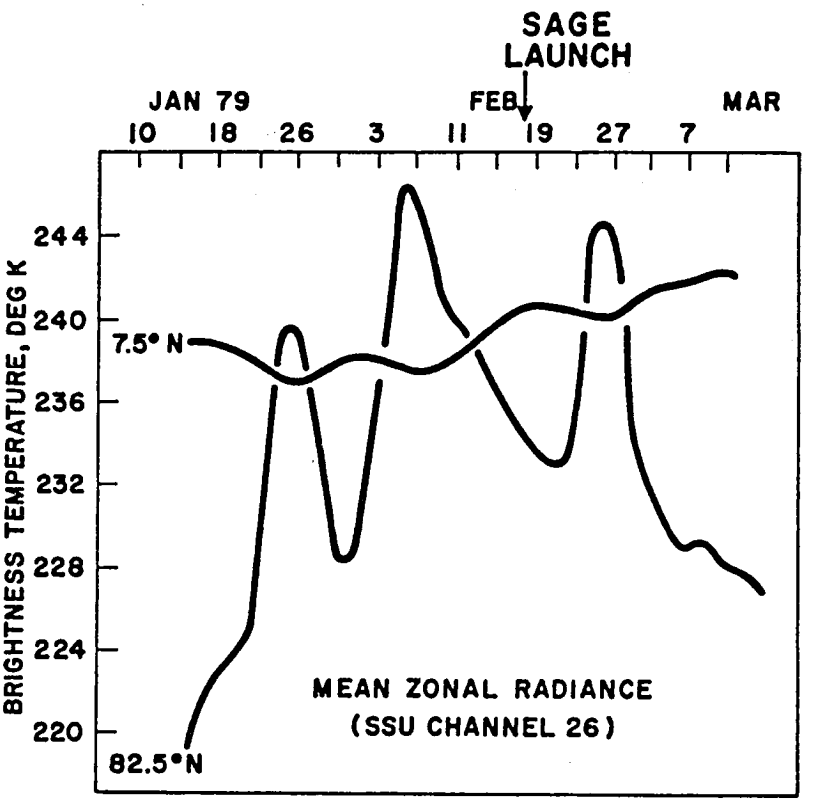

FIG. 4.2: Zonal mean radiance near equator and pole from measurements in SSU Ch. 26 (proportional to mean temperature for layer 50-1 mb). (From Quiroz, 1979).

observations in the period from January 24, 1979 to March 5, 1979, used in this analysis. It covers the three warming pulses that occurred at high latitudes during this January-February 1979 stratospheric warming as shown in Fig. 4.2 (Quiroz, 1979). It should be noted that before January 24, 1979, the stratosphere was characterized by the appearance of polar stratospheric clouds (PSCs), and that the warming ended approximately in the early March as activity of the planetary waves declined (McCormick et al., 1982; Quiroz, 1979; see also McCormick et al., 1981). It is important to note that the overall average latitude is about 75^{o}N; therefore, the interpretation of the analyzed results should be applied to this latitude. Although there is about a $\pm 5^{o}$ latitude range existing in the entire data set, the results of this study are believed to be representative qualitatively since the latitudinal scale of the stratospheric warming is much larger than 15^{o}. Due to the fact that the time scale of a stratospheric warming is about one week or longer, the data are smoothed by using a 3-day running-mean smoothing scheme to avoid high frequency fluctuations. In doing this, the daily data sets at SAM II measurement tangent points are interpolated to obtain information at assigned longitudes from -180^{o} to 180^{o} at 20^{o} increments. The calculation of the zonal mean aerosol extinction ratio as well as the mean temperature for a particular day at a given altitude is straightforward. The results of the calculations are discussed in the next section.

4.3 RESULTS AND DISCUSSION

The calculated zonal mean temperature field, expressed as dashed lines in Fig. 4.3, exhibits three consecutive warming pulses over the time period from January 24 to March 5 in agreement with Quiroz's (1979) report. The peaks of these warmings took place on approximately January 27, February 9,

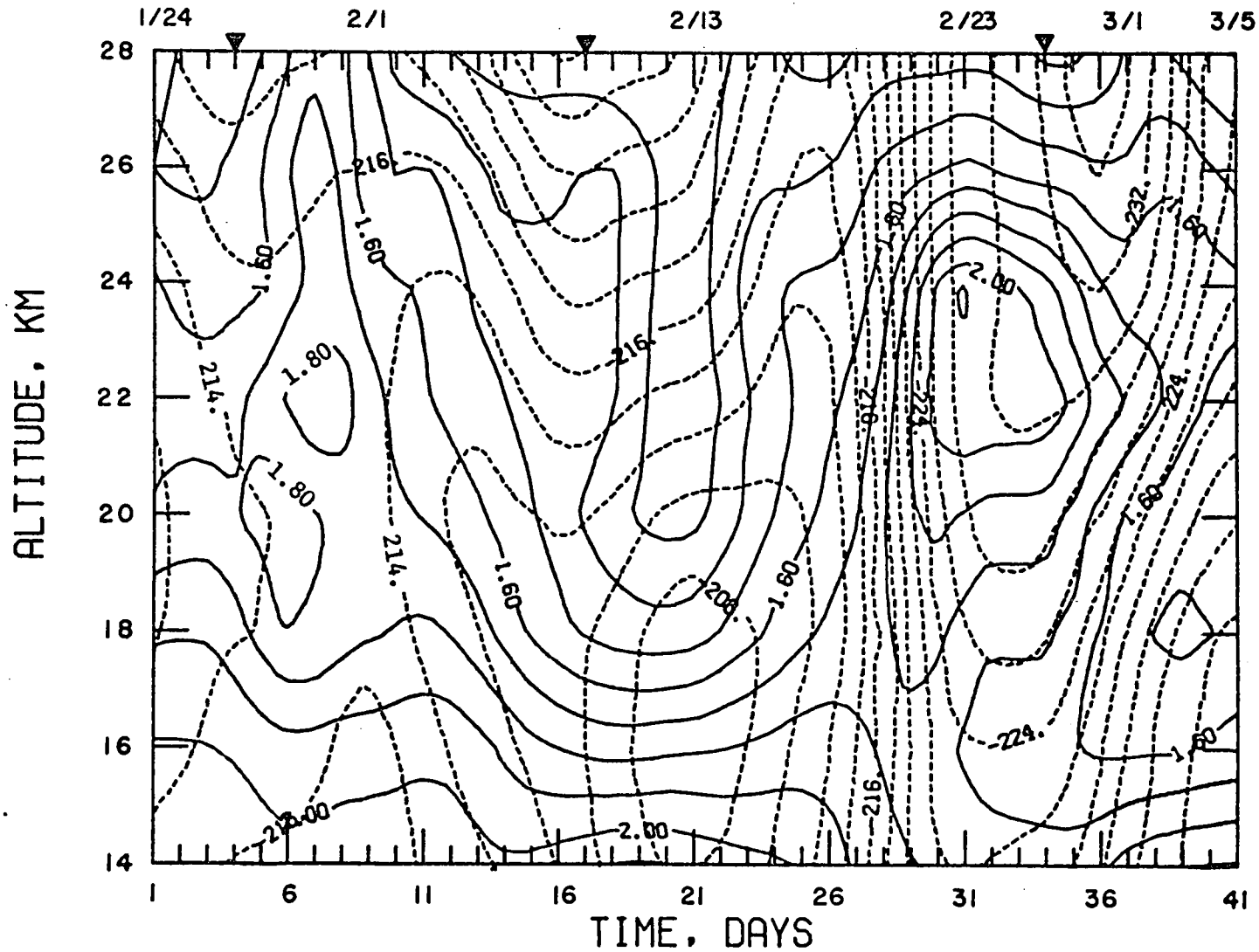

FIG. 4.3: The zonal-averaged aerosol extinction ratio (solid line) and zonal mean temperature (^{o}K, dashed line) near 75^{o}N during the stratospheric warming event of January - February 1979. ∇ denotes the approximate day of each warming peak. The contour interval is .1 for the zonal mean aerosol extinction ratio, and 2^{o}C for the mean temperature.

and February 26 near 75°N. It is interesting to note that these three warming pulses show different vertical extents. The first pulse reaches down to an altitude at approximately 24 km, the second one at 19 km, and the last one covers the entire altitude range of this analysis. Fig. 4.3 shows that the occurrence of the second warming pulse began first at higher altitudes (at 28 km on February 1). It appeared at the level 20 km by February 9. On the other hand, the third warming pulse began first at the lower level (14 km on February 13) and then the higher levels. Since the data cover only a limited part of the first warming pulse, no conclusion about the level of the first appearance of this warming pulse can be drawn. The intensities of the three warming pulses also seem increased according to the sequence of their occurrence. At 28 km, the peak temperatures of the three warming pulses are 219°K, 226°K, and 235°K corresponding approximately to January 27, and February 9 and 2. The rates of the mean temperature change for the development of the last warming pulse are dramatic; a zonal mean temperature increase of ∿5°C from February 20 to 21 at 22 km (12°C from February 19 to 22), and a decrease of ∿3°C from March 2 to 3 at the same level. Quiroz (1979) has shown that the development of the last warming pulse was associated with planetary wave activity, namely the eddy heat transport of wavenumber 2. He also shows that wavenumber 1 was responsible for the second warming. Labitzke (1981) has indicated that, preceeding the development of wavenumber 2, there is an amplification of wavenumber 1 which displaces the stratospheric jet poleward and leads to a situation favorable to the intensification of wavenumber 2.

The solid lines in Fig. 4.3 show the variations of the zonal mean aerosol extinction ratio based on SAM II measurements. Noticeable features are the fluctuations of the aerosol extinction ratio centered approximately at an altitude of 22 km over the entire warming period. From altitude 14 to 17 km,

values of extinction ratio of 1.6 to 2.0 are fairly constant with time. At 22 km, Fig. 4.3 shows the development of peaks in the ratio of about 2, occurring on January 30 and February 23, and the appearance of a relatively low ratio of about 1.2 on February 12. With respect to the latter, also note that the lower stratosphere from 20 to 28 km was characterized by relatively low values of the mean aerosol extinction ratio throughout the entire period of the second warming pulse (from February 3 to 17). The minimum extinction ratio developed on February 12 occurred about 5 days after the second warming peak. It should be noted that the aerosol microphysics, namely the nucleation, condensation, and evaporation processes, suggest that the background aerosol in the stratosphere is related inversely to the local temperature (Yue and Deepak, 1981, 1982). It is anticipated that the relatively low values of the zonal mean aerosol extinction ratio should occur in the region above altitude $\sim$20 km during the second warming pulse. On the other hand, the dynamics may also affect the aerosol distribution through transport processes. This seems to be the case in the region below altitude $\sim$20 km during the second warming pulse. One may notice that during the period from February 1 to 13, both the mean aerosol extinction ratio and the temperature in the region below altitude $\sim$20 km were decreasing while they both increased afterward. This feature suggests that the aerosol microphysics may not be important in this particular development in the region below altitude $\sim$20 km, and that dynamics seem to play a dominant role. The development of the peak of the mean aerosol extinction ratio on February 23 is of particular interest. It can be seen that during the period from February 17 to 23, both the mean aerosol extinction ratio and the mean temperature show rapid increase. This joint increase in mean temperature and aerosol extinction ratio provide an additional interesting incidence which suggests that

the dynamics may play a significant role in the development of the mean aerosol extinction ratio during stratospheric sudden warmings.

5. OZONE TRANSPORT DUE TO PLANETARY WAVES; THE LATE FEBRUARY 1979 STRATOSPHERIC WARMING

5.1 BACKGROUND

One of the most interesting aspects of atmospheric ozone is the so-called northern spring maximum in the yearly variation of total ozone in high latitudes of the northern hemisphere. It has been suggested that ozone transports due to large-scale quasihorizontal eddies are responsible for this spring ozone buildup (Newell, 1964; Craig, 1965; Dütsch, 1969; Prabhakara, 1963; Cunnold et al., 1980; and, Holton, 1980a). Recently, Hartmann and Garcia (1979) have described theoretically the mechanism of ozone transport due to forced planetary waves (wavenumber 1 and wavenumber 3) based on a linearized numerical model which takes into account the coupling between radiation, chemistry, and dynamics. Their model results indicate that ozone perturbations exhibit a phase shift of nearly 180^{o} between the region of dynamical control and the region of photochemical control. This phase shift takes place mainly in a layer (the transition region) in which the effect of the dynamics on the ozone concentration is about equal to that of the ozone photochemistry. In this altitude region, an in-phase relationship between ozone perturbations and wave motion may occur and leads to enhanced poleward and downward ozone transports. A similar model analysis has been given by Kawahira (1982).

In the ozone photochemically controlled region, the effect of ozone transport due to planetary waves on the zonal mean ozone distribution is vanishingly small. Nevertheless, equatorward eddy ozone transport is expected to occur in accompanying the intense poleward eddy heat transport developed during stratospheric sudden warmings because of a negative correlation between

ozone and temperature in the upper stratosphere (Barnett et al., 1975; Kawahira, 1982). In the dynamical controlled region, the ozone transport effect of planetary waves depends on the nature of the waves. For steady nondissipative waves with nonzero Doppler-shifted frequency the eddy tracer transport is exactly cancelled by the transport due to wave-induced mean meridional circulation--the so-called nontransport theorem (Andrews and McIntyre, 1978a,b). On the other hand, net tracer transport can be brought about by dissipative or transient waves. It is well known that during stratospheric sudden warming events, rapid changes in wave amplitude occur. Thus, during the warming period net ozone transport due to planetary waves can be very significant in understanding the stratospheric ozone budget. The dynamical aspects of sudden stratospheric warmings have been subject to extensive investigation , and have recently been reviewed by McInturff (1978), Schoeberl (1978), and Holton (1980b). There can be little doubt that the wave-mean flow interaction processes are responsible for the generation of stratospheric sudden warmings and for the significant poleward and downward transport of stratospheric ozone and other passive tracers during a warming event (Holton, 1980b).

The purpose of this chapter is to study the planetary wave transport of ozone during the late February 1979 sudden stratospheric warming by computing the ozone eddy flux using SAGE and auxiliary meteorological data, and to assess the current understanding of the ozone transport effect of large scale disturbances in winter stratosphere by comparing the calculated results with those of existing model and observational analyses (Hartmann and Garcia, 1979; Kawahira, 1982; Gille et al., 1980). As mentioned in Chapter 4, some aspects of this January-February 1979 warming have been discussed by Quiroz (1979). There are three

successive reversals of the meridional gradient of zonal mean stratospheric temperature during this warming (Fig. 4.2). The behavior of the warming also reveals strong tropospheric-stratospheric interactions through intense upward geopotential flux from the troposphere in the form of wave 1 and 2 amplifications. Furthermore, Quiroz (1979) has shown that the third warming pulse occurring during the late February 1979 can be attributed mainly to the effect of wavenumber 2.

5.2 DATA AND METHOD OF APPROACH

The characteristics of SAGE ozone measurements have been described in Chapter 2. The instrument was launched on February 18, 1979. Since February 22, 1979 (four days after the launch of the SAGE instrument), profiles of ozone as well as aerosol and nitrogen dioxide have been collected by SAGE. Although the January-February 1979 warming began about a month before the launch of the SAGE instrument, the measurements cover the period of the third warming pulse of the zonal mean temperature in high latitudes, which was associated with a reversal of the mean zonal wind (Quiroz, 1979). In this chapter, the SAGE ozone measurements, in conjunction with the meteorological data, will be used to investigate the ozone transport due to planetary waves during the late February 1979 stratospheric warming. Due to the fact that the meteorological data above 10 mb ($\sim$30 km) are missing for five consecutive days beginning on March 3, 1979, the data used in this study cover from February 23, 1979, to March 2, 1979. As indicated by Quiroz (1979), the development of the wavenumber 2 was beginning approximately on February 11 with a maximum amplitude at 10 mb around February 22. Thus, this study covers the declining phase of this January-February warming event.

As indicated in Chapter 2, there are temperature and height data at 18 standard pressure levels associated with each ozone profile measured by the SAGE instrument. The daily height data are first used to determine the zonal averaged height by performing harmonic analysis at each of the standard pressure levels. These mean heights of the 18 pressure levels allow us to determine the height deviations from zonal averages at assigned altitude mesh points, namely from 10 to 50 km with a 2 km increment, using an interpolation scheme. Similarly, an interpolation scheme is used to obtain the temperature at these assigned altitudes. This interpolation is needed because the height parameter of the SAGE ozone mixing ratio is measured in kilometers. At these assigned altitudes, the ozone mixing ratio can be obtained based on the SAGE observations. To ensure compatibility between the SAGE data and the meteorological data, the SAGE ozone profiles have been vertically smoothed with a 5 km running-mean triangular filter. This vertical smoothing on the SAGE ozone profile also reduces the uncertainties to typically below the 5% level. The typical altitude-longitude distribution of the ozone mixing ratio, temperature, and height deviation for February 25, 1979, are displayed in Figs. 5.1a to 5.1c, respectively. The tickmarks on the abscissae denote the longitudes where SAGE made measurements on that particular day. Figure 5.1 clearly indicates the wave structure in the longitudinal direction. For the convenience of performing Fourier analysis, these data are further used to determine the ozone mixing ratio, temperature and height deviation at every 20° in longitude at assigned altitudes using a two-dimensional Lagrangian interpolation scheme. These altitude-longitude interpolation procedures for the 24-hour data sets can be justified by the fact that stratospheric warmings are characterized by a time scale about a week or longer. This

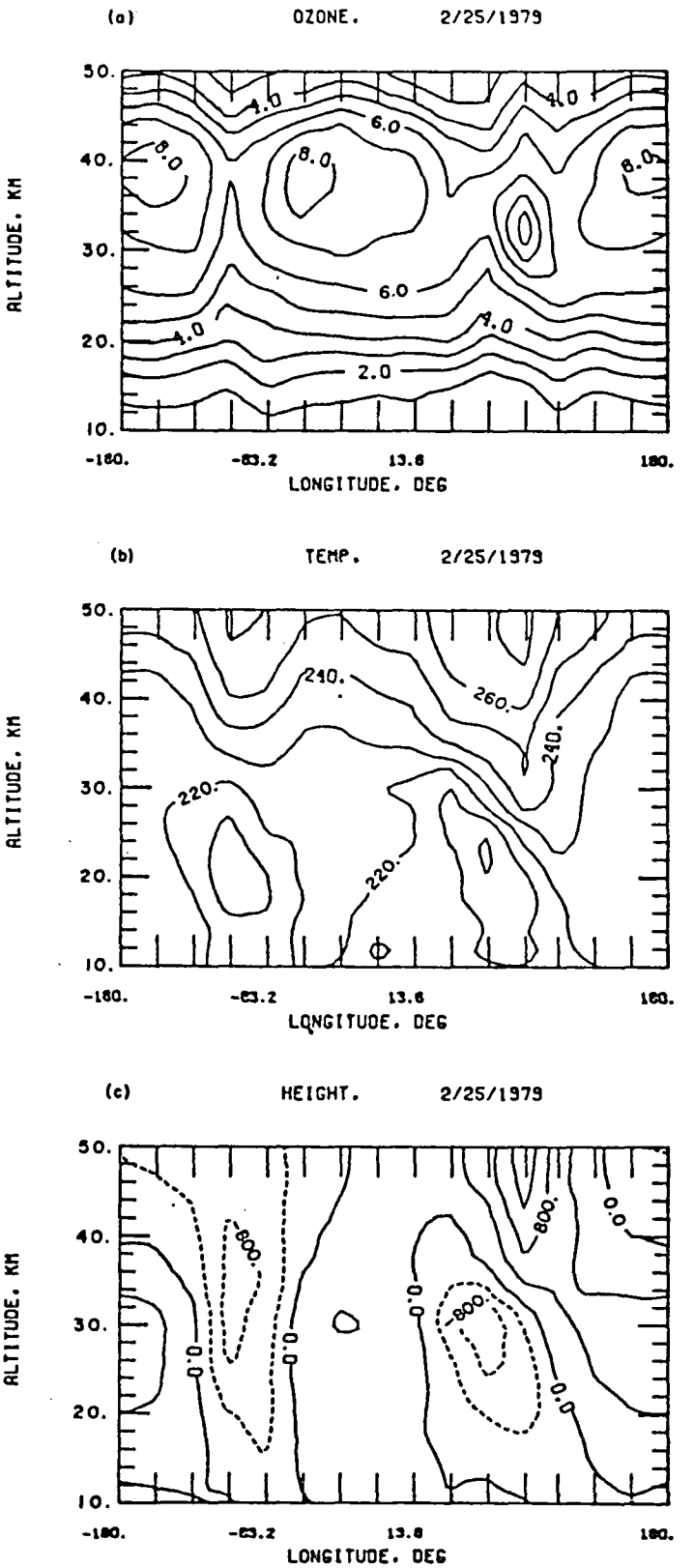

FIG. 5.1: Typical height-longitude distribution (~55°N) of (a) ozone mixing ratio, ppmv, contour interval 2 ppmv; (b) temperature, °K, contour interval 10°C; and, (c) height deviation, m, contour interval 400 m (February 25, 1979).

feature also allows us to apply a 3-day running-mean smooth procedure to the data set to suppress high frequency noise components. After this smoothing procedure, the Fourier analysis is carried out over the longitudinal circle for each of the deduced daily data sets, including ozone mixing ratio, temperature, and height deviation, for each day from February 23 to March 2. Due to the fact that there may be one or more of the SAGE measuring events missing in any day, we feel that it is appropriate to include only up to the third component in the harmonic analysis. Since the third wave component is generally smaller than the first two, we will discuss mainly the results of wavenumbers 1 and 2. The number of profiles and the averaged latitude of SAGE daily observations from February 23, 1979 to March 2, 1979, are given in Table 5.1. Note that the overall averaged latitude is about 55^{o}N; therefore, this is the latitude where the results of the analysis should be interpreted. Finally, the latitudinal velocities associated with the large-scale disturbances can be deduced from the harmonic components of the height field based on the geostrophic wind relationship. The determination of the zonally-averaged horizontal ozone transport across the latitude circle ($\sim 55^{o}$N) as a result of planetary waves is straight-forward. The results of the harmonic analysis and the calculated ozone transport are given in the next section.

5.3 RESULTS AND DISCUSSION

In this section, we show the results of the harmonic analysis of temperature, eddy meridional velocity, and ozone mixing ratio followed by a discussion of the results of the horizontal ozone and temperature transports by the planetary waves. In the last part of this section, the interpretation of the ozone and temperature transports will be given based on the phase relationships between the waves of temperature, eddy meridional velocity, and

TABLE 5.1: The number of profiles and the averaged latitude of SAGE observations from February 23 to March 2, 1979

Date	Number of Profiles	Averaged Latitude
Feb 23	14	52.43
Feb 24	14	53.71
Feb 25	15	54.74
Feb 26	11	55.57
Feb 27	14	56.35
Feb 28	14	56.93
March 1	14	57.33
March 2	15	57.54

the ozone mixing ratio.

A. Evolution of the Planetary Waves

The wave amplitudes of the first two harmonic components of the temperature as well as the zonal mean temperature, during the late February 1979 stratospheric warming are given in Figs. 5.2a to 5.2c, respectively. In the upper stratosphere, above 35 km, both components exhibit distinct amplifications of the waves from February 23 to 27, followed by a reduction of their strength during the remainder of the third warming pulse. The peak values for both waves take place at 42 km corresponding to February 28 and 26 for wavenumber 1 and 2, respectively. On these days, the upper stratosphere showed the third reversal of the meridional gradient of zonal mean temperature (Quiroz, 1979; see also Fig. 4.2). The maximum amplitude of 11.6°K of the temperature wavenumber 2 is slightly greater than that of wavenumber 1 (10.9°K).

Below altitude about 30 km, the behavior of these waves is more complex. Figure 5.2 shows that the temperature of wavenumber 2 was the dominant component and that it was declining during the entire late February 1979 warming. We have compared the results of the temperature waves 1 and 2 in the region below altitude 30 km (∿10 mb) with those of Quiroz (1979). In general, they show similar behavior during this third warming pulse even though Quiroz's (1979) analysis is applied to 65° N while ours is made at about 55° N (Table 5.1). In regard to the variation of zonally averaged temperature, Fig. 5.2c indicates that it increased slightly in the lower stratosphere below about 31 km, while it decreased in the upper stratosphere over the period of the third warming pulse.

Since the eddy meridional velocity field is directly related to the

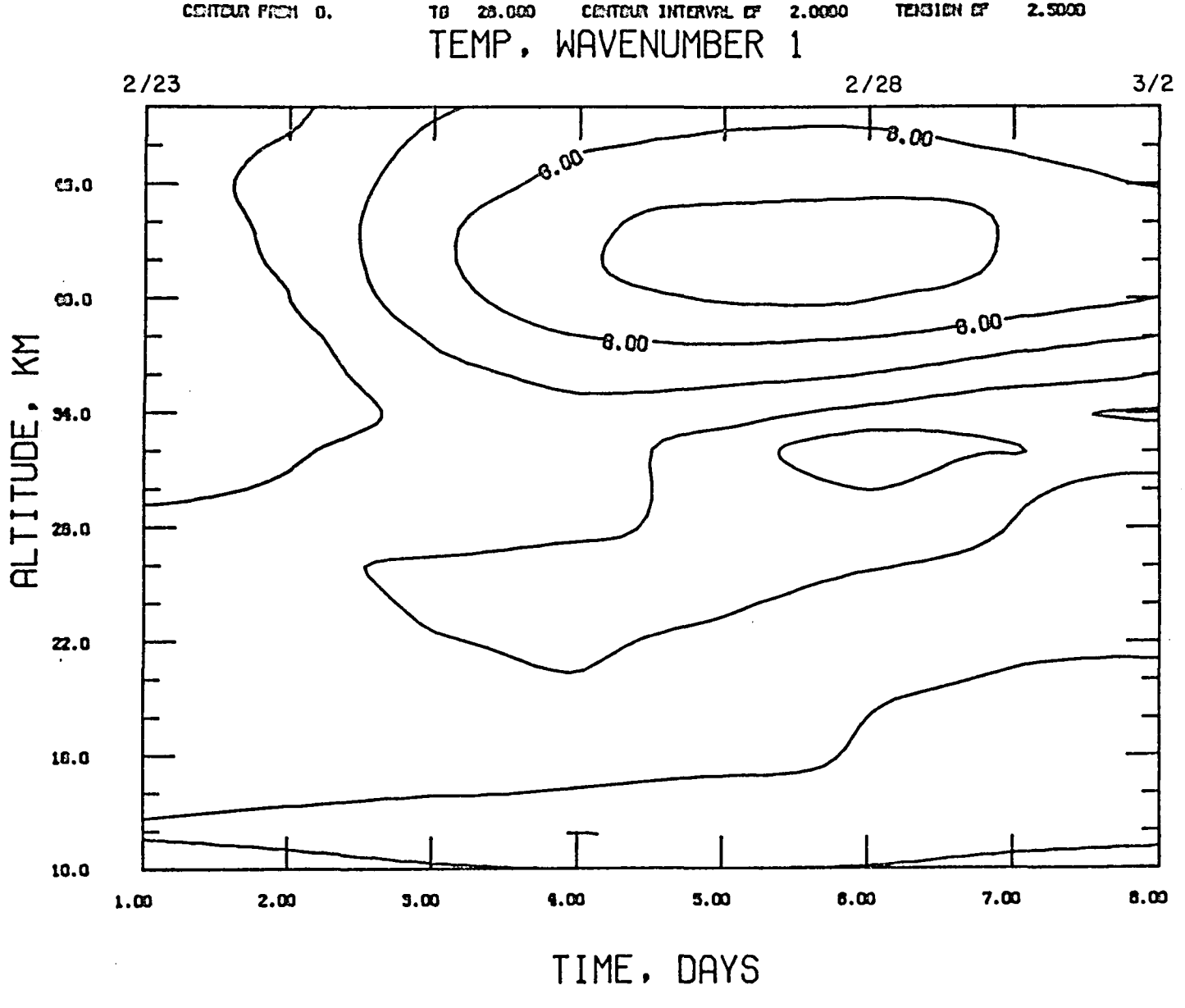

FIG. 5.2a: Evolution of the amplitudes, in unit ^{o}C, of the temperature wavenumber 1 during the late February 1979 warming (~55^{o}N). Contour interval 2^{o}C.

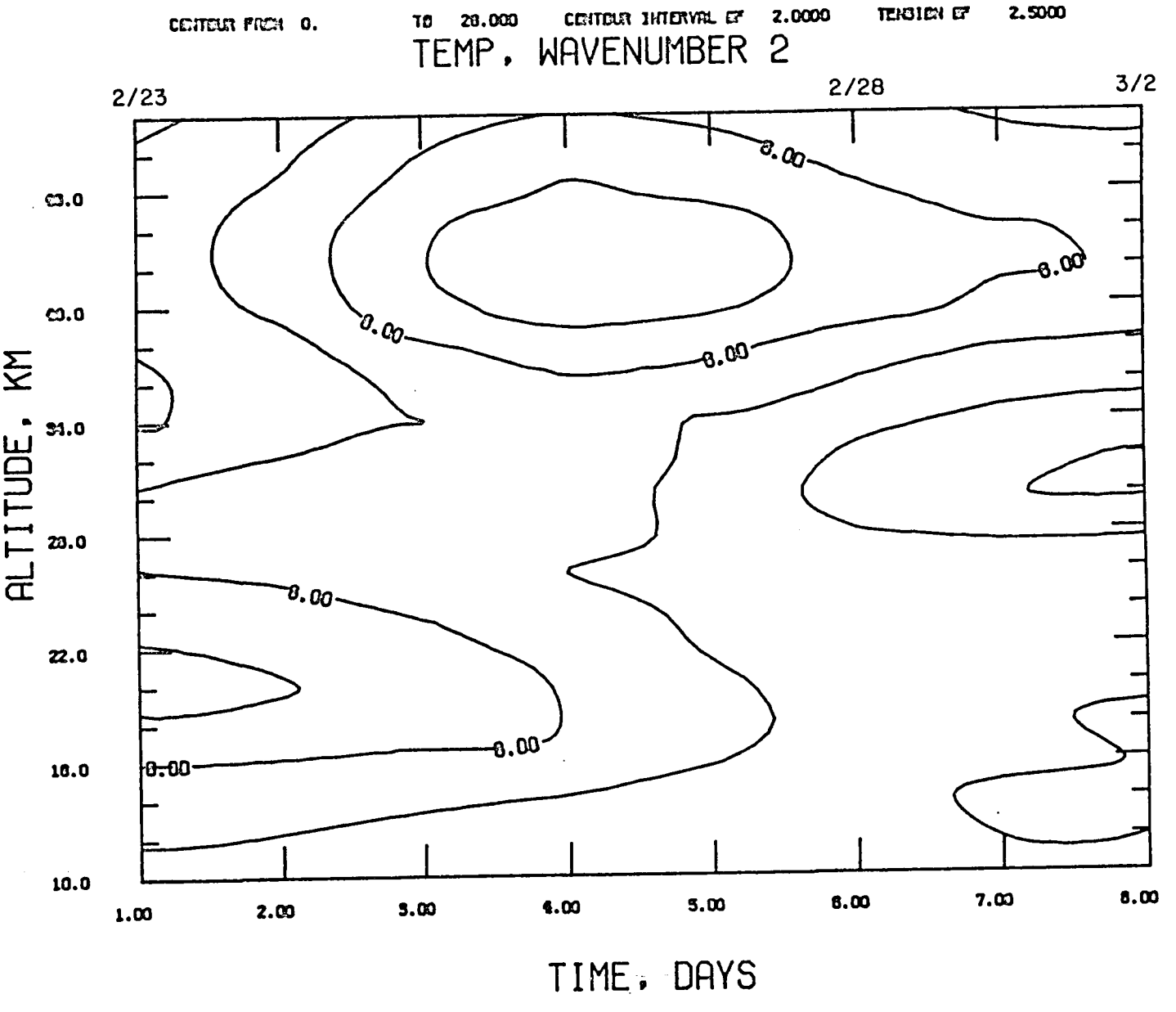

FIG. 5.2b: Evolution of the amplitudes (in unit ^{o}C) of the temperature wavenumber 2 during the late February 1979 warming (~55^{o}N). Contour interval 2^{o}C, zonal mean temperature, K^{o} (Contour interval 3^{o}C).

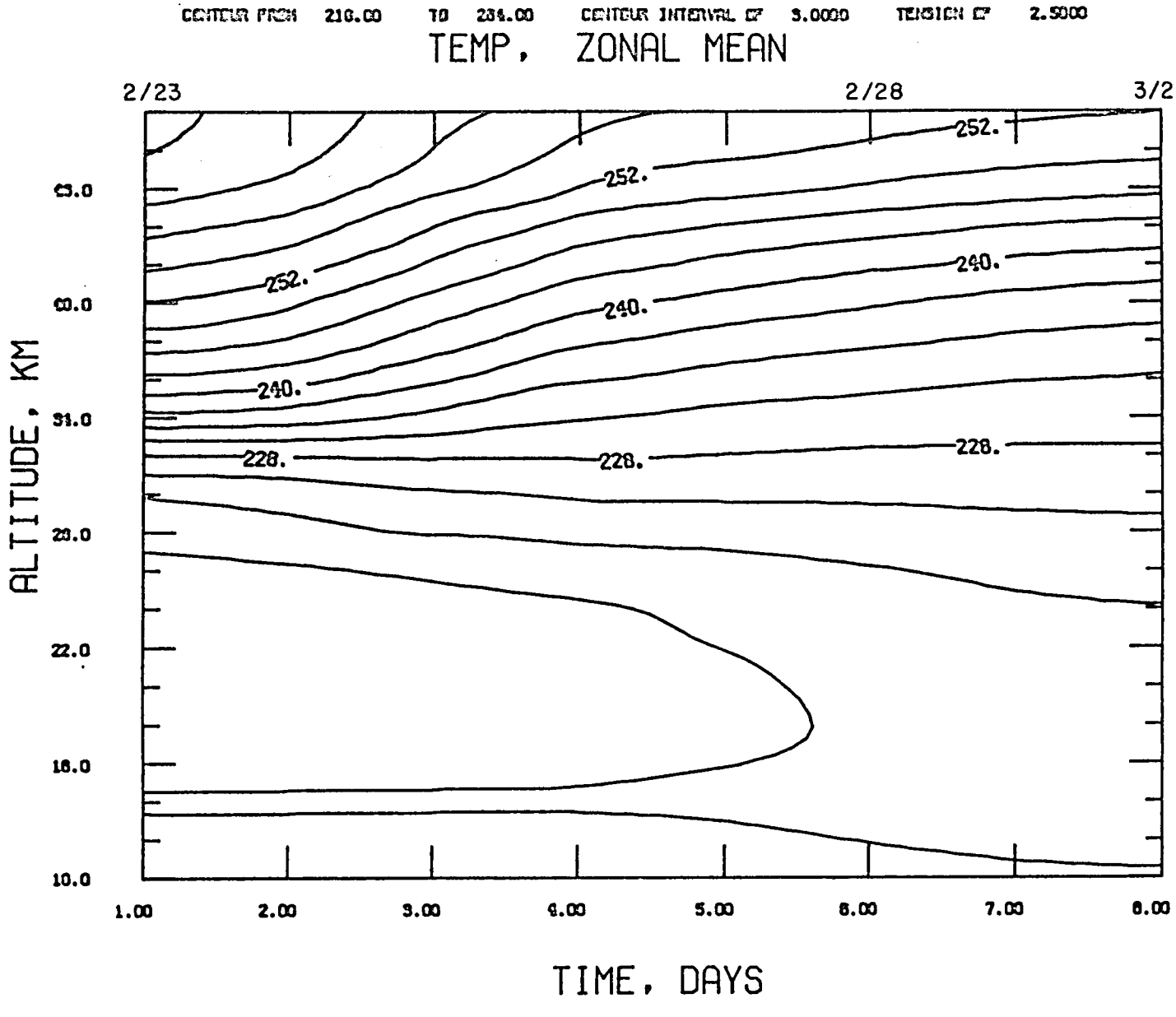

FIG. 5.2c: Evolution of the zonal mean temperature, K^{o} (contour interval $3^{o}C$) during the late February 1979 warming ($\sim 55^{o}N$).

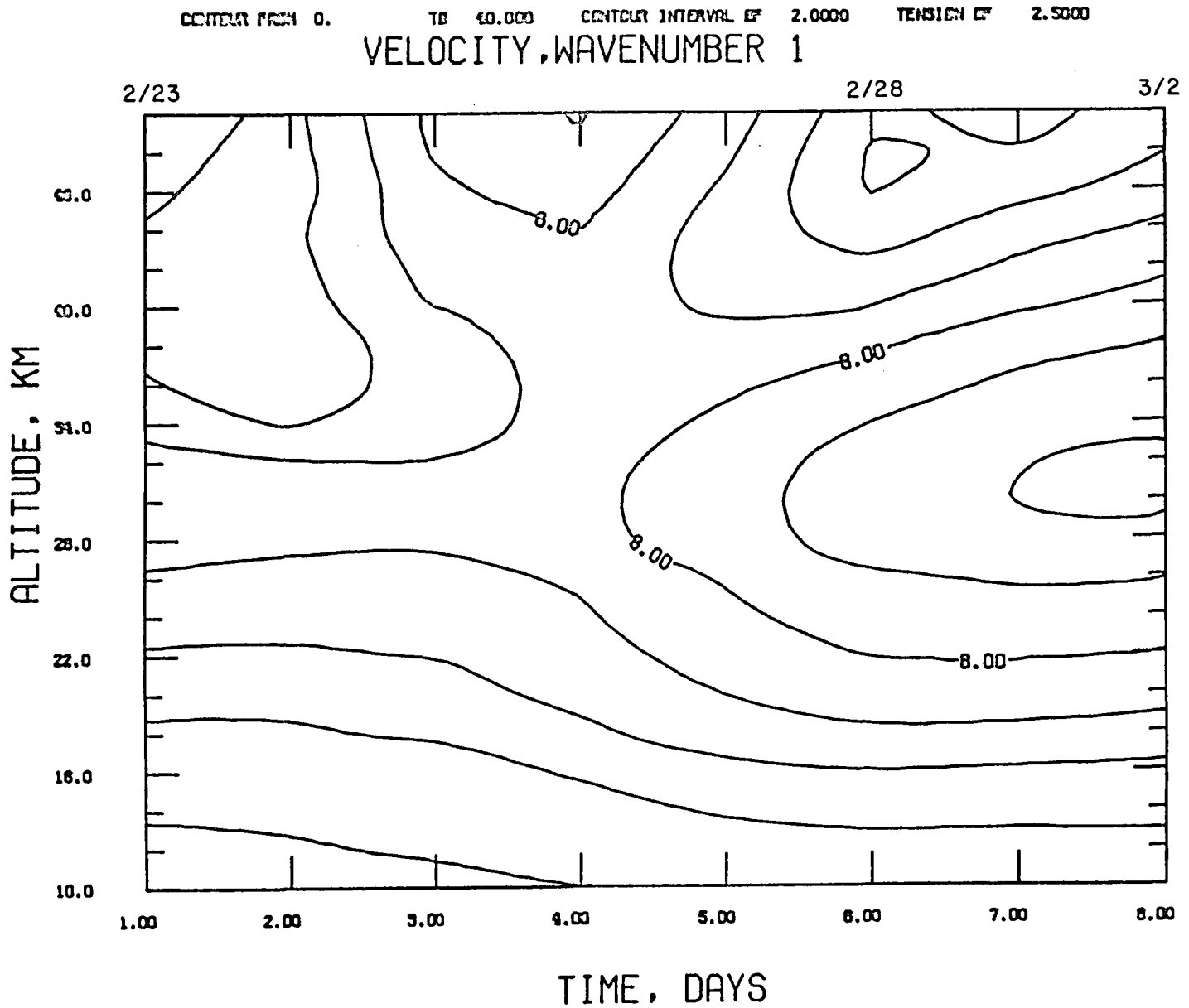

FIG. 5.3a: Evolution of the wavenumber 1 amplitudes (in unit m/s) of meridional velocity waves during the late February 1979 warming (~55°N). Contour interval 2 m/s.

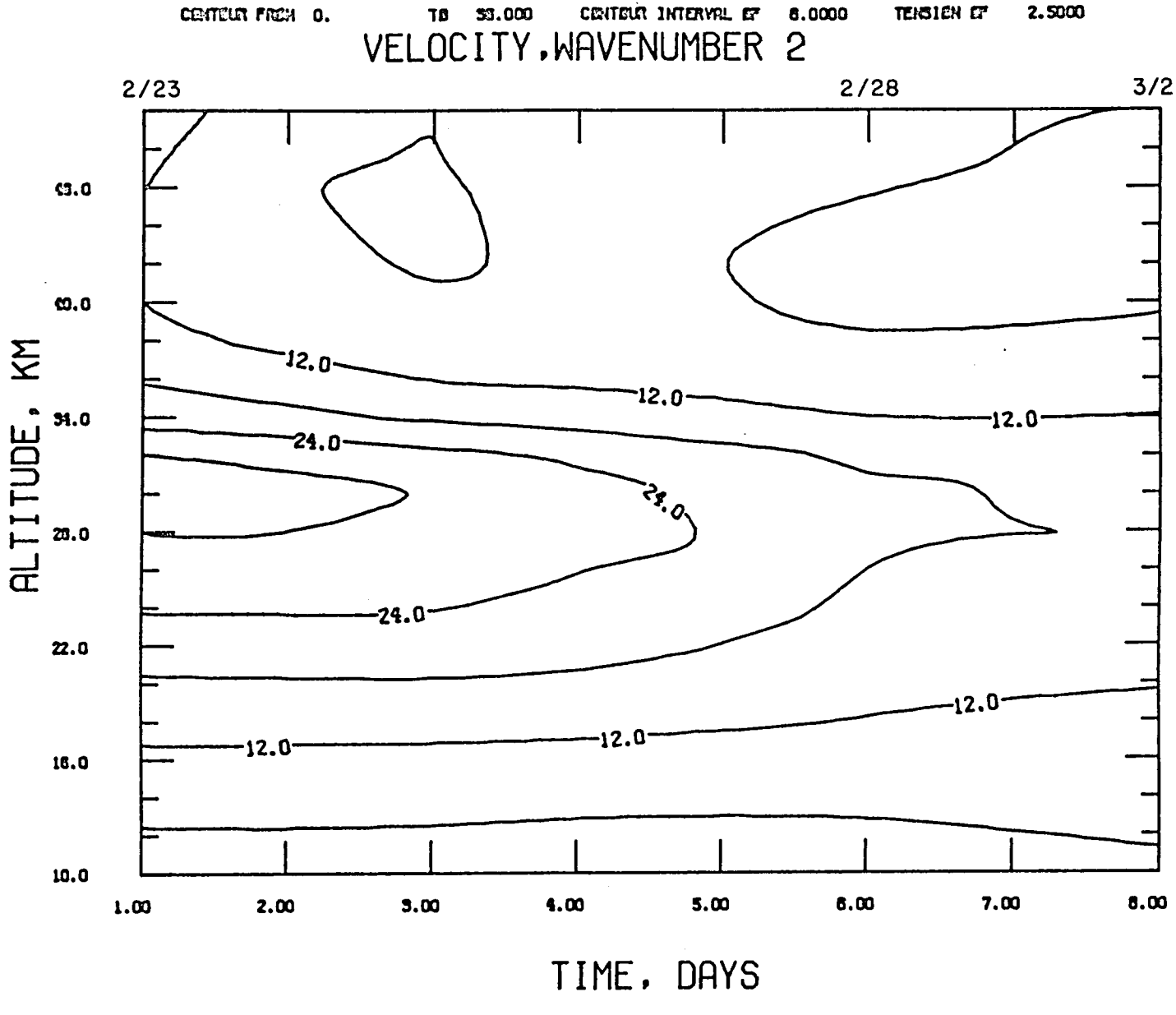

FIG. 5.3b: Evolution of the wavenumber 2 amplitudes (in unit m/s) of meridional velocity during the late February 1979 warming (~55°N). Contour interval 6 m/s.

height deviation field with only a $\pi/2$ phase difference, the features of the harmonic components of meridional eddy velocity discussed below apply equally well to that of height deviation except for the phase. The analyzed results of the first two harmonic components of the eddy meridional velocity are shown in Figs. 5.3a and 5.3b, respectively. The wave component 1 shows an intensification from February 26 to March 2 at altitudes between 24 and 42 km (Fig. 5.3a). On the other hand, the wavenumber 2 (Fig. 5.3b) exhibits a decline at these altitudes over the entire data period of this analysis. Quiroz (1979) has noted the intensive wavenumber 2 development beginning at about February 11. A maximum height amplitude of 1100 m at 10 mb took place around February 22. This is the first day of the SAGE experiment. Unfortunately, only seven SAGE profiles were measured in the northern hemisphere during that day. As a result, the data set for this analysis begins on February 23. Despite the difference in latitudes between Quiroz's (1979) analysis and ours, the wavenumber 2 shown in Fig. 5.3b exhibits a similar behavior as his over the same period in the lower stratosphere below about 30 km. Particularly, the peak of the eddy meridional velocity (height deviation) wavenumber 2 at 30 km appeared on February 23 (Fig. 5.3b) seems to be associated with the maximum height amplitude (1100 m) of wavenumber 2 in his analysis.

Figures 5.4a to 5.4c give the isolines of the first two harmonic components and the zonal mean of the ozone mixing ratio, respectively. Above altitude 34 km, wavenumber 1 exhibits an intensification from February 23 to 28, and it becomes declining afterward (Fig. 5.4a). A maximum amplitude of 1.5 ppmv appeared at 42 km on February 23. This evolution of ozone wavenumber 1 seems to be associated with that of the temperature

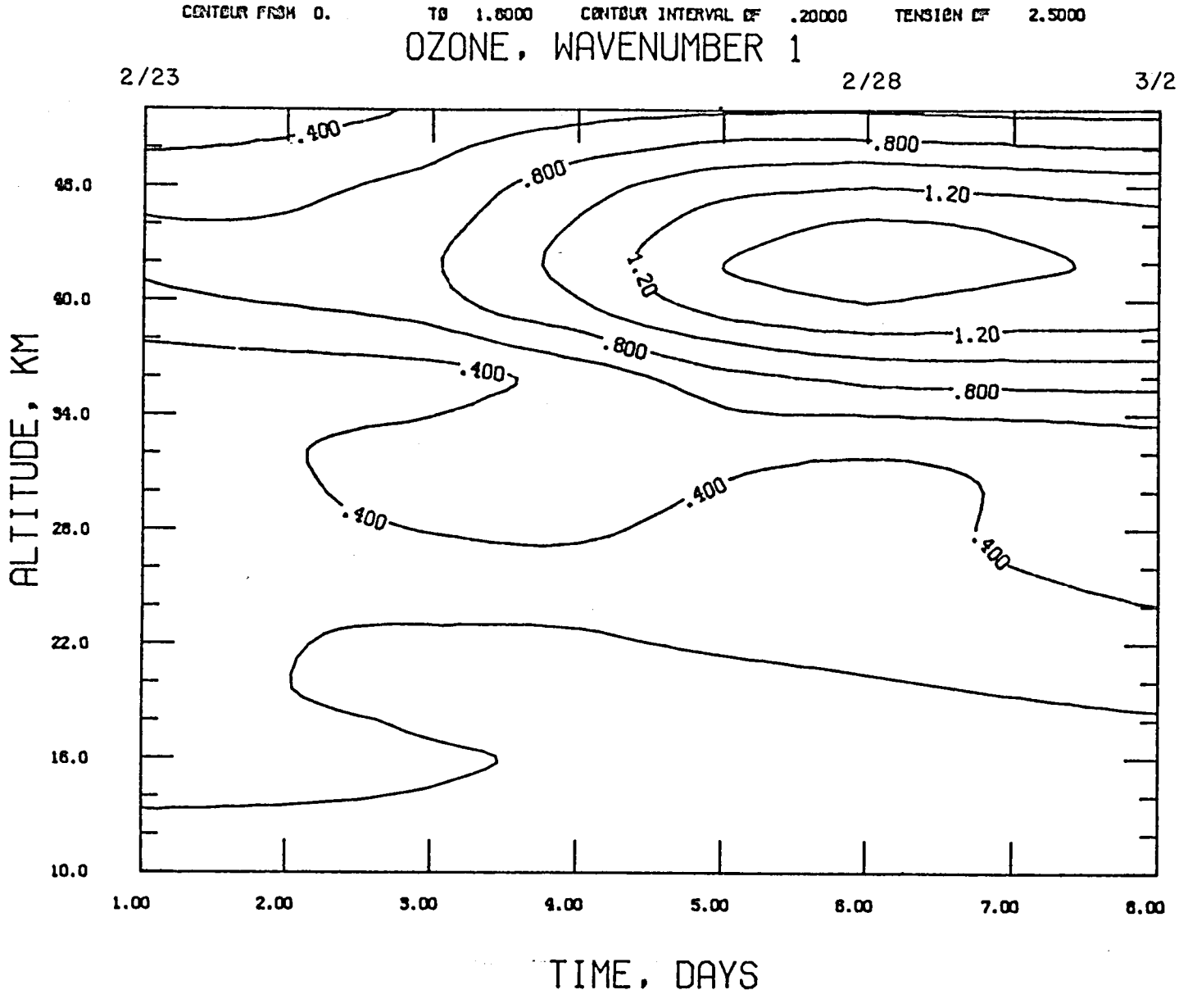

FIG. 5.4a: Evolution of the ozone wavenumber 1 amplitudes during the late February 1979 warming (in unit ppmv). Contour interval .2 ppmv.

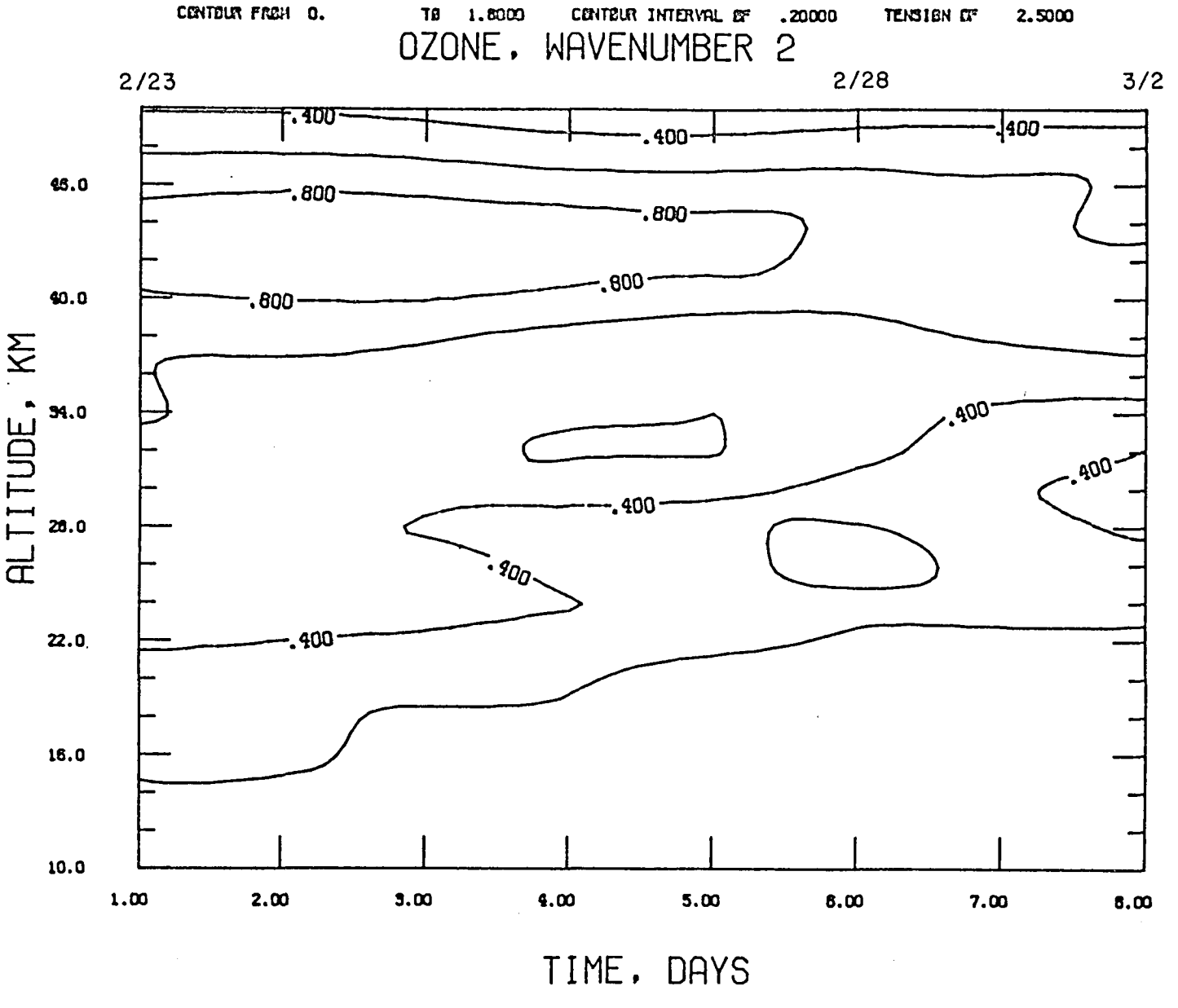

FIG. 5.4b: Evolution of the ozone wavenumber 2 amplitudes during the late February 1979 warming (in unit ppmv). Contour interval .2 ppmv.

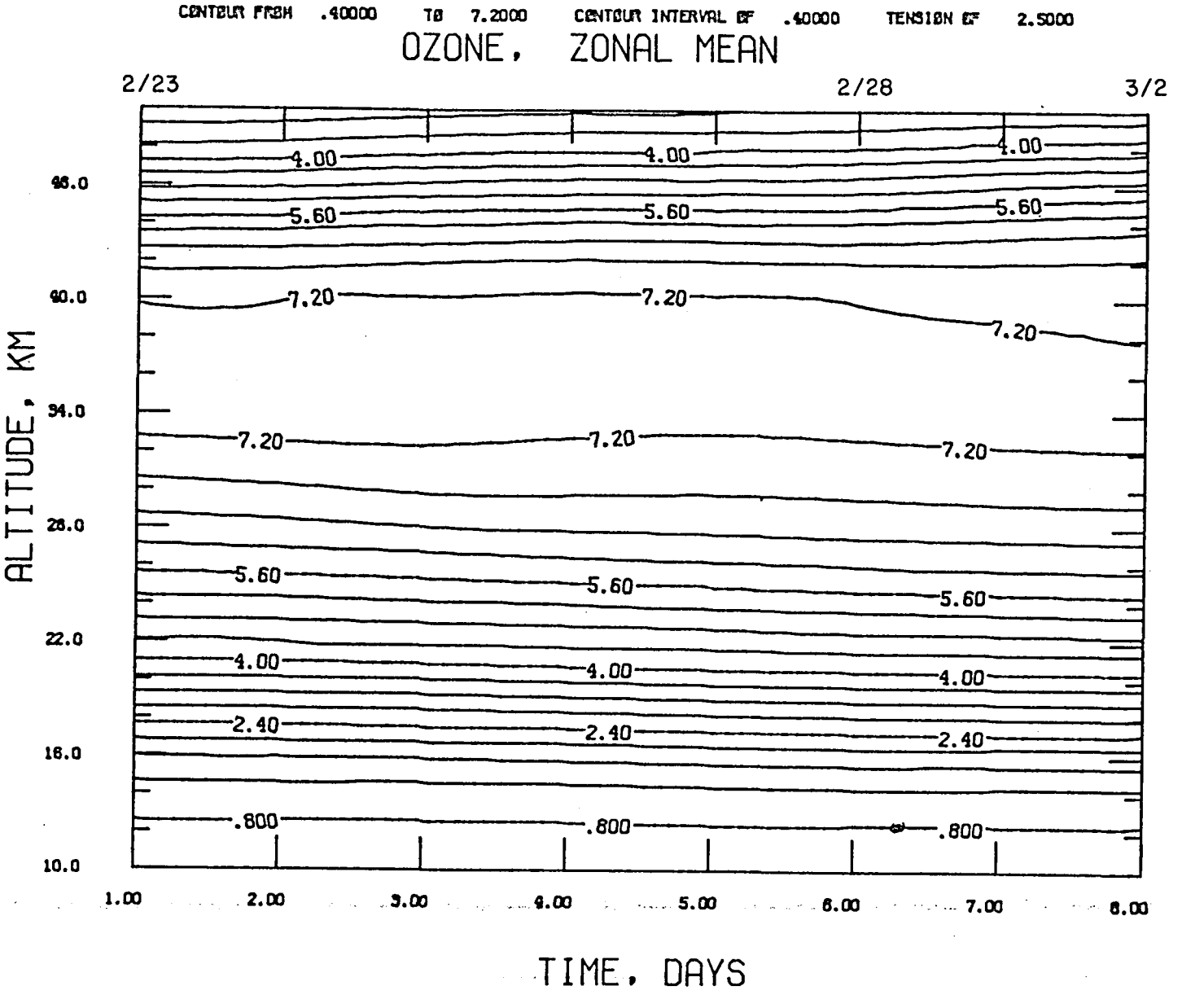

FIG. 5.4c: Evolution of zonal mean ozone during the late February 1979 warming (in unit ppmv). Contour interval .8 ppmv.

wave in the upper stratosphere as displayed in Fig. 5.2a; a feature that indicates the condition of photochemical control (Hartmann and Garcia, 1979, Eq. 13). In the lower stratosphere below about 30 km, ozone wavenumber 1 shows only mild variation. In the case of ozone wavenumber 2 (Fig. 5.4b), the wave is generally declining over the entire period of the third warming pulse except in the three layers centered at 16, 33, and 43 km. Within these layers, the wave exhibits slow intensification during the first 4 to 5 days of the analysis followed by the declining of the wave. Perhaps the development of an ozone wavenumber 2 centered at 43 km is related to that of thermal wavenumber 2 in the upper stratosphere (Fig. 5.2b). The behavior of zonal mean ozone profile (Fig. 5.4c) shows a rather slow increase of ozone mixing ratio below 30 km, and also above 40 km. There seems to be no significant variation of zonal mean ozone mixing ratio between 30 and 40 km during this warming.

Since the yearly variation of the surface total ozone is characterized by the so-called northern spring maximum in the high latitude northern hemisphere, it is interesting to investigate the temporal variation of the columnar ozone above 10 km during the late February 1979 warming. Figure 5.5a shows the evolution of the zonal mean ozone number density over this period. The mean ozone density exhibits a significant increase in the lower stratosphere (below 25 km). The increase near the peak of ozone density ($\sim$20 km) is particularly distinct. At 20 km, the mean ozone density is increased by $\sim$6 percent from February 23 to 28. Above 25 km, there seems to be no significant changes in ozone density. The associated change of columnar ozone above 10 km is given in Fig. 5.5b. It shows a monotonic increase over the data period as expected. This increase is

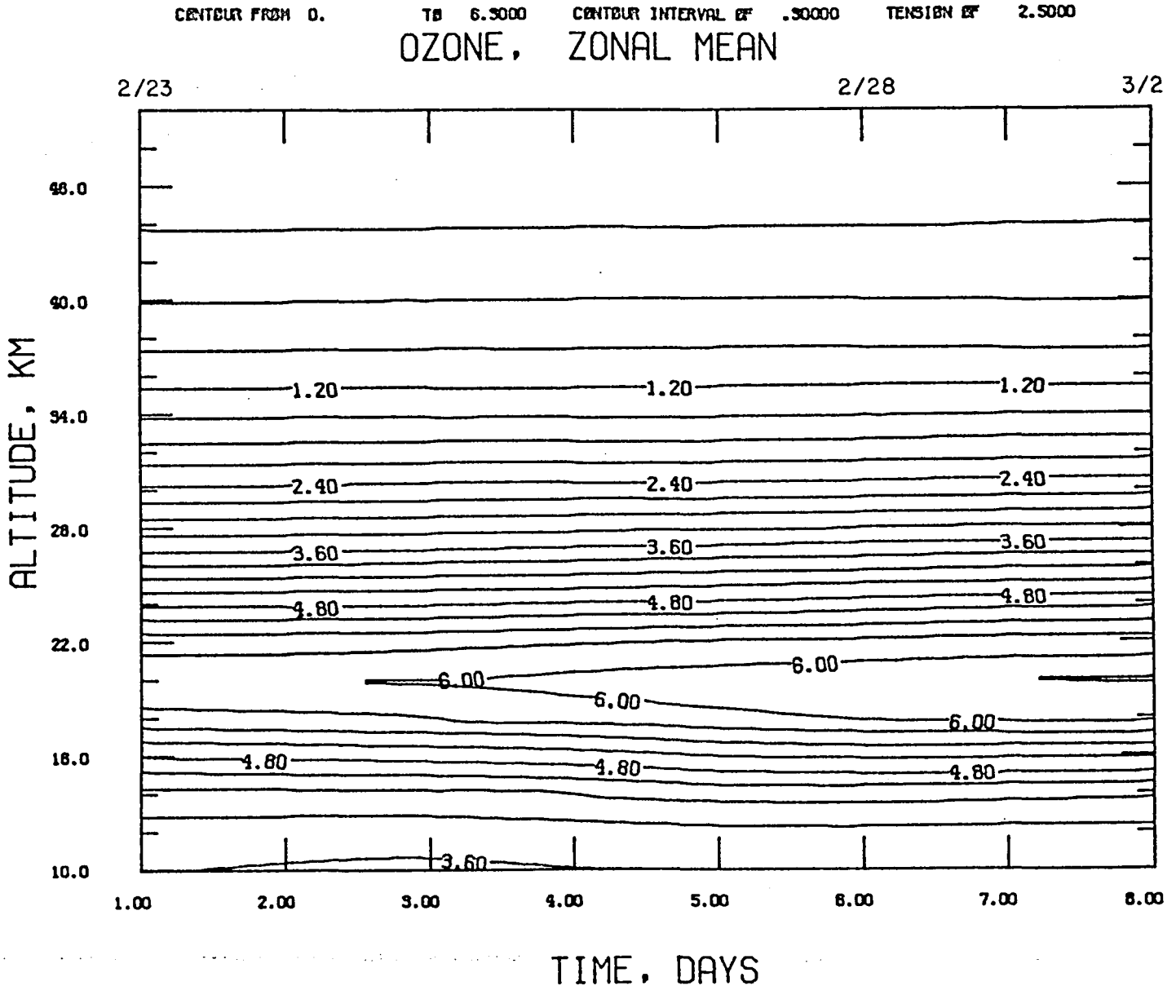

FIG. 5.5a: Evolution of zonal mean ozone number density during the late February 1979 warming (~55°N), contour interval .6, scaled by 10^{-12} in unit cm^{-3}.

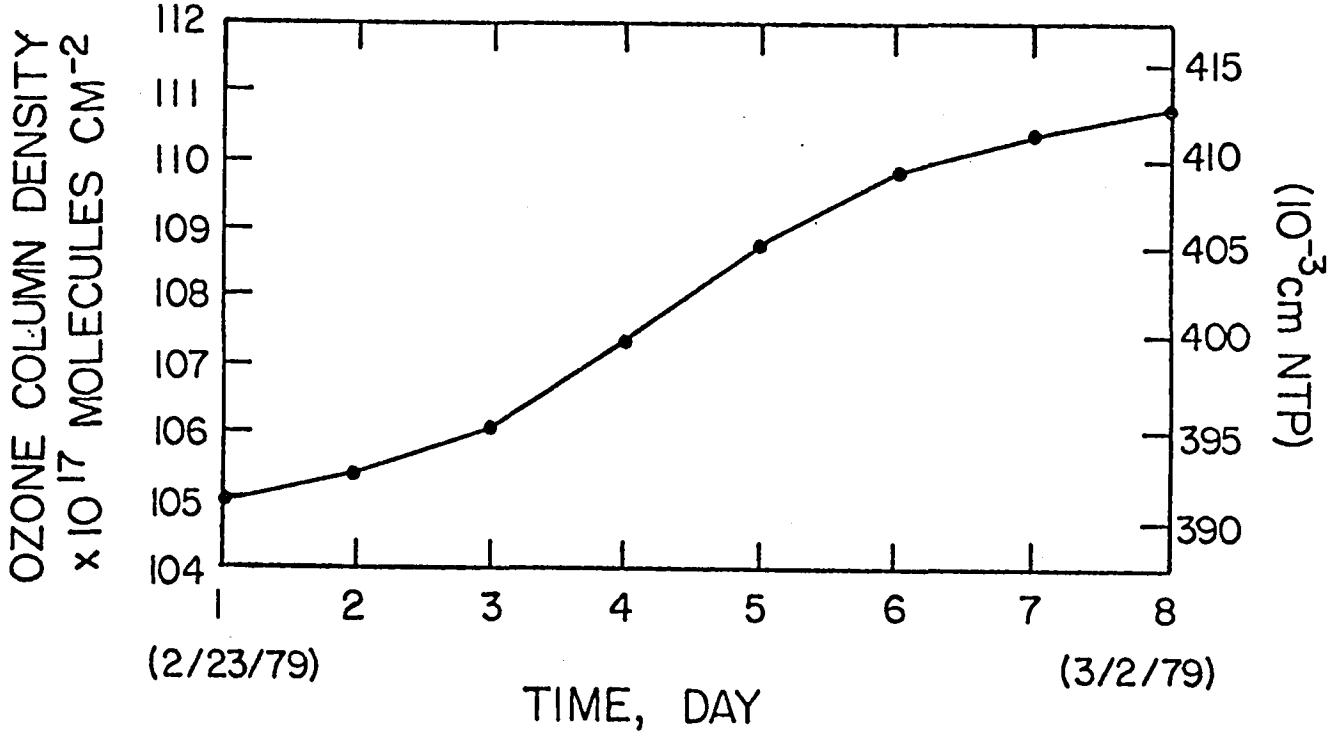

FIG. 5.5b: Time variation of ozone columnar density at altitude 10 km during the late February 1979 warming (~55°N).

primarily a response to the change of mean ozone density in the lower stratosphere as illustrated in Fig. 5.5a. Cunnold et al. (1980) have also indicated that the spring maximum in columnar ozone results from ozone variations below 40 mb (∿22 km) in their model calculation.

B. Horizontal Ozone and Temperature Transports by Planetary Waves

The behavior of the eddy ozone transport associated with the first two wave components is shown in Fig. 5.6. The distinct features of the wavenumber 1 component (Fig. 5.6a) above altitude 35 km are the development of the equatorward eddy ozone transport over the period from February 23 to 28, and the poleward transport afterwards. The situation below 35 km seems to be just the opposite; Fig. 5.6a shows the significant poleward eddy ozone transport from February 23 to 28 followed by the equatorward transport. In the case of wavenumber 2 (Fig. 5.6b), an intense poleward eddy ozone transport appeared in the middle stratosphere between approximately altitudes 25 and 36 km throughout the entire data period of this analysis. Above altitude ∿38 km, ozone was mainly transported to lower latitudes during the late February 1979 warming. The net ozone transport as a result of the first three waves is given in Fig. 5.6c. The behavior of this net ozone transport resembles very much that of wavenumber 2 since ozone transport due to wavenumber 2 is predominant. As one may notice, an intense poleward transport occurred in the middle stratosphere centered at altitude 30 km from February 23 to 27. This center shifted to a higher altitude (∿38 km) by March 2. At approximately 32 km altitude, a maximum poleward eddy ozone transport of 9.9 (ppm ms^{-1}) occurred on February 24. Figure 5.6c also shows the development of an equatorward eddy ozone transport centered at 45 km. The maximum equatorward transport

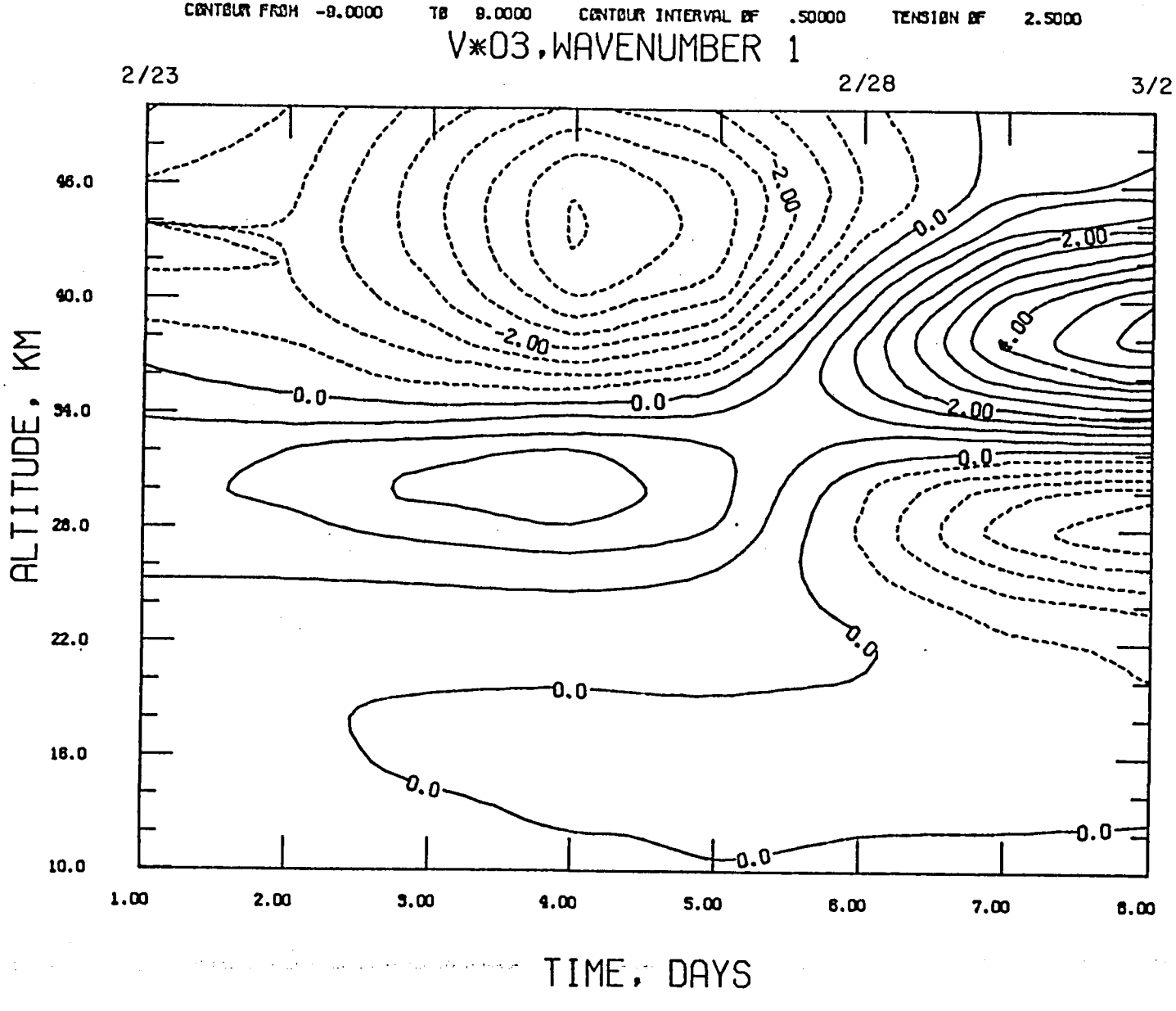

FIG. 5.6a: Time variations of eddy ozone flux, in unit ppm ms^{-1}, due to wavenumber 1, contour interval 1 ppm ms^{-1}.

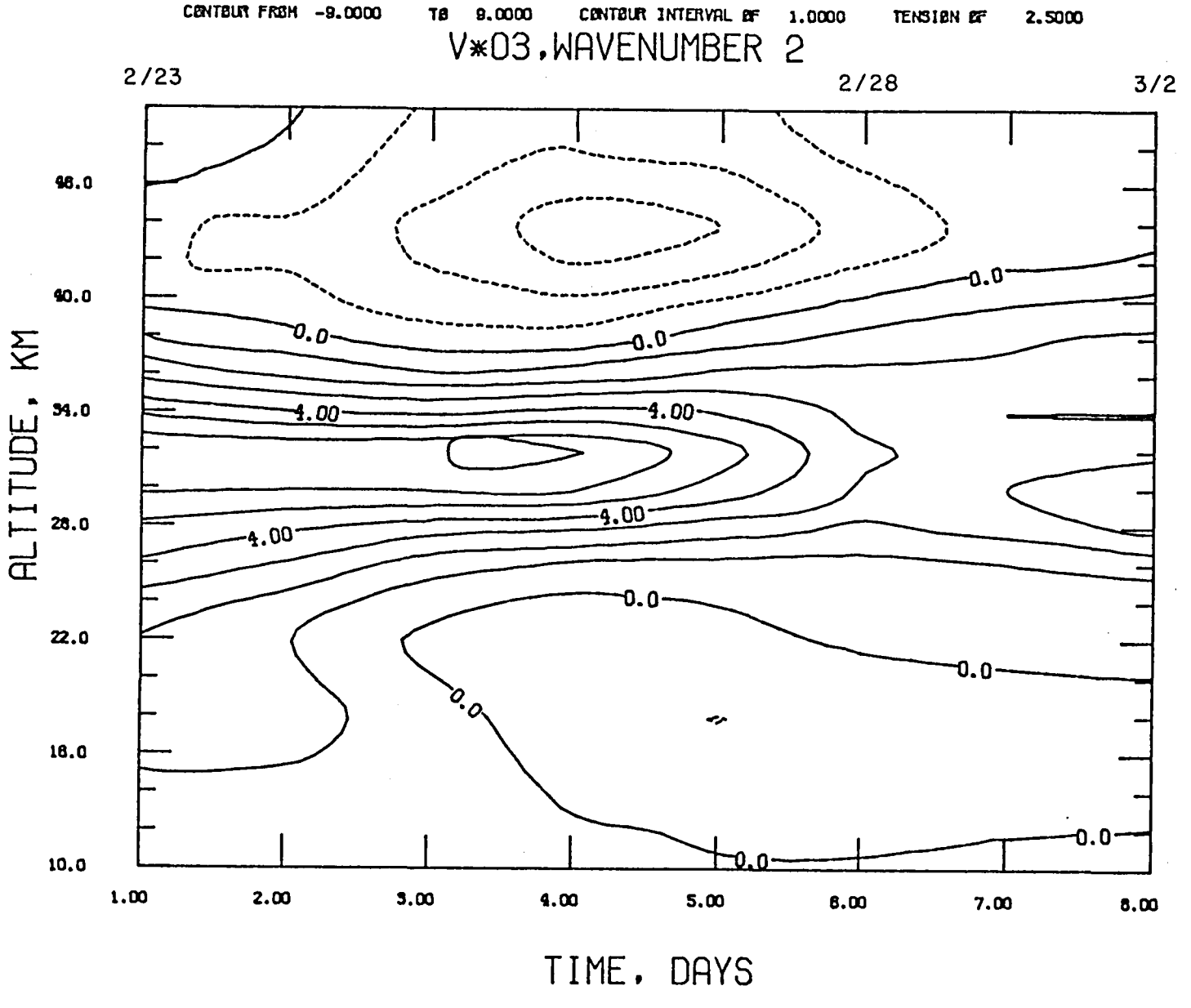

FIG. 5.6b: Time variations of eddy ozone flux, in unit ppm ms^{-1}, due to wavenumber 2, contour interval 2 ppm ms^{-1}.

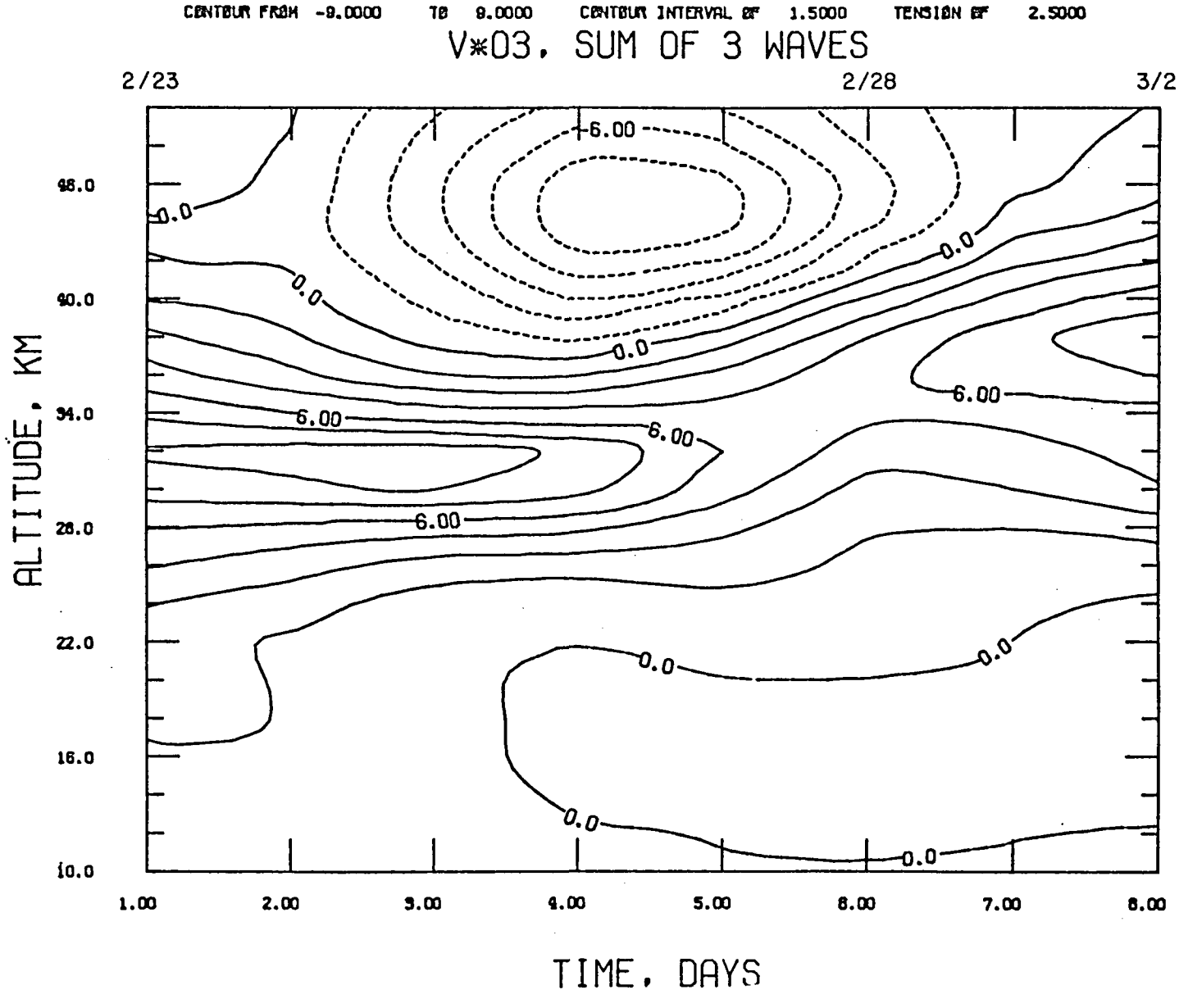

FIG. 5.6c: Time variations of eddy ozone flux (sum of the first three waves) in unit ppm ms^{-1}. Contour interval 3 ppm ms^{-1}.

is 8.6 (ppm ms^{-1}) appeared on February 26. Below altitude 24 km, Fig. 5.6c indicates that the transport is much smaller than those in the regions above.

Since the major contribution to the SAGE derived ozone column changes comes from the lower stratosphere as illustrated in Fig. 5.5a, it is of interest to investigate the eddy ozone mass transport during this time period. The eddy ozone mass transport associated with the first two wave components is illustrated in Fig. 5.7. The characteristics of the ozone mass transport induced by wavenumber 1 and 2 are similar to those exhibited by the ozone mixing ratio transport as in Fig. 5.6. They show the predominant wavenumber 2 activity which is found to be responsible for the intense poleward transport in the middle stratosphere. For example, on the third day (February 25) during the maximum of transport activities, $(1.12\pm.04)\times10^{20}$ (molecules/cm^2) x (m/sec) of integrated mass flux of ozone was transported poleward in the lower stratosphere (10 to 30 km altitude) as deduced from the data. However, this horizontal eddy mass transport cannot account totally for the ozone column changes at 55^{o} because it is not the entire ozone transport effect of the planetary waves. There are also those due to wave-induced meridional circulation and vertical eddies. Unfortunately, the investigation of the latter contributions is hampered by lack of sufficient data. Nevertheless, the mean and eddy cancellation for tracers is particularly incomplete and a net transport of ozone may occur as a result of planetary waves during stratospheric warmings (Mahlman and Moxim, 1978).

It has been recognized that eddy heat transport plays a significant role in stratospheric warmings (Holton, 1975). As indicated in Section 5.1, in the upper stratosphere equatorward/poleward eddy ozone

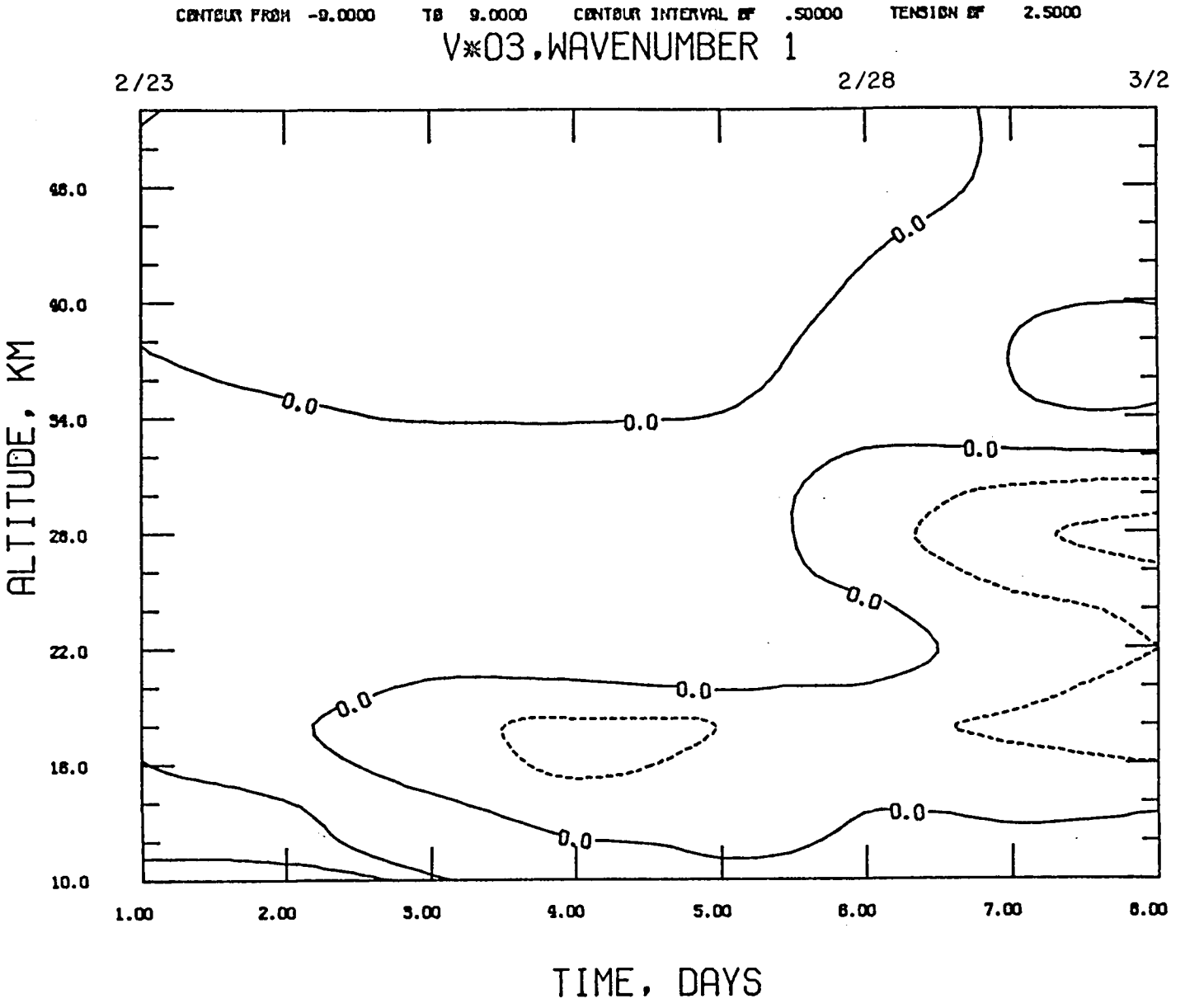

FIG. 5.7a: Time variations of eddy ozone mass transport, in unit molecule cm^{-3} ms^{-1}, due to wavenumber 1, contour interval .5 molecule cm^{-3} ms^{-1}. Scaled by 10^{-12}.

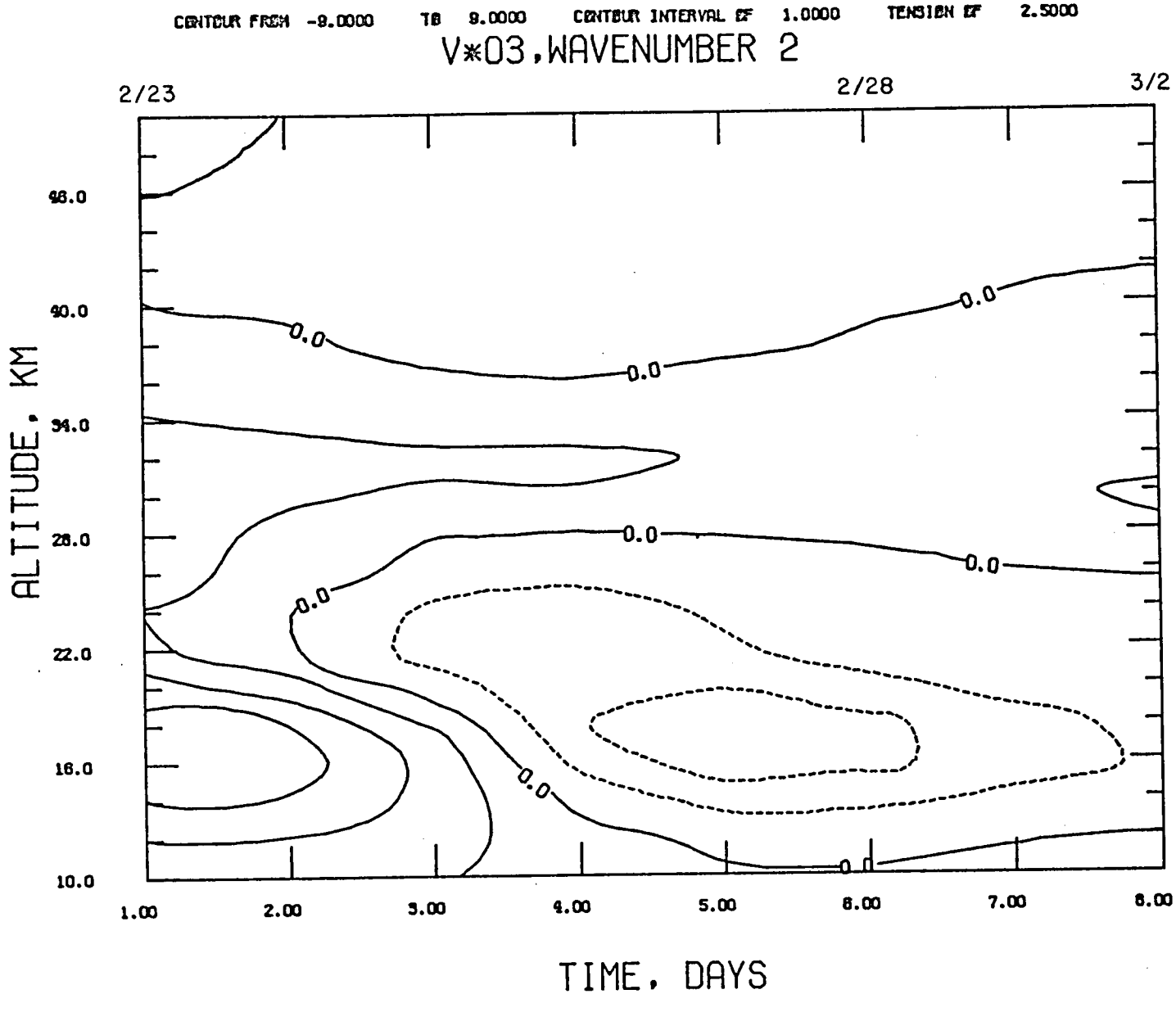

FIG. 5.7b: Time variations of eddy ozone mass transport, in unit molecule cm^{-3} ms^{-1}, due to wavenumber 2, contour interval 1. Molecule cm^{-3} ms^{-1}. Scaled by 10^{-12}.

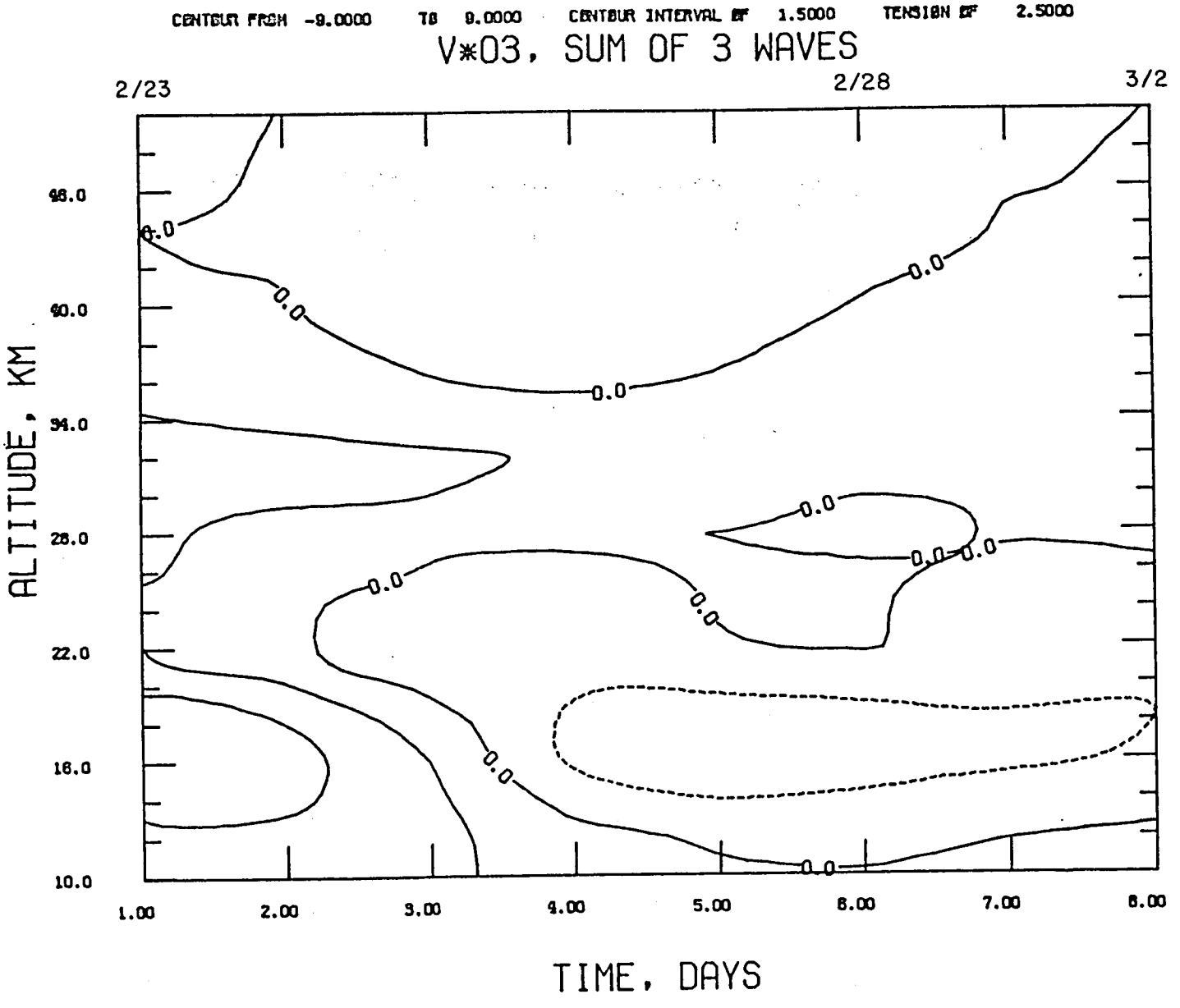

FIG. 5.7c: Time variations of eddy ozone mass transport (sum of the first three waves) in unit molecule cm^{-3} ms^{-1}. Contour interval 1.5 molecule cm^{-3} ms^{-1}. Scaled by 10^{-12}.

transports are expected to be associated with poleward/equatorward eddy heat transports because of the negative correlation between ozone and temperature due to ozone photochemistry. To examine this feature, the calculated results of eddy heat transports due to wavenumber 1 and 2 are given in Figs. 5.8a and 5.8b, respectively. Noticeable features of wavenumber 1 development (Fig. 5.8a) are the poleward eddy heat transport centered at 42 km peaked on February 26, and the equatorward transport centered at 28 km beginning on February 28. Note also the reversal of the transport occurred just before March 1 above 38 km. By inspecting the wavenumber 1 of ozone and temperature eddy transports, it is found that the behavior of the eddy ozone and heat transports above $\sim$35 km altitude is indeed closed to the expected feature just discussed. Especially, the date and altitude of the development of the maximum center of the equatorward eddy ozone transport are found to be coincident with that of the poleward heat transport in this particular event. In addition, the reversals of the transport direction of both the eddy ozone and heat transports above 38 km seem to take place between days six and seven. For wavenumber 2, Fig. 5.8b shows the poleward eddy heat transport in the entire altitude region from 10 to 50 km during this late February 1979 warming. In particular, an intense poleward eddy heat transport occurred between 20 and 32 km, with a maximum centered at 30 km on February 25. Above 38 km, Fig. 5.8b also shows the development of a local maximum center of the poleward transport at approximately 44 km on February 26. Perhaps this development was related to that of the equatorward eddy ozone transport above $\sim$38 km (Fig. 5.6b). The net eddy heat transports due to the first three waves are displayed in Fig. 5.8c. It shows an intense poleward eddy heat transport between altitudes 22 and 32 km with the peak centered

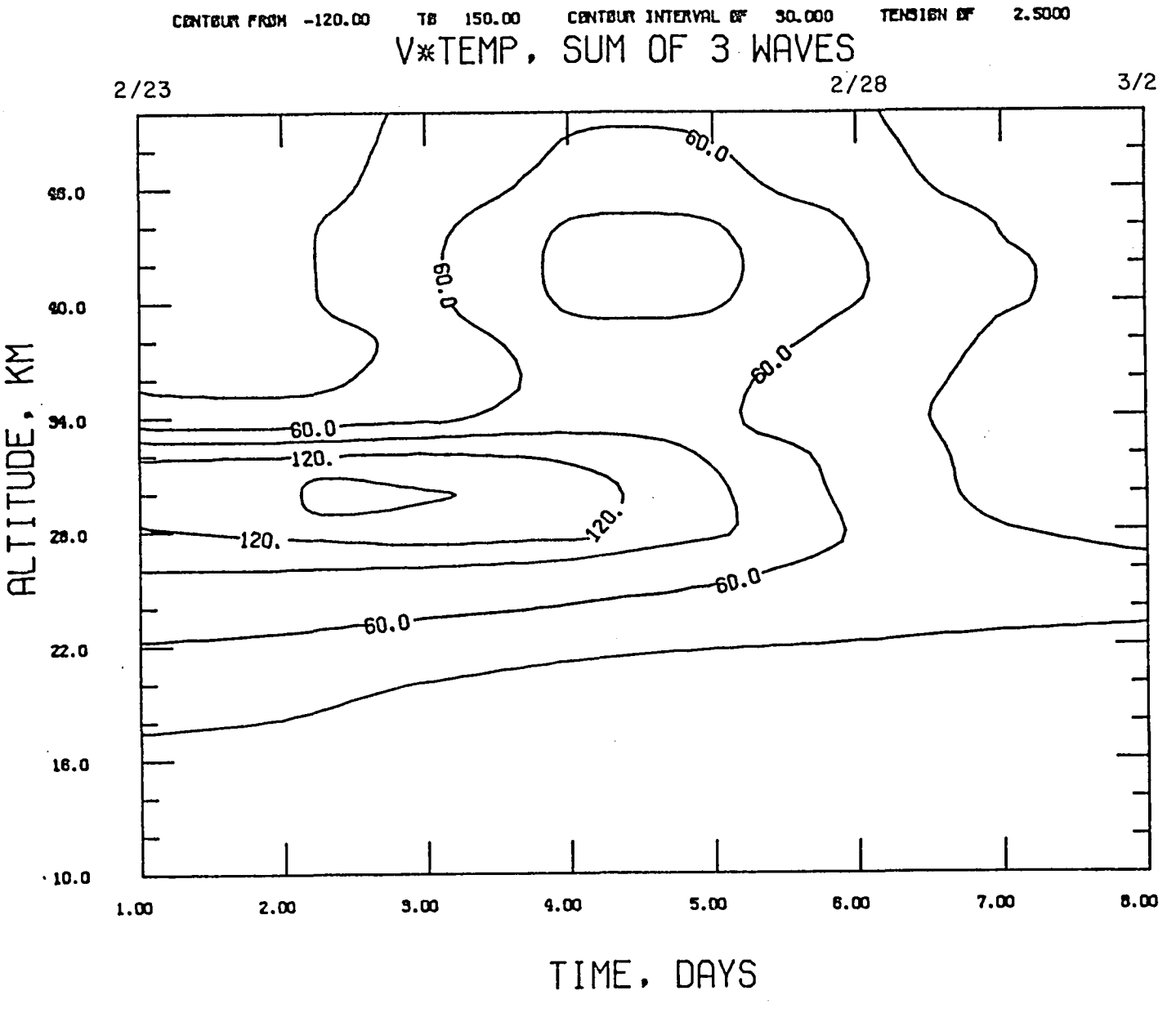

FIG. 5.8c: Time variation of eddy heat flux, sum of the first three waves, contour interval 30°C ms^{-1}, in unit °K ms^{-1}.

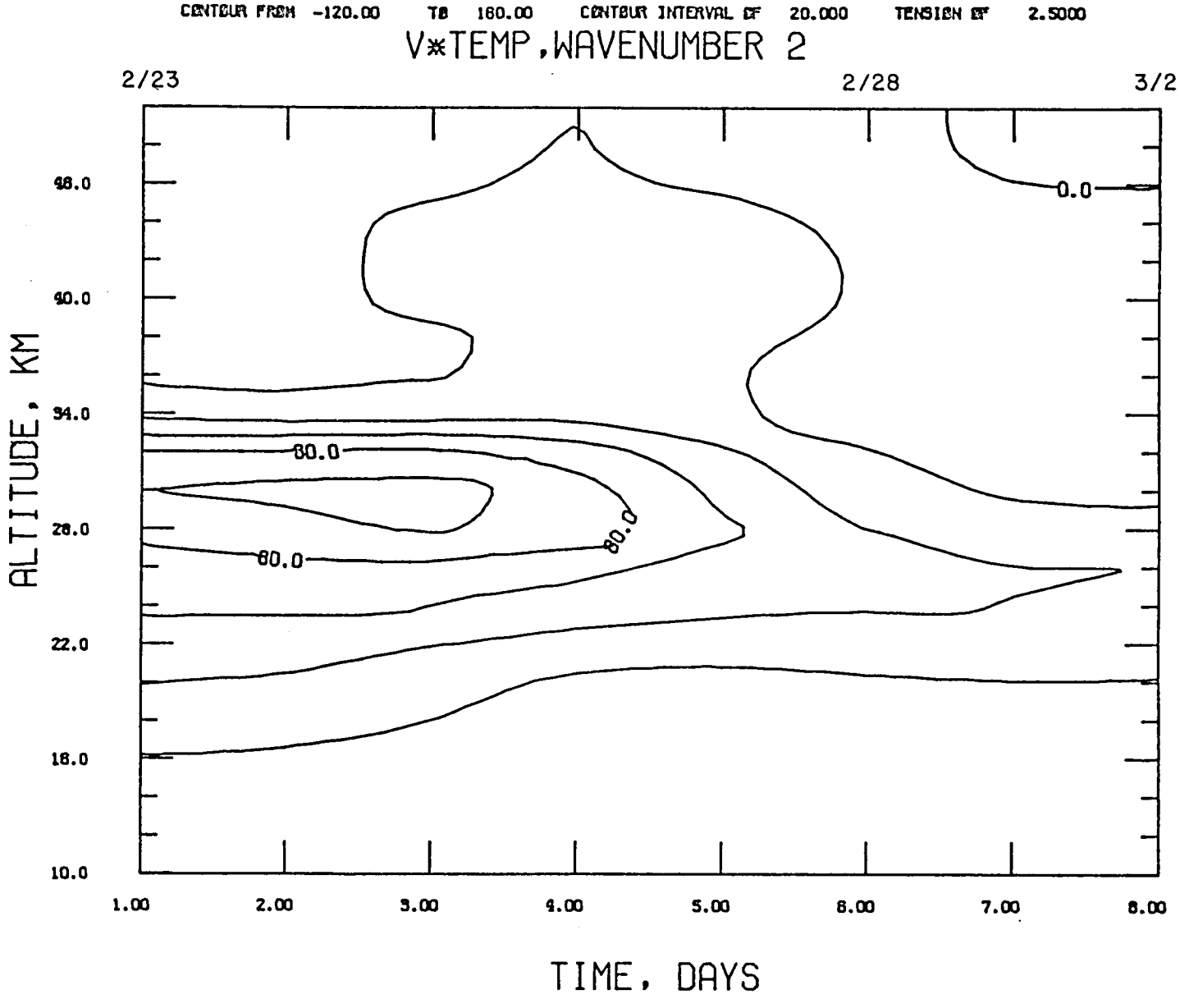

FIG. 5.8b: Time variation of eddy heat flux, wavenumber 2, contour interval 20°C ms^{-1}, in unit °K ms^{-1}.

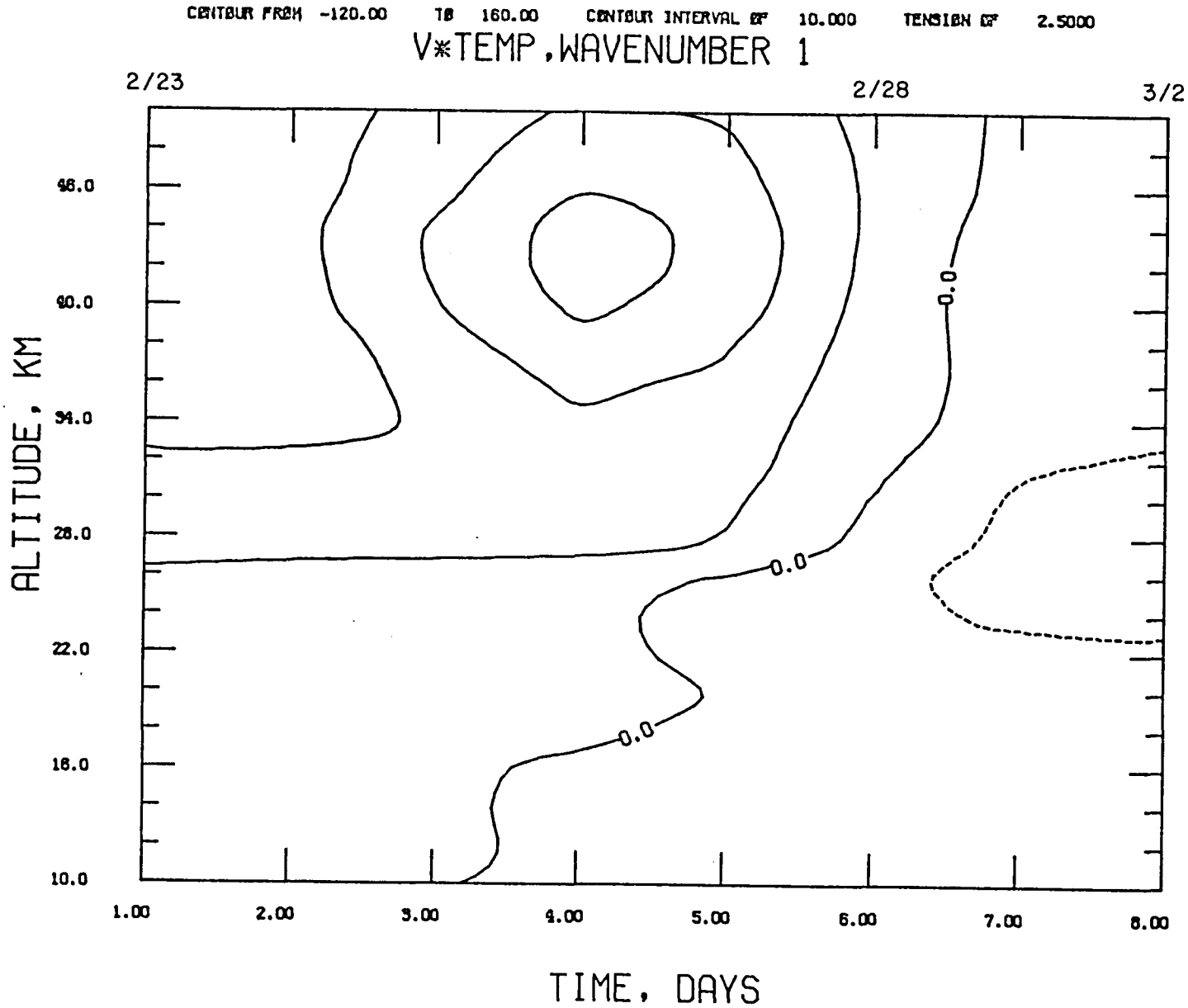

FIG. 5.8a: Time variation of eddy heat flux, wavenumber 1, contour interval 10°C ms^{-1}, in unit °K ms^{-1}.

at 30 km. The maximum of this poleward transport took place approximately on February 24. Above altitude ∿38 km, one can also find significant poleward eddy heat transport from February 25 to 28. These were the days that significant equatorward eddy ozone transports took place above ∿38 km, and that the stratosphere shows intense warming in high latitudes.

C. Analysis in Terms of Phase Relationship Between the Eddy Fields

As mentioned in Chapter 3, in the midlatitude below about 25 km (15 to 25 mb), the ozone distribution is mainly controlled by dynamical processes while photochemical reactions play a decisive role in determining ozone concentrations above 35 km. The relative importance of the dynamical and photochemical processes in determining ozone concentration can be simply estimated based on their relaxation effects on the ozone perturbations. It should be noted that the relaxation concept does not concern primarily the origin and development of the disturbances. However, in reality, especially during winter and spring equinox, the stratosphere is characterized by activities of large scale eddies, which are believed to be responsible for the northward transport of O_3 and the distinct spring total ozone buildup in the northern hemisphere. There is no doubt that the development of these large-scale disturbances in the stratosphere are related intimately to the meteorological activities in the troposphere. As mentioned in Chapter 3, ozone and temperature perturbations will show an out-of-phase relationship in the photochemically controlled region and an in-phase relationship in the dynamically controlled region in response to the forced disturbances at the lower boundary. Consequently, there is a shift of the phase relationship between ozone and temperature perturbations from dynamical controlled region to photochemically controlled region. This shift in the phase relationship

between ozone and temperature may lead to an in-phase relationship between ozone perturbation and eddy meridional velocities at certain levels in the transition region and results in a large poleward ozone transport. Recently, Hartmann and Garcia (1979) have investigated this development in the form of wavenumber 1 and also wavenumber 3 by introducing a large scale disturbance at their model lower boundary, and have discussed the potential importance of phase relationships between planetary waves of stratospheric ozone, temperature, and meridional eddy velocity in ozone transport, especially in the transition region (see also Kawahira, 1982). In this section, we will examine these phase relationships for the late February 1979 warming based on SAGE measurements and meteorological information, and compare the results with that of the model analyses (Hartmann and Garcia, 1979; Kawahira, 1982) and the observed phase results on November 1, 1975, at 60° N (Gille et al., 1980).

The evolution of the phases of ozone mixing ratio (solid line), temperature (dashed line), and meridional velocity (solid and dashed line) for wavenumber 1 on February 25, 1979, is given in Fig. 5.9a. The horizontal bars are the computed uncertainty of the calculated phase based on the given uncertainty of the SAGE and meteorological data. Ozone and temperature perturbations indeed show a nearly in-phase relationship in the lower stratosphere between about 18 km and 30 km. Above approximately altitude 35 km, the ozone and temperature waves are approximately out-of-phase. These results suggest that the ozone in the upper stratosphere (above 35 km) is under photochemical control, and is determined by dynamical processes below altitude ∿30 km. A transition region seems to exist between approximately 30 and 35 km. This region is much thinner than the one

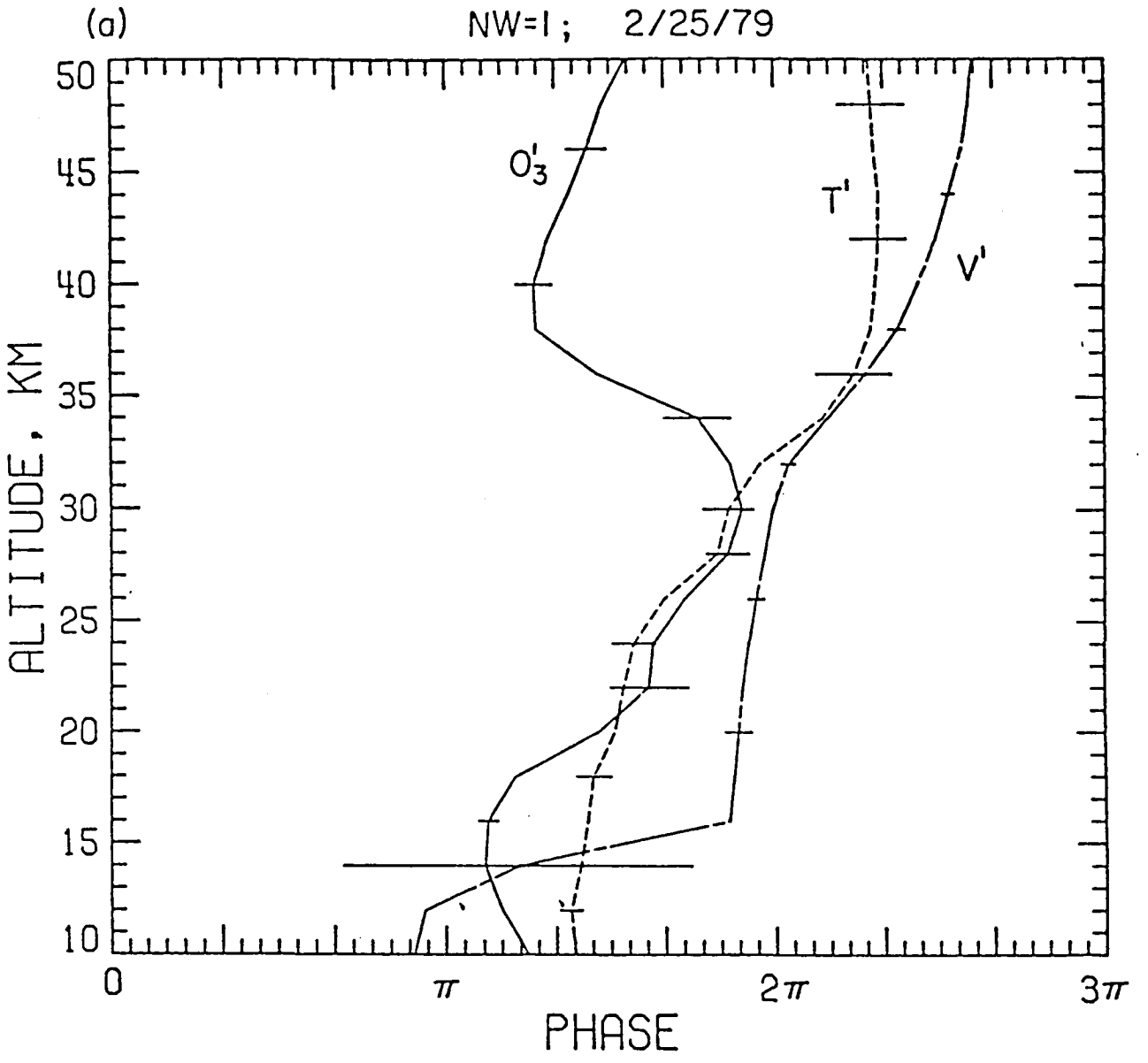

FIG. 5.9a: The phase relationship between ozone (solid line), temperature (dashed line), and eddy meridional velocity (solid and dashed line) for wavenumber 1, February 25, 1979. Phase increases westward.

suggested by the model analyses (Hartmann and Garcia, 1979; Kawahira, 1982). In addition, it is centered at a lower altitude. Gille et al. (1980) have shown the wavenumber 1 phase of temperature, height, and ozone mixing ratio for November 1, 1975 at 60° N from satellite observations. Although their results show slightly lower altitude of the phase transition compared to that of model analyses, their observational results have confirmed the phase behavior predicted on the basis of photochemical model. As noted by Hartmann (1981), the difference in the altitude of phase transition could be attributed to the differences in solar zenith angle, zonal wind profile, or to deficiencies in the parameterization of photochemistry in the model. In comparison with Gille et al.'s (1980) results, the transition region in Fig. 5.9a is still thinner and centered at a slightly lower altitude. It should be mentioned that this late February 1979 stratospheric warming was associated with a mean zonal wind reversal. The mean zonal wind could be relatively weak during this period. Hartmann and Garcia (1979) have noted that the advective time scale is inversely proportional to the mean zonal wind. As a result, the advective time scale during the late February 1979 warming could be relatively long, and the transition region took place at lower altitudes.

In the upper stratosphere (above 35 km), Fig. 5.9a also shows a nearly out-of-phase relationship between ozone and meridional velocity waves, and a phase difference of about $\pi/3$ between altitude approximately 20 and 35 km. This phase behavior between ozone and meridional velocity waves explains the poleward eddy ozone transport in the middle stratosphere and the equatorward transport in the upper stratosphere on February 25, 1979 (Fig. 5.6a). As for the wavenumber-1 phase relationship between temperature and meridional

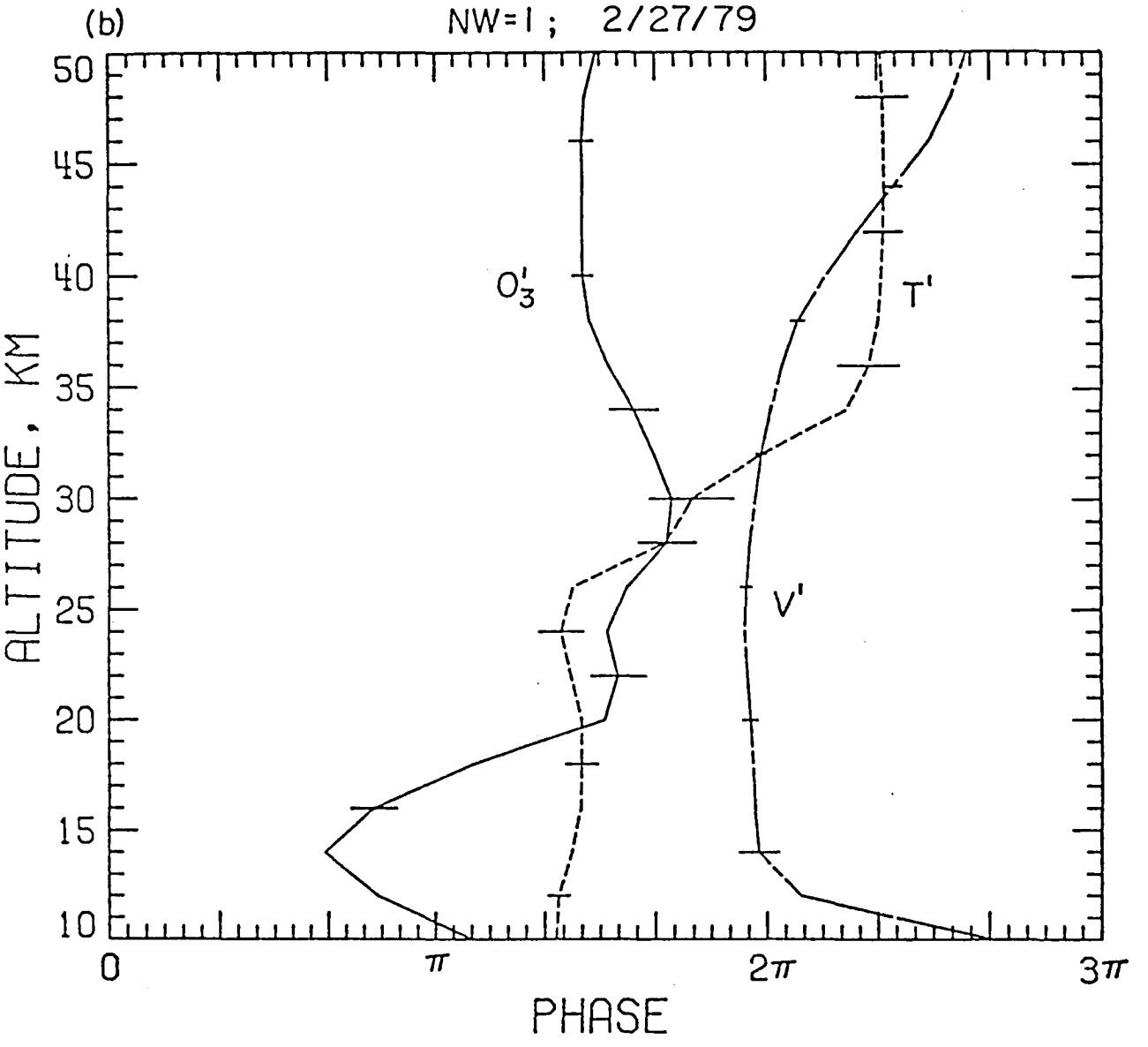

FIG. 5.9b: The phase relationship between ozone (solid line), temperature (dashed line), and eddy meridional velocity (solid and dashed line) for wavenumber 1, February 27, 1979. Phase increases westward.

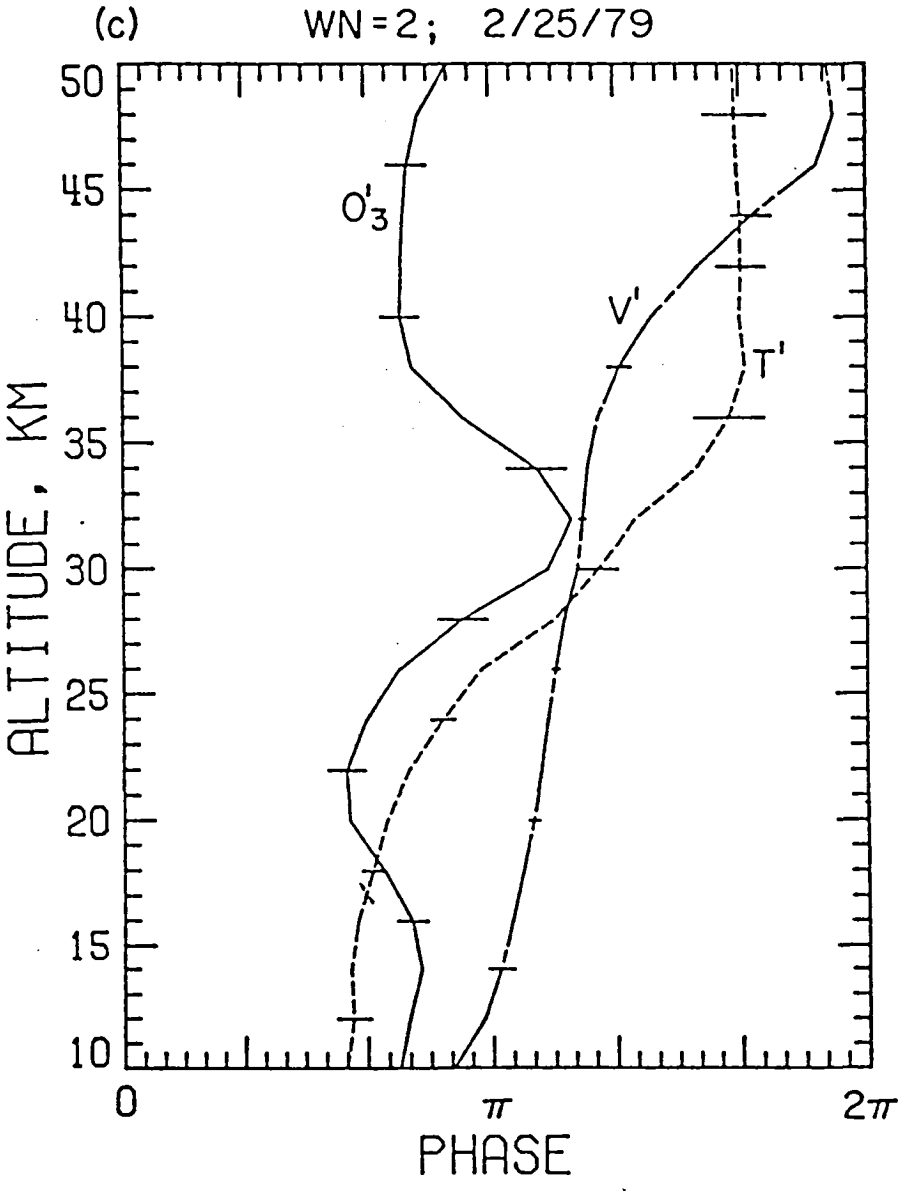

FIG. 5.9c: The phase relationship between ozone (solid line), temperature (dashed line), and eddy meridional velocity (solid and dashed line) for wavenumber 2, February 25, 1979. Phase increases westward.

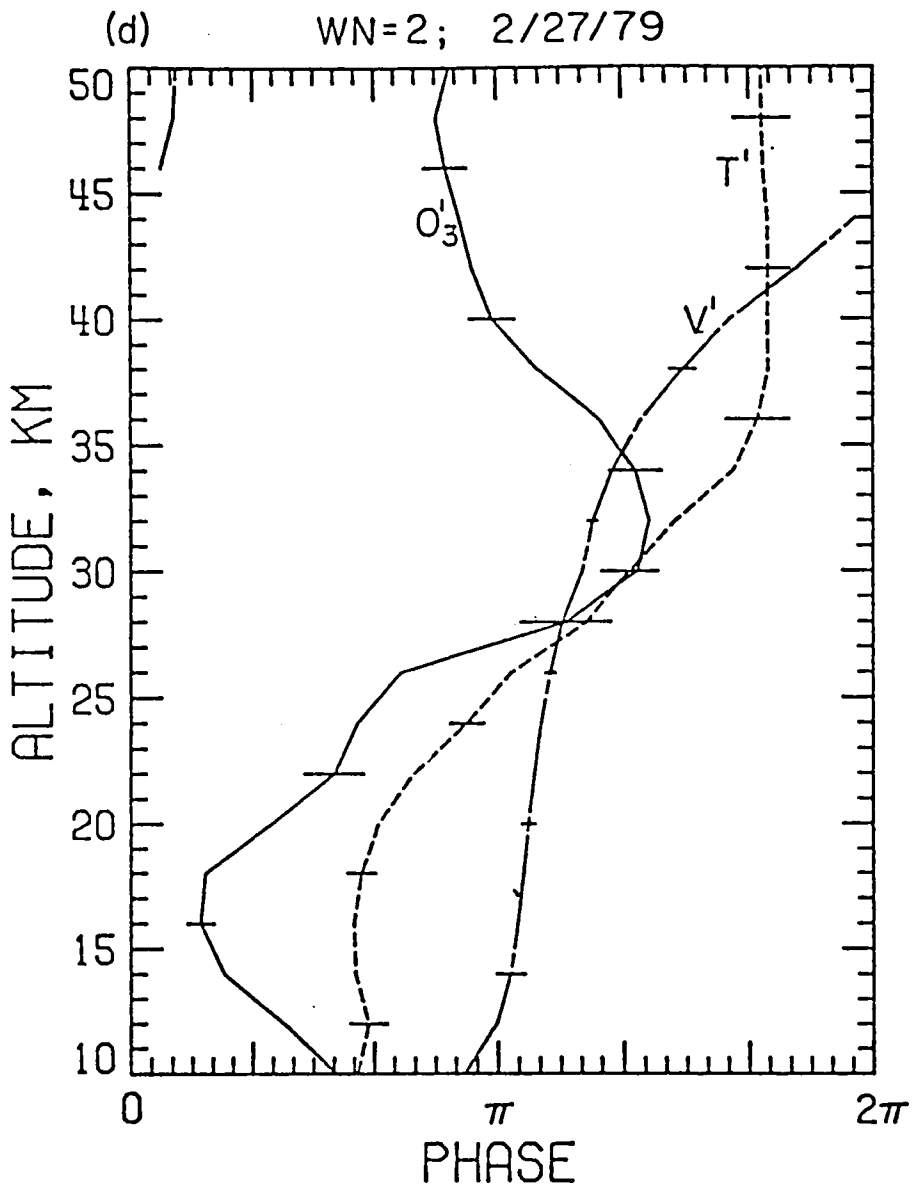

FIG. 5.9d: The phase relationship between ozone (solid line), temperature (dashed line), and eddy meridional velocity (solid and dashed line) for wavenumber 2, February 27, 1979. Phase increases westward.

velocity waves, they show approximately an in-phase relationship in the upper stratosphere (above 30 km) and a phase difference of $\sim\pi/3$ below altitude $\sim$30 km. This phase relationship explains the poleward eddy heat transport in the entire altitude range of this study which occurred on February 25, 1979 (Fig. 5.8a). Figure 5.8b is the same as Fig. 5.8a except for February 27, 1979. Figure 5.9b shows a quite similar feature between ozone, temperature and meridional velocity waves as in Fig. 5.9a. It is interesting to note that below $\sim$20 km, the nearly in-phase relationship between ozone and temperature waves becomes less evident than that in the altitude region between 20 and 30 km. This feature can also be noticed in the report of Gille et al. (1980).

The phase results for wavenumber 2 on February 25, 1979, are given in Fig. 5.9c. It shows a similar phase relationship between ozone and temperature waves as Fig. 5.9a; they are in-phase below altitude 32 km, out-of-phase above altitude 38 km, and a transition region exists approximately between altitudes 32 and 38 km. This transition region is only slightly higher than that for wavenumber 1. Figure 5.9c also shows a close in-phase relationship between ozone and meridional velocity waves at altitude 32 km and an out-of-phase relationship at altitude 45 km. This feature explains the poleward eddy ozone transport centered at 32 km and the equatorward transport centered at $\sim$45 km occurred on February 25, 1979 (Fig. 5.6b). Between altitudes 18 and 27 km, ozone and meridional velocity waves show a phase difference approximately $\pi/2$ (Fig. 5.9c). This altitude region corresponds to a layer with relatively weak eddy ozone transport as shown in Fig. 5.6b on February 25, 1979. Figure 5.9c also shows the phase relationship between temperature and meridional waves. They show a phase difference less than $\pi/2$ in the entire altitude range between

10 and 50 km. In particular, their phase lines cross each other at altitudes about 29 and 43 km. Thus, on February 25, 1979, only poleward eddy heat transport occurred between altitudes 10 and 50 km with two locate maximum centers of poleward transport at altitudes of about 30 and 42 km (Fig. 5.8b). Figure 5.9d is the same as Fig. 5.9c except for February 27, 1979. It shows a similar behavior of the phase relationship between ozone, temperature, and meridional velocity waves as Fig. 5.9c.

It should be pointed out that the approximate in-phase relationship between ozone and temperature waves in the upper stratosphere and their nearly out-of-phase relationship in the lower stratosphere are found to be evident throughout the entire data period of this analysis. This feature is illustrated in Fig. 5.10. Figures 5.10a and 5.10b are the time variation of the phase relationship between ozone, temperature, and meridional velocity waves for wavenumber 1 at altitudes of 44 and 26 km, respectively. Figures 5.10c and 5.10d are the result of wavenumber 2 at the corresponding altitudes.

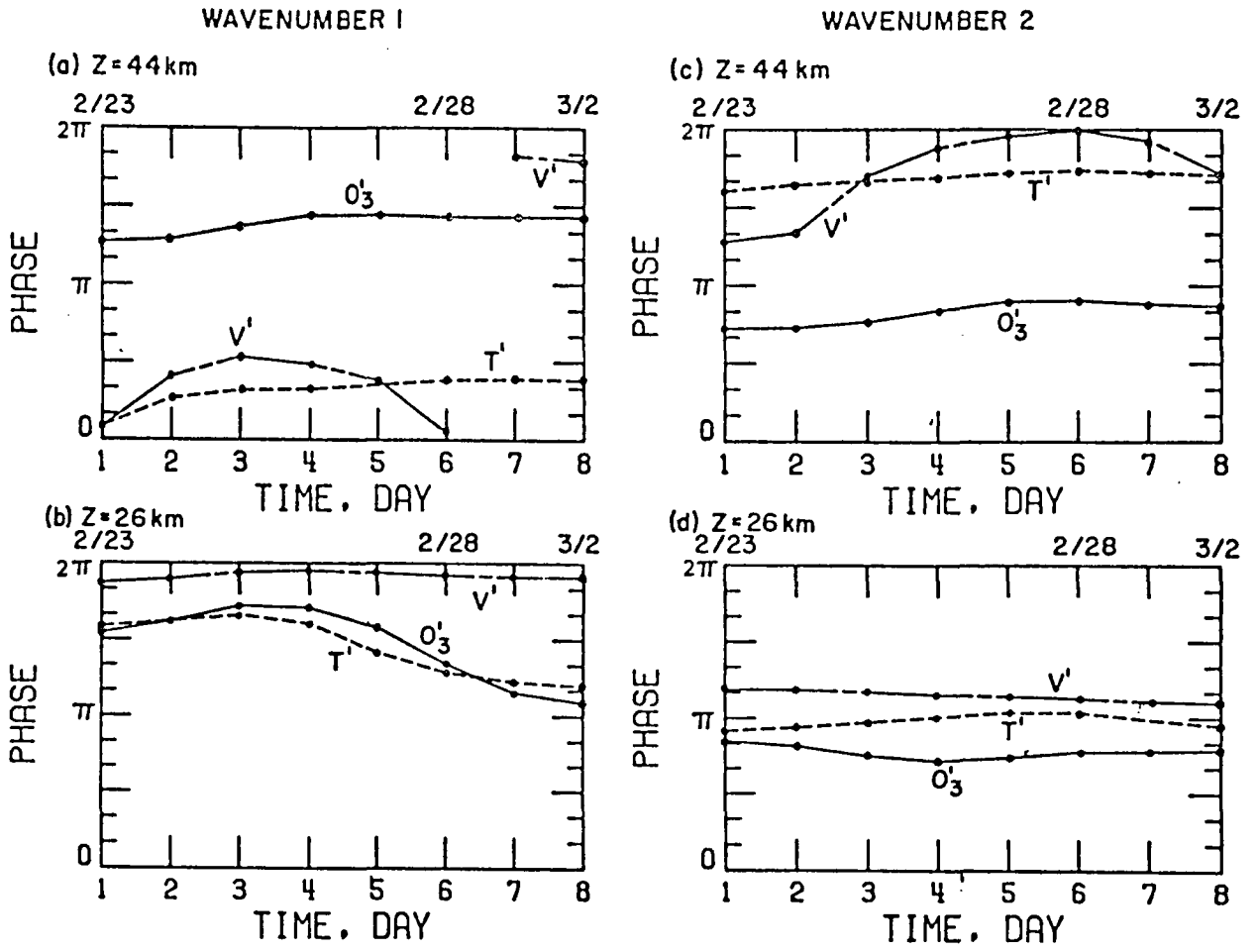

FIG. 5.10: The time variation of the phase relationship between ozone (solid line), temperature (dashed line), and eddy meridional velocity (solid and dashed line) waves during the late February 1979 warming. Phase increases westward. (a) Wavenumber 1 at altitude 44 km; (b) Wavenumber 1 at 26 km; (c) Wavenumber 2 at 44 km; and, (d) Wavenumber 2 at 26 km.

6. RADIATIVE DAMPING OF PLANETARY WAVE

6.1. BACKGROUND

In this chapter, we examine the coupling mechanism between radiation and dynamics by determining the radiative damping associated with planetary waves during stratospheric warming using SAGE data set. It is well known that the behavior of ozone, temperature, and motion waves in the stratosphere is determined by the strong coupling of radiation, photochemistry and dynamics (Hartmann, 1981). Dickinson (1968) has shown theoretically that the amplitude of planetary waves propagating out of the troposphere to the mesopause is reduced substantially by Newtonian cooling. Infrared radiation is capable of destroying the eddy available potential energy which is produced through the local conversion of eddy kinetic energy by the rising of cold air and sinking of warm air associated with amplifying waves.

As to the effect of solar radiation on the planetary waves, earlier analyses indicate that the temperature dependence of ozone photochemistry almost doubles the rate of relaxation of temperature perturbations in the upper stratosphere from that due to infrared radiative transfer alone (Craig and Ohring, 1958; Lindzen and Goody, 1965; and Blake and Lindzen, 1973). Strobel (1977) further showed theoretically that this acceleration in the relaxation is somewhat reduced by the so-called opacity effect when the effective optical depth is less or about equal to 1.

Hartmann (1981) also examined this opacity effect with the analysis extended to regions where ozone is under dynamical control. His results show that, below the transition level (Hartmann, 1981, Fig. 1), the sign and magnitude of the effect of opacity changes on the relaxation of temperature perturbations depends on the vertical structure of the temperature and ozone perturbations. Recently, Ghazi et al. (1979) have shown a strong negative correlation between variations in the temperature and ozone solar heating in the upper stratosphere by using satellite observations in the Southern hemisphere for the period of October 16-20, 1970. This correlation between temperature and ozone was shown to almsot double the rate of radiative damping of temperature perturbations in the upper stratosphere from that due to infrared radiation alone. Furthermore, the opacity effect accounted for about 40% of this enhancement.

The amplification of large-scale disturbances (planetary waves) during the winter and early spring is one of the prevailing characteristics of the high latitude stratosphere. Both theoretical and observational analyses indicate that this development is a manifestation of the stratosphere in response to the tropospheric activities (Matsuno, 1971; Holton, 1976; Quiroz, 1979, etc.). It has been shown that the observed features, including stratospheric warming and the northern spring high latitude total ozone maximum, are intimately related to the heat and ozone transports associated with these wave activities (e.g. Mahlman, 1979; Mahlman et al., 1979; Hartmann and Garcia, 1979).

Thus, the knowledge about the controlling mechanism of planetary waves is important to understanding of the stratospheric warming and the trace gas transports and for the model simulation of winter stratospheric circulation.

6.2. DATA AND METHOD OF APPROACH

In this section, we will describe a simple formulation that allows us to utilize the recent observational data during stratospheric warming periods to determine the radiative damping associated with planetary waves. Following Ghazi et al. (1979), the governing equation of the temperature departure from zonal average (T') can be written as

$$\frac{\partial T'}{\partial t} = PW + Q'_{IR} + Q'_{S} \qquad (1)$$

where PW represents the effect of planetary waves on T'; and Q' perturbation radiative heating (or cooling) with subscripts S and IR denoting solar and infrared terms. It is understood that, at a given latitude, T' and Q' are functions of altitude and longitude only. Approximately, Q'_{IR} and Q'_{S} can be expressed by

$$Q'_{IR} = - a T' \qquad (2a)$$

and

$$Q'_{S} = -b T' \qquad (2b)$$

respectively, where a and b are the radiative damping coefficients. They describe the damping (or relaxation) effect of infrared radiation and solar heating on temperature

fluctuations, respectively., To determine the values of a and b based on observational data is the main objective of this analysis. The coefficient a bears the well known meaning of the Newtonian cooling (Goody, 1964; Rodgers and Walshaw, 1966). However, as will be shown, the definition of a in this paper is slightly different from the Newtonian cooling coefficient. The coefficient b is essentially the second term in the bracket on the righthand side of Eq. 5 of Hartmann (1981). Its appearance is primarily a result of the coupling between radiation and photochemistry in the stratosphere, and is proportional to the temperature dependence of the ozone concentration (Craig and Ohring, 1958; Lindzen and Goody, 1965; Hartmann, 1981). This coupling leads to an enhancement of the thermal relaxation rate due to infrared effect in the upper stratosphere. By multiplying both sides of Eqs. 2a and 2b by T' and then averaging over longitudes, we have

$$a = - \frac{\overline{Q'_{IR} T'}}{\overline{T'^2}} \qquad (3a)$$

and

$$b = - \frac{\overline{Q'_S T'}}{\overline{T'^2}} \qquad (3b)$$

where overbar indicates the zonal average. In applying Eqs. 3a and 3b, the following steps have been taken.

(1.) Calculate the longitudinal distributions of Q_S based on

SAGE ozone profiles;

(2.) Determine the longitudinal distribution of Q_{IR} using associated temperature distributions;

(3.) Determine the fluctuations T', Q'_{IR}, Q'_{S};

(4.) Compute the zonal average quantities $\overline{T'^2}$, $\overline{Q'_{IR}\,T'}$, and $\overline{Q'_{S}\,T'}$; and

(5.) Calculate coefficients a and b.

The heating/cooling terms Q_S and Q_{IR} are determined by adapting the radiative transfer model of Ramanathan (1976). The one-dimensional model extends from the ground to about 55 km in altitude, including the contribution due to CO_2, H_2O and O_3. It accounts for surface and cloud reflections and the Rayleigh scattering effects, and also the Doppler-broadening effects for CO_2 and O_3. In addition, the exchange of infrared radiation between the level under consideration and the layers below is also included. The albedos of Rayleigh scattering and cloud are a function of solar zenith angle. In this study, the mean solar zenith angle and fractional length of daytime are determined by the third approximation of Cogley and Borucki (1976).

As to the data sets, the SAGE ozone density profiles are employed in determining Q_S at 11 pressure levels between 50-0.5

mb. Below 50 mb, we have used the ozone values from the vertical ozone distribution given in the U.S. Standard Atmosphere (1976). The solar absorption by CO_2 and H_2O is also included. Their concentrations are assumed to be uniformly distributed with 320 ppmv and 3 ppmm, respectively. Since we are mainly interested in the effect of ozone solar heating associated with the waves on the damping processes, and since the solar absorption by CO_2 and H_2O in the stratosphere are of secondary nature, we consider only the contribution of O_3 in determination of the coefficient b.

In determining Q_{IR}, resulting from infrared radiation of CO_2, H_2O, and O_3, we have used the meteorological information provided by NOAA's National Meteorological Center (NMC). This information, including temperature and geopotential height at 18 standard pressure levels from 1000 to 0.4 mb, is interpolated at SAGE sampling locations and time based on the NWC's routine operational analyses (Gelman et al., 1981). For the calculations, a cloud top altitude of 6 km and a fractional cloud cover of 0.45 are used. In order to gain the insight in the wave damping mechanism, we have carried out the Fourier decomposition of T, Q_{IR}, and Q_S in determining T', Q'_{IR}, and Q'_S (step 3). Since the winter stratospheric disturbances consist largely of long waves, we consider only wavenumber 1 and 2 in this analysis. The calculation of the zonal averages (step 4) and the damping

coefficients a and b (step 5) are straight forward. The results of the calculation are given in the next section.

Before describing the computed results, it is important to mention that, in this analysis, we have selected observational data sets of three particular days with large longitudinal ozone and temperature variations in the high latitudes during stratospheric warmings. They are the SAGE measurements on February 25, 1979, February 15, 1981, and September 8, 1979. On these three particular days, SAGE sampling location reaches, on the average, the latitudes 55^{o} N (Fig. 2.2), 53^{o} N, and 54^{o} S, respectively. Note that the one on September 8, 1979 is a case in the Southern hemisphere.

6.3. RESULTS AND DISCUSSION

(a) Height-Longitudinal Distributions of Q_3, T, Q_S, and Q_{IR}

As indicated earlier, we have examined three particular daily data sets. For the sake of brevity, we will describe only the results on February 25, 1979 in detail. As to the other two days, i.e., February 15, 1981 and September 8, 1979, their calculated results are shown for comparison only. Figures 6.1a to 6.1d are the analyzed results for February 25, 1979. It should be noted that this is about the peak date of the late February 1979 stratospheric warming (Quroiz, 1979; Wang et al. 1983). As shown in Figure 2.2, this major warming is characterized by large disturbances associated with a wavenumber 2 circulation pattern

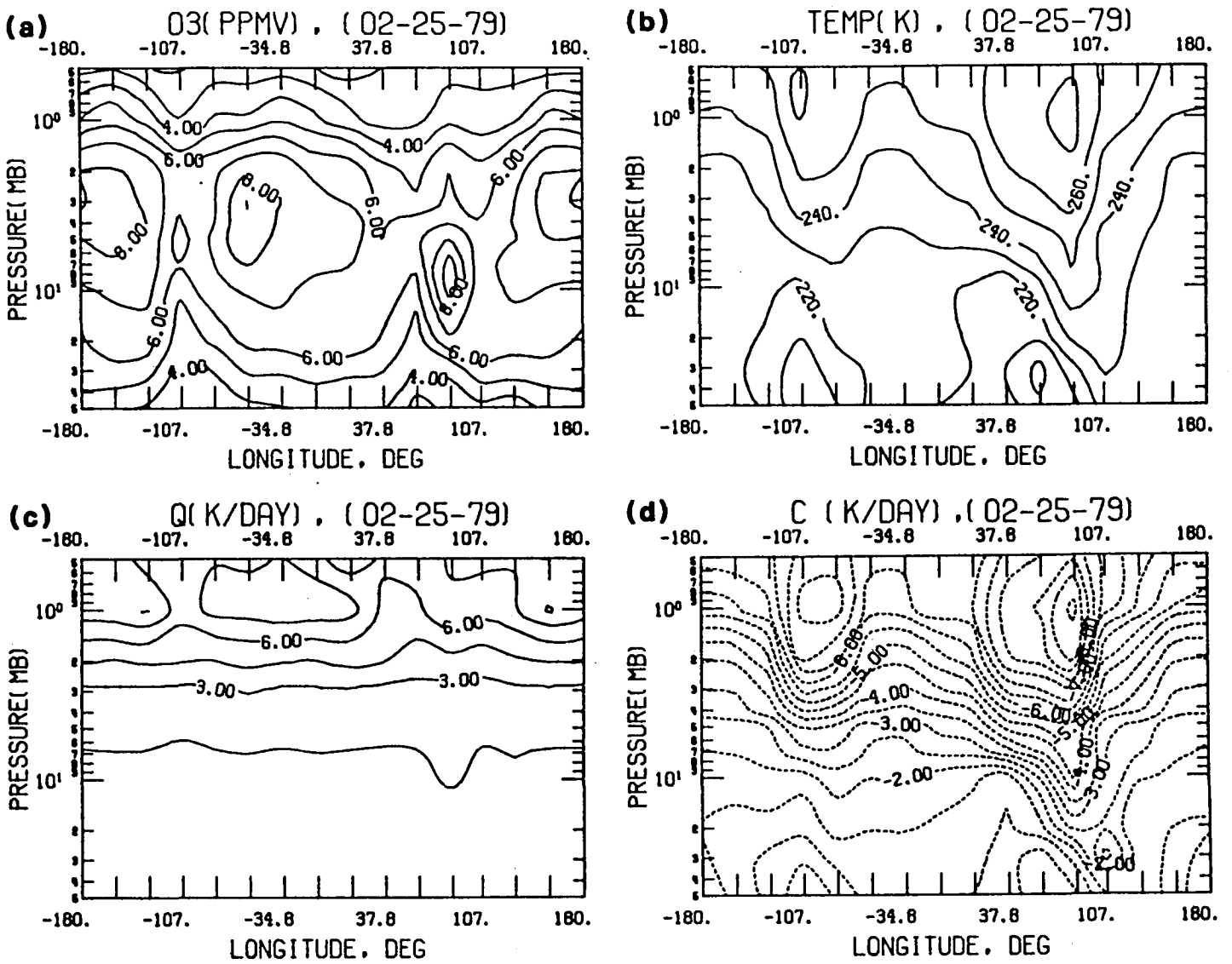

Fig.6.1. The height (in pressure, mb) - longitudinal distributions of (a) ozone mixing ratio (ppmv), (b) ozone solar heating, k/day, (c) temperature, k, and (d) infrared cooling k/day, near 55°N on February 25, 1979.

at 30 mb with the polar vortex being split into two low pressure systems. The large longitudinal fluctuations in O_3 and T are clearly evident in Figs. 6.1a and 6.1b, respectively. The calculated ozone solar heating (Fig. 6.1c) shows a peak centered at ~ 1 mb pressure level. It decreases rather rapdily with height below this level. Figure 6.1c also reveals distinctively the longitudinal variations of ozone solar heating in the upper stratosphere above ~ 2 mb. The result of infrared radiation calculations is given in Fig. 6.1d. It shows two local infrared cooling centers. They are located approximately at longitudes -100^{o} and $+100^{o}$ at ~ 1 mb, with the value of 7.5 and 9.5 k/day, respectively. As expected, the temperature and the calculated infrared cooling show quite similar contour patterns, especially in the upper stratosphere. This is not surprising, since the infrared cooling depends strongly on the temperature distribution, particularly in the upper stratosphere. The results for February 15, 1981 and September 8, 1979 are given in Figs. 6.2 and 6.3, respectively.

(b) Radiative Damping

Table 6.1 shows the values of radiative damping coefficients a and b for wavenumber 1 and 2 at six pressure levels from 0.5 to 10 mb for the three selected days mentioned earlier. Many features can be noticed in Table 6.1. First of all, it shows that the coefficient a exhibits a maximum at about the 2 mb pressure level. On the other hand, the highest values of b occurs

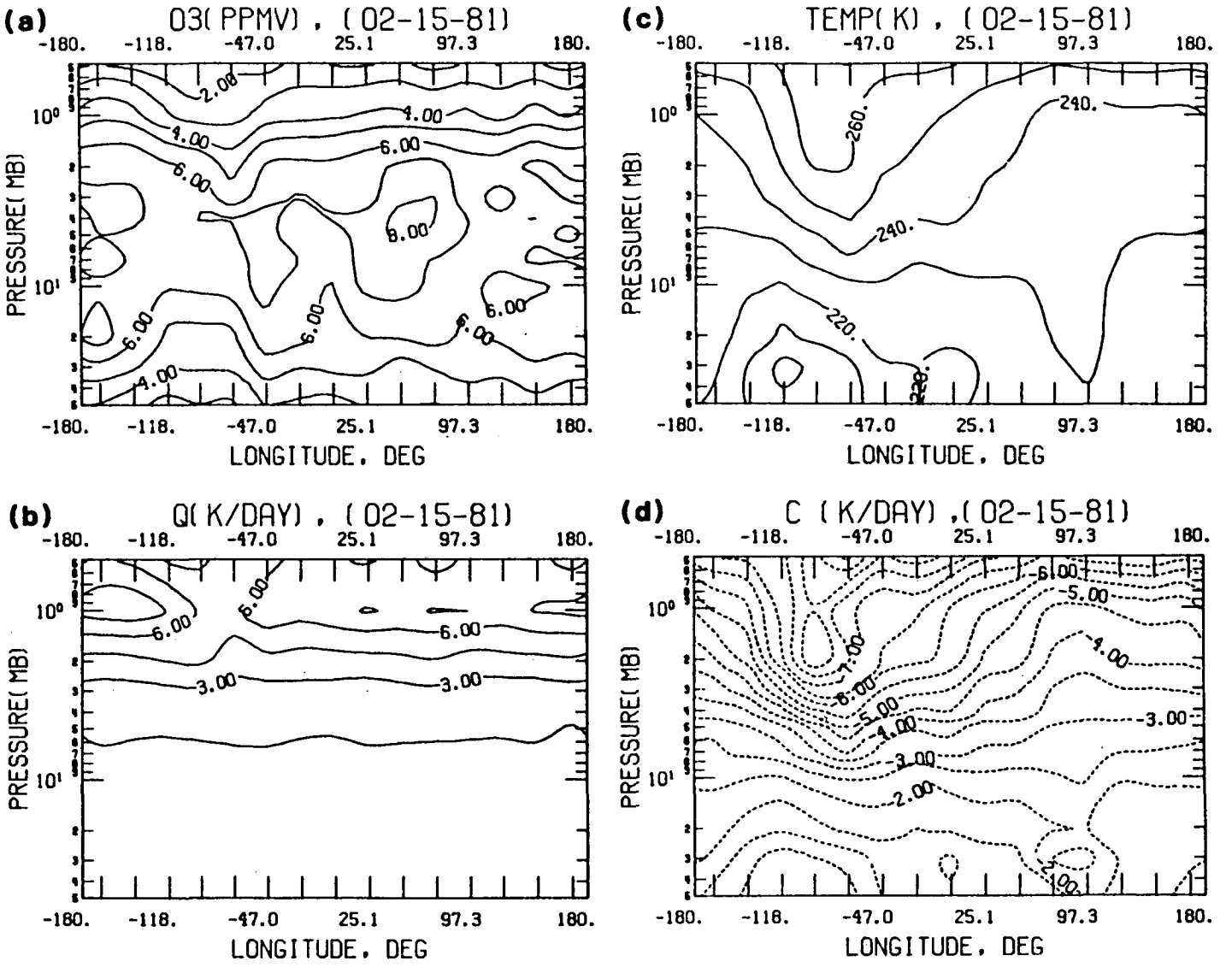

Fig. 6.2. The same as Fig. 6.1, except for 53°N on February 15, 1981.

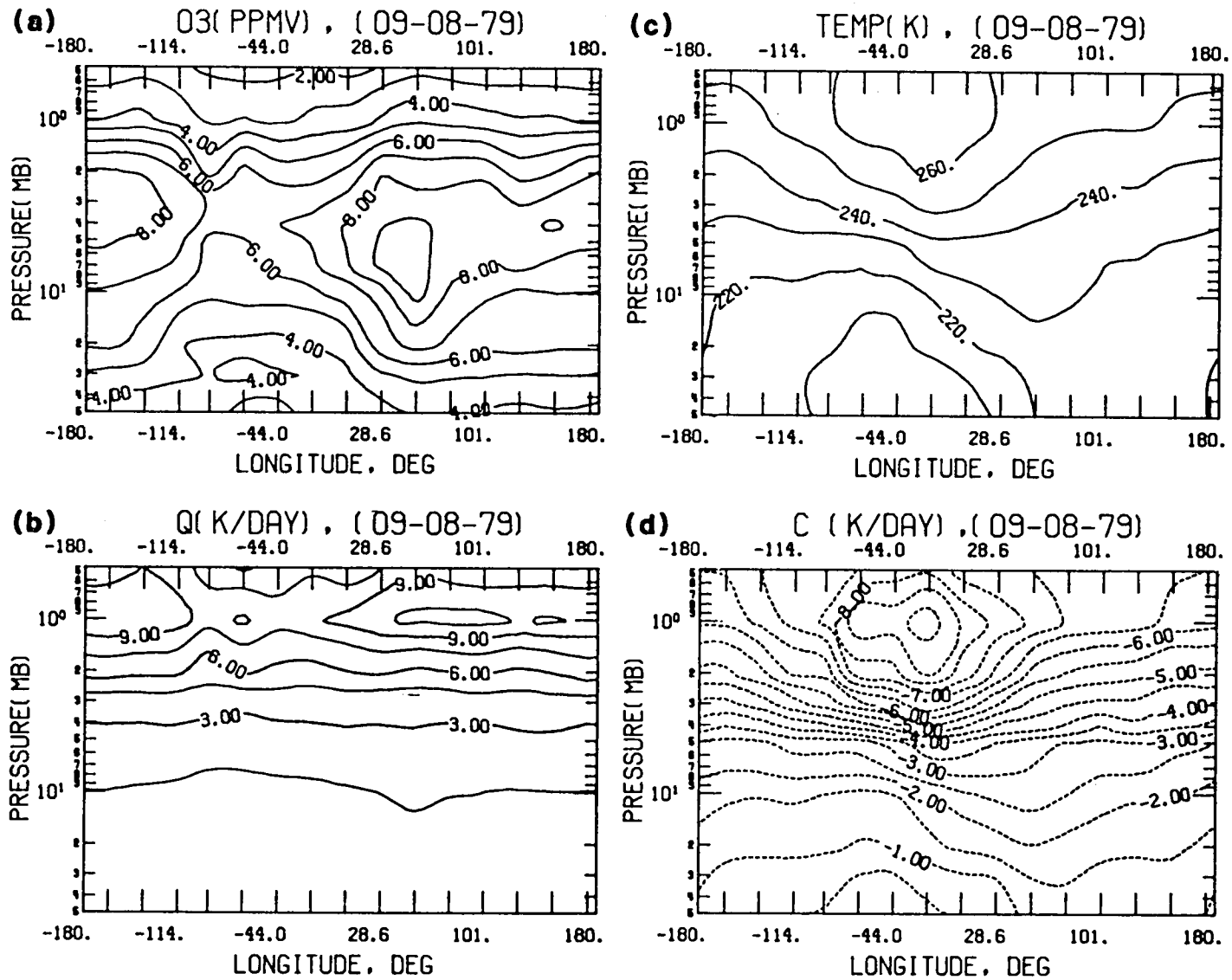

Fig. 6.3. The same as Fig. 6.1, except for 54°S on September 8, 1979.

TABLE 6.1. Radiative Damping Coefficients a and b (Day^{-1})

WAVENUMBER 1

P(mb)	Feb 25, 1979 55°N		Feb 15, 1981 53°N		Sep 8, 1979 54°S	
	a	b	a	b	a	b
.5	.09	.08	.11	.06	.09	.14
1	.11	.09	.12	.05	.14	.10
2	.13	.01	.15	.00	.16	.03
5	.12	-.01	.15	.01	.09	.02
10	.01	-.01	.03	.00	.06	.02

WAVENUMBER 2

P(mb)	Feb 25, 1979 55°N		Feb 15, 1981 53°N		Sep 8, 1979 54°S	
	a	b	a	b	a	b
.5	.10	.02	.12	.11	.08	.35
1	.12	.09	.08	.20	.13	.19
2	.14	.01	.15	-.03	.16	.06
5	.12	.00	.13	-.02	.12	-.07
10	.08	-.01	.06	.02	.07	-.04

generally at 1 mb. In addition, the values of b at 0.5 and 1 mb as a whole are comparable to those of a at these two pressure levels. This particular feature implies a significant enhancement of the infrared damping rate by ozone solar heating in the upper stratosphere as discussed by Hartmann (1981), and also support the analysis given by Ghazi et al. (1979). Note the rapid decrease of the value of b below 2 mb and also the negative values of b which occur in some of the cases mostly below 5 mb. These negative values of b are mainly the result of a nearly in-phase relationship between the ozone solar heating and temperature waves. Under such a circumstance, the effect of ozone solar absorption associated with the waves is to intensify the temperature disturbances instead of suppressing them. Thus, in the region below about 5 mb, the relaxation effect of ozone solar heating associated with the waves depends intimately on the wave structures of the temperature and ozone concentration. A further discussion of this particular aspect is given in the last part of this section. From Table 6.1, one may notice the relatively large fluctuation of individual b values at 0.5 and 1 mb when compared with coefficient a at the same levels. This behavior of b can be attributed to the fact that b depends not only on the state of the stratosphere but also on the incoming solar radiation. In other words, the value of b is sensitive to the mean solar zenith angle, and varies from day to day even at the same latitude. A case of poleward decrease of b value has been reported by Ghazi et al. (1979).

Newtonian cooling accounts approximately for the damping by infrared radiative transfer of a large-scale temperature perturbation in the atmosphere (Rodgers and Walshaw, 1966). Perhaps, the most widely used set of Newtonian cooling coefficient is the one developed by Dickinson (1973). This set of coefficients allows us to perform a very fast evaluation of the approximate perturbations of infrared cooling associated with small departures of the atmospheric temperature from that of the 1962 U.S. standard temperature profile. The necessary correction of this set of coefficient to a wide range of departure temperature from this reference temperature was also suggested by Dickinson (1973). Since his Newtonian cooling coefficient was developed based on a model atmosphere with an imposed small temperature perturbation, it is interesting and worthwhile to compare his coefficient with our calculated infrared damping coefficient based on observational data sets. In doing this, we have combined all the values of the damping coefficient at a given pressure level from the six independent cases listed in Table 6.1 to obtain an averaged value. The results are given in Table 6.2. Similar procedure is also applied to the coefficient b at 0.5, 1, and 2 mb. The results are also listed in Table 6.2. Table 6.2 includes also their corresponding standard deviations. For comparison, we have marked the values of Table 6.2 on the figure taken from Fels (1982), who calculated the infrared relaxation time with consideration of the vertical-scale dependence, and compared his results with Dickinson (1973) and Blake and Lindzen (1973). The comparison is presented in Fig.

TABLE 6.2 Mean and Standard Deviation (σ) of Radiative Damping Coefficients a and b (day^{-1})

P(mb)	a		b	
	Mean	σ	Mean	σ
.5	.10	.016	.13	.12
1	.12	.021	.12	.06
2	.15	.010	.023	.021
3	.15	.020	--	--
4	.13	.023	--	--
5	.12	.019	--	--
7	.10	.022	--	--
10	.07	.020	--	--

6.4. In Fig. 6.4 the enhanced damping rates resulting from ozone solar heatings, at pressure levels 0.5, 1, and 2 mb are also shown as denoted by solid triangles. It can be seen that, there is a good agreement in the values of the damping coefficient between Dickinson's (1973) and the calculated result in this study, except at 0.5 (~ 53 km) and 1 mb (~48 km) pressure levels. At these levels, the computed results are smaller than Dickinson's (1973) and also than that of the uniformly perturbed case of Fels' (1982). It should be remembered that, in this analysis, the calculation of Q_{IR} at a given level includes the contribution of cooling to space and the radiative exchange between the level considered and the layers below. Only the exchanges of energy with the region of stratosphere above is neglected. This exchange of energy is, however, negligibly small when compared with the other contributions (Ramanathan, 1976). Therefore, the derived infrared damping coefficient a does include the effect of vertical-scale dependence to alarge extent. This would explains why the infrared damping coefficients of this analysis are slightly larger than the Newtonian cooling rate of Fels (1982), as shown in Fig. 6.4. It should be mentioned that Fels (1982) attributed half of the difference in the Newtonian cooling rate between his calculation and Dickinson's to the difference in CO_2 concentration and half to O_3 distribution.

Several papers have been addressed on the importance of the

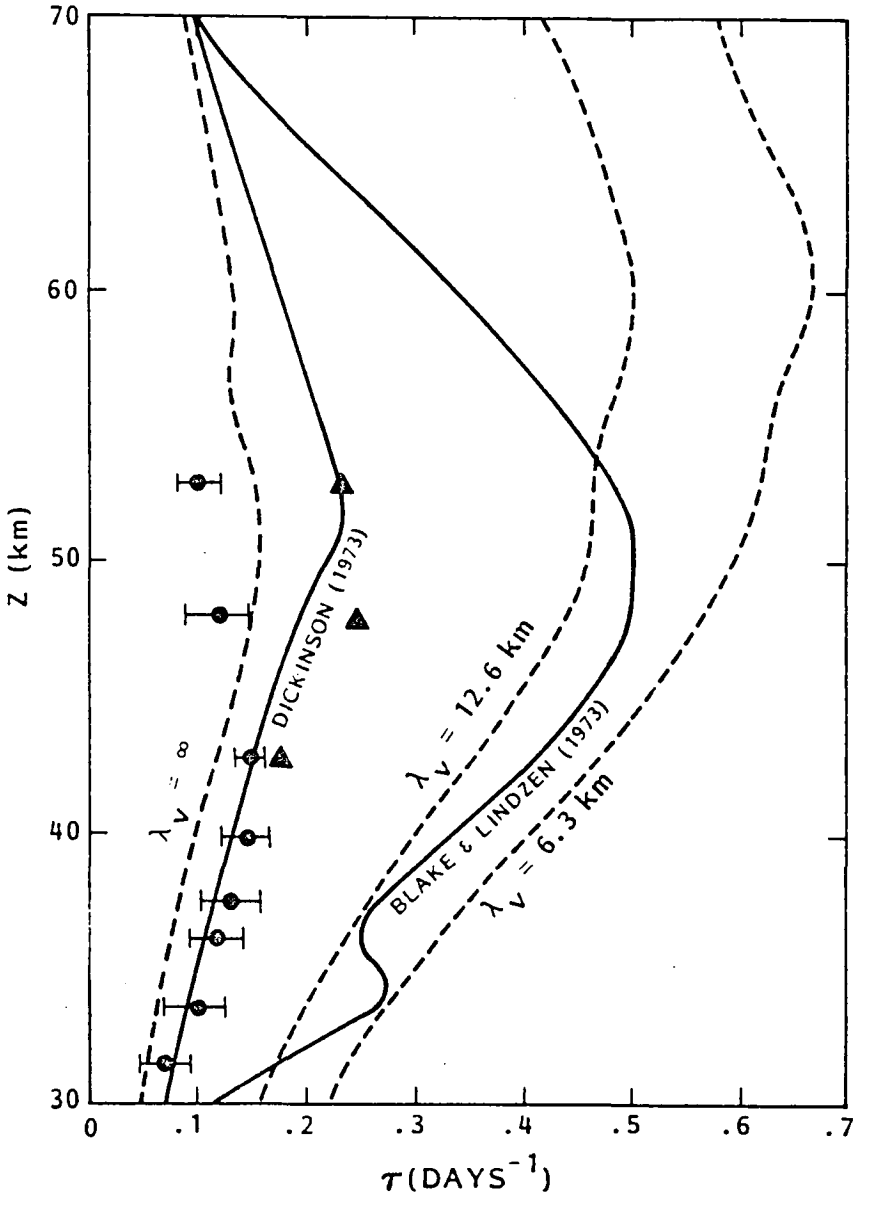

Fig. 6.4. Comparison of infrared radiative relaxation times (after Fels, 1982). Solid circles and the horizontal bars are the means and standard deviations listed in Table 6.2, respectively. Solid triangles are the enhanced relaxation at .5, 1, and 2 mb due to the negative correlation between solar heating and temperature.

dependence of infrared damping rate on the vertical wavelength of temperature disturbances in the atmosphere (Sasamori and London, 1966; Fels, 1982, 1984; Alimandi and Visconti, 1983; Schoeberl et al., 1983; Apruzese and Strobel, 1984; etc.). Although, the infrared radiation calculations in this analysis have taken into account the exchange of energy between the level considered and the layers below, as mentioned earlier, no attempt is made here to quantitatively derive the vertical scale dependent infrared damping coefficient using observational data sets. Fels (1982) has pointed out the technique difficulties in practical use of this detailed coefficient and said "It is therefore simpler (and more accurate) in this case to make use of some version of the fully non-local radiative treatment." It should be noted that the main aim of this analysis is to use observational data sets to examine the radiative damping processes associated with planetary waves. Especially, the derived infrared cooling coefficients based on observational data can be easily calculated and readily used to validate the theoretical Newtonian cooling coefficient. The values of coefficients a and b can be incorporated into the circulation models to provide very fast radiative damping calculations. Although the results of such a model calculation may not be sufficiently accurate, it may provide guiding information which can be very useful for further detailed quantitative circulation analysis using a much more elaborated computation scheme.

c. Analysis in terms of the phase relationship of the

planetary waves

As shown earlier (Section 6.3b), ozone solar absorption associated with planetary waves may suppress or enhance the temperature disturbances in the stratosphere. In order to gain insight into the specific effect of ozone solar heating on the temperature disturbances, it is worthwhile to examine the phase relationship between the planetary waves of ozone, temperature, and ozone solar heating,. The vertical variations of the phase of these waves are given in Fig. 6.5. This figure illustrates many interesting features. First of all, the phase relationship between ozone and temperature waves on the three selected days, including both wavenumber 1 and 2, shows generally a transition layer in which a change from the close in-phase relationship in the region below (lower stratosphere) to the nearly out-of-phase relationship in the region above (upper stratosphere) takes place. Some variations in the thickness and height of the center of this transition layer on the three selected days are also depicted. Detailed discussions of such a transition layer in the stratosphere have been given by Hartmann and Garcia (1979), and Kawahira (1982), based on model analyses, and by Gille et al. (1980) and Wang et al. (1983; see also Chapter 5) based on observations.

As to the phase relationship between ozone and solar heating waves, (Fig. 6.5) exhibit a close in-phase relationship above ~ 1 mb and also below ~ 10 mb. Between 1 and 10 mb, they show a departure from the in-phase relationship. The in-phase

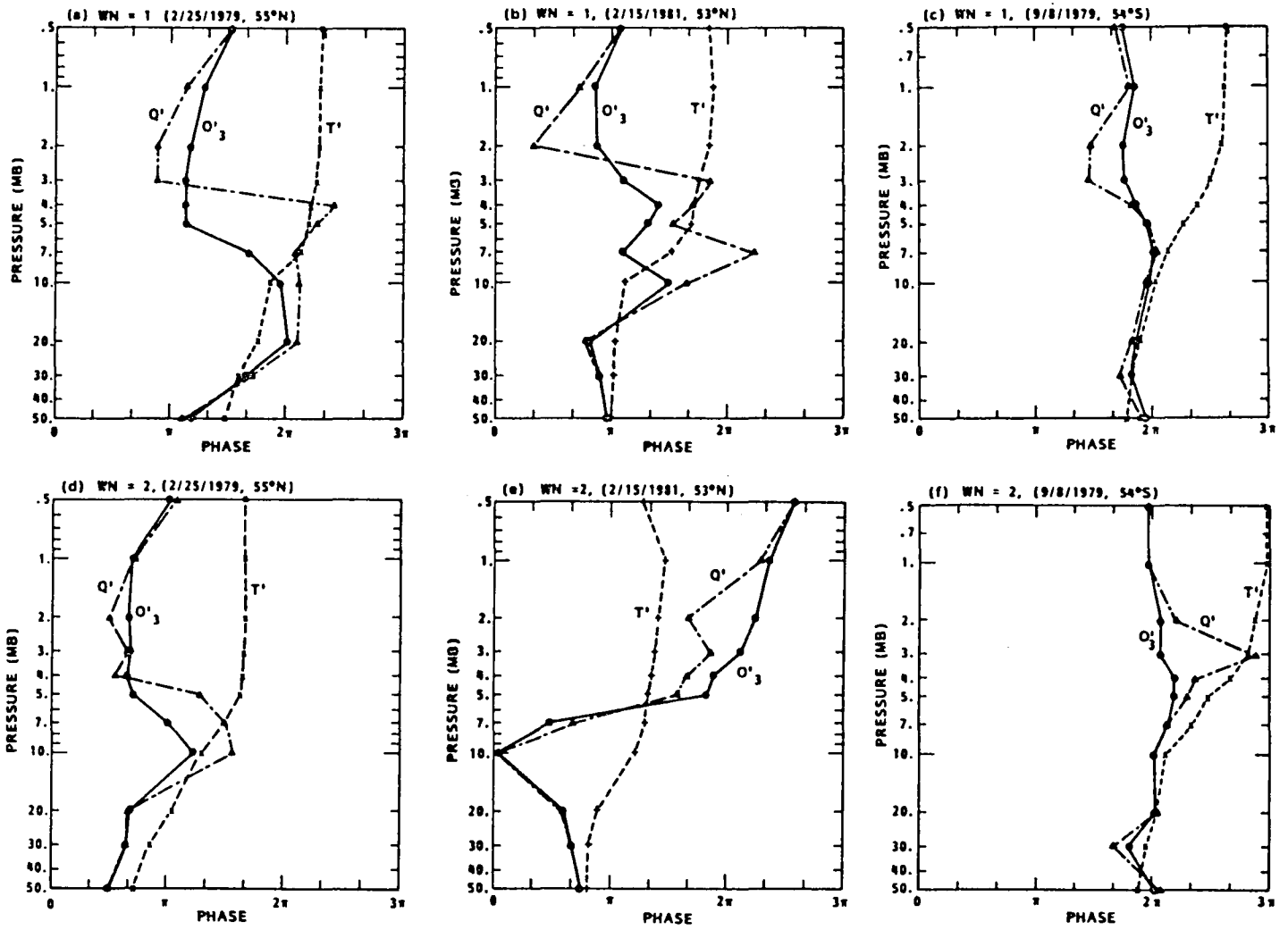

Fig. 6.5. Phase relationship between ozone, temperature, and ozone solar heating waves.

relationship above 1 mb and below 10 mb are interesting and can be attributed to somewhat different reasons. In the region above 1 mb (~ 45 km) the solar absorption due mainly to ozone ultraviolet (Hartley and Huggins) bands is not saturated, thus the absorption of the solar beam is proportional mainly to the local ozone concentration. As a result, the perturbations in the ozone solar heating follow closely the variations of ozone concentration, and result in a close in-phase relationship between the corresponding waves. On the other hand, in the region below 10 mb (~ 30 km), the ozone solar absorption is expected to be saturated due to the absorption above. Therefore, the ozone absorption below 10 mb is insensitive to further increase in the ozone column and depends mainly on the local ozone concentration. Thus, ozone and ozone solar heating also show an in-phase relationship in this region. As to the region between approximately 1 and 10 mb, the departure from an in-phase relationship between ozone solar heating and ozone waves can be attributed to the opacity effect. Since in this region the optical depth approaches the value of 1, ozone solar heating is sensitive to changes in the optical path length, as well as local ozone concentration (Hartmann, 1981). This feature can be illustrated schematically in Figure 6.6. The locations of points A and B in Fig. 6.6 are the centers of regions with positive and negative fluctuations in ozone concentrations, respectively. Thus, the air element near point A/B will experience a larger/smaller optical depth than that around B/A at the same height. As a result in the region between 1 and 10 mb, where

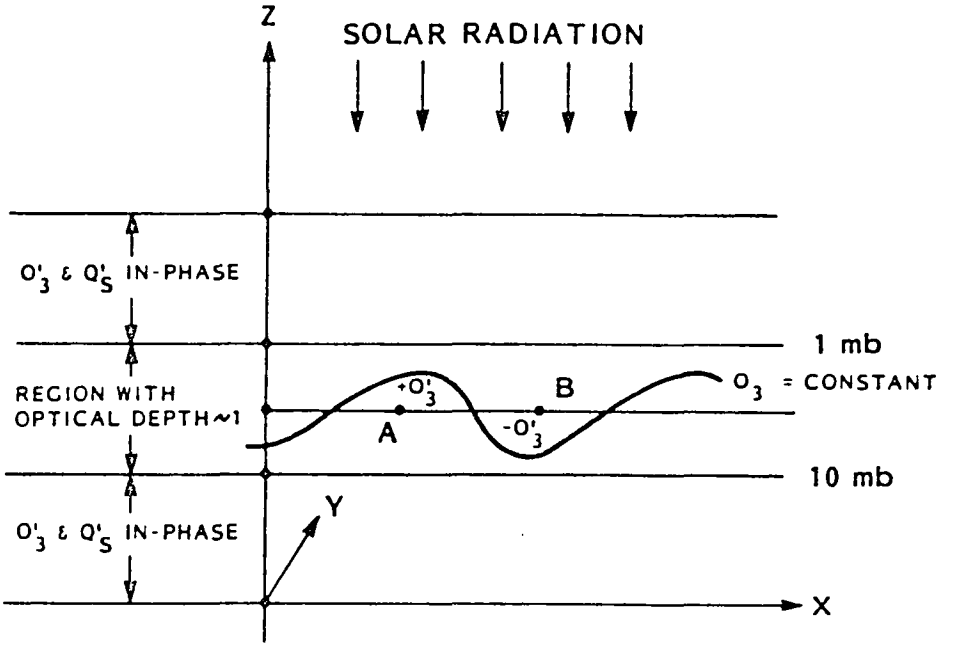

Fig. 6.6. A schematic diagram illustrating the departure from in-phase relationship between ozone and ozone solar heating waves in the transition region (approximately between 1 and 10 mb), in which the optical depth approaches 1.

ozone absorption is most sensitive to the change in optical depth, it is possible to have less ozone solar heating in a region with high ozone concentration, than in a region with low ozone concentration. A direct consequence of this "opacity effect" is a departure from the in-phase relationship between ozone and ozone solar heating.

Figure 6.5 also shows the phase relationship between temperature and the ozone solar heating waves. As mentioned earlier, this phase relationship is important in determining the sign of the damping rate due to ozone solar heating. By inspection, one may find that all the negative damping rates appeared in Table 1 are basically associated with cases of a nearly in-phase relationship between ozone solar heating and temperature waves.

7. SUMMARY AND CONCLUDING REMARKS

7.1 STRATOSPHERIC AEROSOL

The SAM II and auxiliary meteorological measurements during the January-February 1979 stratospheric sudden warming have been used for studying the variation of zonal mean aerosol extinction ratio and its relationship with the mean temperature in the lower stratosphere from 14 to 58 km near 75°N (Chapter 4). Results of this analysis indicate distinct changes in the distribution of the mean aerosol extinction ratio during this warming event. In addition, relatively low mean aerosol extinction ratios are found during the second warming pulse in regions above altitude 20 km. Below 20 km, however, the variations of the mean aerosol extinction ratio are showing positive correlation with the mean temperature. During the period of the third warming pulse, they are found to be positively correlated in most of the altitude range and during most of the time. In addition, the joint rapid increase of the mean aerosol extinction and mean temperature from February 17 to February 25, 1979 is of particular interest. Due to the fact that positive correlation observed between zonal mean aerosol extinction ratio and temperature cannot be explained on the basis of aerosol microphysics, dynamical processes can be very important during the warming periods. Since this is a single case study, analyses based on different winters are highly desirable.

7.2 STRATOSPHERIC OZONE

SAGE ozone measurements were used, in concert with the meteorological information, to infer the ozone controlling mechanism in different regions in the stratosphere and to study the ozone transport due to planetary waves

during the late February 1979 stratospheric warming. The calculated results of the correlation coefficients (R) between stratospheric ozone and temperature (Chapter 3) show that the values of R are negative in the upper stratosphere and positive in the lower stratosphere in agreement with the ozone theory, including both photochemistry and dynamics. A transition region has been defined by taking the absolute value of R to be less than .5 as a criterian. Under this condition, the effects of photochemistry and dynamics are about equal in determining the ozone distribution. The zero line of R, which represents the center of the transition region, is found to be tilted generally in such a way that its altitude increases with latitude. The results also show that the vertical extension of this transition region increases with the latitude. It is found that these features are in agreement with the model results of Gunnold et al. (1980) and also with those from observation (Gille et al., 1980).

As for the ozone transport due to planetary waves during this late February stratospheric warming, the results show an intense poleward eddy ozone transport occurred in the middle stratosphere between altitudes 24 and 32 km, while equatorward transport took place in the upper stratosphere above 38 km. The results also show that the equatorward ozone transport appearing in the upper stratosphere was accompanied by a poleward eddy heat transport as expected on the basis of ozone photochemistry. In the lower stratosphere (below 25 km), there was an equatorward ozone eddy transport, but it is secondary. The transport effect of planetary wavenumber 2 can account largely for the net ozone eddy flux. Furthermore, the ozone columnar density above 10 km shows a rapid increase during this late February warming. This increase is found to be a response primarily to the change

of mean ozone number density in the lower stratosphere. In regard to the phase relationship, we have found that ozone mixing ratio and temperature waves exhibit a nearly in-phase relationship in the lower stratosphere except the lower few kilometers around the tropopause. In the upper stratosphere, they generally show an out-of-phase relationship; a condition indicating photochemical control. With regard to the transition layer between photochemical and dynamical dominance, we found that this layer is thinner and is centered at a lower altitude than the model predictions (Hartmann and Garcia, 1979; Kawahira, 1980) and the measurements reported by Gille et al. (1980). The reason for this difference can be attributed to the weak mean zonal wind during this late February 1979 warming. It is interesting to note that Cunnold et al. (1980) have derived a transition region, which is located between altitudes 25 and 40 km at latitude 55^{o}, using a spectrum 3-D photochemical-dynamical model. Although the results in this study show a lesser vertical extending of the transition layer, the altitude range of this layer does fall into their model estimate. Since the manifestation of stratospheric warming is different for different winters, ozone transport analyses based on warming events from different winters are highly desirable.

Finally, we have also examined the planetary wave controlling mechanism due to damping effect of ozone solar heating associated with the wave itself. It is found that the ozone solar heating in the upper stratosphere enhances the damping rate of the waves due to infrared radiation alone. This result is in agreement with that of theoretical studies, and also an earlier observational analysis (Ghazi et al.).

ACKNOWLEDGMENTS

This work was supported by Contract NAS1-16362. It is a pleasure to acknowledge M. P. McCormick, W. Chu, and L. R. McMaster of NASA-Langley Research Center (LaRC) for giving valuable assistance on many aspects during the course of this work. In addition, thanks are also due to G. Yue of NASA LaRC (formerly of IFAORS) and G. S. Kent, IFAORS, for helpful assistance in the successful completion of the work reported here. Special assistance of A. Ghazi, Commission of the European Communities, in the analysis presented in Chapter 6 is also gratefully acknowledged.

REFERENCES

Alimandi, G., and G. Visconti, 1983: Radiative damping and amplitude of long-wavelength modes in the stratosphere, *J. Atmos. Sci.*, *40*, 2243-2250.

Andrews, D.G. and M.E. McIntyre, 1978a: An exact theory of nonlinear waves on a Lagrangian-mean flow, *J. Fluid Mech.*, *89*, 609-646.

Andrews, D.G. and M.E. McIntyre, 1978b: Generalized Eliassen-Palm and Charney-Drazin theorems for waves on axisymmetric mean flows in compressible atmospheres, *J. Atmos. Sci.*, *35*, 175-185.

Apruzese, J. P., and D. F. Strobel, 1984: Radiative relaxation rates for individual 15-u CO_2 lines in the upper stratosphere and lower mesosphere, *J. Geophys. Res.*, *89*, 7187-7194.

Arnold, F., R. Fabian, and W. Joos, 1981: Measurements of the height variations of sulfuric acid vapor concentrations in the stratosphere, *Geophys. Res. Lett.*, *8*, 293-296.

Bandeen, W.R., and R.S. Fraser, Eds 1982: *Radiative Effects of the El Chichon Volcanic Eruption: Preliminary Results Concerning Remote Sensing,* NASA Technical Memorandum 84959.

Barnett, J.J., J.T. Houghton, and J.A. Pyle, 1975: The temperature dependence of the ozone concentration near the stratopause, *Quart. J.R. Met. Soc.*, *101*, 245-257.

Blake, D. and R.S. Lindzen, 1973: The effect of photochemical models on calculated equilibria and cooling rates in the stratosphere, *Mon. Wea. Rev.*, *101*, 783-802.

Cadle, R.D., C.S. Kiang, and J.-F. Louis, 1976: The global scale dispersion of the eruption clouds from major volcanic eruptions, *J. Geophys. Res.*, *81*, 3125-3132.

Cadle, R.D., F.G. Fernald, and C.L. Frush, 1977: Combined use of lidar and numerical diffusion models to estimate the quantity and dispersion of volcanic eruption clouds in the stratosphere: Vulcan Fuego, 1974, and Augustine, 1976, *J. Geophys. Res.*, *82*, 1783-1786.

Chu, W.P. and M.P. McCormick, 1979: Inversion of stratospheric aerosol and gaseous constituents from spacecraft solar extinction data in the 0.38-1.0 μm wavelength region, *Appl. Opt.*, *18*, 1404-1413.

Cogley, A.C., and W. J. Borucki, 1976: Exponential approximation for daily average solar heating or photolysis, *J. Atmos. Sci.*, *33*, 1347-1356.

Craig, R. A., and G. Ohring, 1958: The temperature dependence of ozone radiational heating in the vicinity of the mesopeak, *J. Meteorol.*, *15*, 59-62.

Craig, R.A., 1965: *The Upper Atmosphere, and Physics,* Academic Press, 509 pp.

Cunnold, D.M., F.N. Alyea, and R.G. Prinn, 1980: Preliminary calculations concerning the maintenance of the zonal mean ozone distribution in the northern hemisphere, *Pure Appl. Geophys., 118,* 284-306.

Dickinson, R. E., 1969: Vertical propagation of planetary Rossby waves through abn atmosphere with Newtonian cooling., *J. Geophys. Res., 74,* 929-938.

Dickinson, R. E., 1973: Method of parameterization for infrared cooling between altitudes of 30 and 70 kilometers, *J. Geophys. Res., 78,* 4451-4457.

Dütsch, H.U., 1969: Atmospheric ozone and ultraviolet radiation, *World Survey of Climatology, Vol. 4, Climate of the Free Atmosphere,* D.F. Rex, Ed., Elsevier, 383-432.

Fels, S. B., 1982: A parameterization of scale-dependent radiative damping rates in the middle atmosphere, *J. Atmos. Sci., 39,* 1141-1152.

Fels, S. B., 1984: The radiative damping of short vertical scale waves in the mesosphere., *J. Atmos. Sci., 41,* 1755-1764.

Fleig, J., J. C. Gille, M. P. McCormick, D. W. Rusch, and J. M. Russell III, 1984: Intercomparison of satellite ozone profile measurements, paper presented at the International Quadrennial Ozone Symposium, Halkidiki, Greece, 3-7 September 1984.

Gelman, M.E., A.J. Miller, J.D. Laver, and F.G. Finger, 1981: An evaluation of stratospheric meteorological analyses using satellite sounder and rocketsonde data, *Middle Atmosphere Program Handbook, Vol. 2,* 1-9 (available from SCOSTEP Secretariat, University of Illinois, 1406 W. Green St., Urbana, IL 61801).

Ghazi, A., V. Ramanathan, and R. E. Dickinson, 1979: Acceleration of upper stratospheric radiative damping: Observational evidence, *Geophys. Res. Lett., 6,* 437-440.

Gille, J. C., G. P. Anderson, W. J. Kohri, and P. L. Bailey, 1980: Observations of the interaction of ozone and dynamics. *Proceedings of the Quadrennial International Ozone Symposium,* IAMAP, J. London, editor, 1007-1011, 1980.

Gille, J.C., P.L. Briley, and J.M. Russell III, 1980: Temperature and composition measurements from the l.r.i.r. and l.i.m.s. experiments on Nimbus 6 and 7, *Phil. Trans. R. Soc. Lond., A296,* 205-218.

Goody, R. M., 1964: *Atmospheric Radiation 1*: Theoretical Basis, Clarendon Press, Oxford.

Hamill, P., C.S. Kiang, and R.D. Cadle, 1977: The nucleation of H_2SO_4-H_2O solution aerosol particles in the stratosphere, *J. Atmos. Sci.*, *34*, 150-162.

Hamilton, K., 1982: Some features of the climatology of the northern hemisphere stratosphere revealed by NMC upper atmosphere analyses, *J. Atmos. Sci.*, *39*, 2737-2749.

Hartmann, D.L., 1978: A note concerning the effect of varying extinction on radiative-photochemical relaxation, *J. Atmos. Sci.*, *35*, 1125-1130.

Hartmann, D.L., and R.R. Garcia, 1979: A mechanistic model of ozone transport by planetary waves in the stratosphere, *J. Atmos. Sci.*, *36*, 350-364.

Hartmann, D.L., 1981: Some aspects of the coupling between radiation, chemistry, and dynamics in the stratosphere, *J. Geophys. Res.*, *86*, 9631-9640.

Hidy, G.M., J.L. Katz, and P. Mirabel, 1978: Sulfate aerosol formation and growth in the stratosphere, *Atmos. Environ.*, *12*, 887-892.

Holton, J.R., 1975: *The Dynamic Meteorology of the Stratosphere and Mesosphere*, American Meteor. Soc., Boston, 218 pp.

Holton, J. R., 1976: A semi-spectral numerical model for wave-mean flow interactions in the stratosphere: Applications to sudden stratospheric warmings, *J. Atmos. Sci.*, *33*, 1639-1649.

Holton, J.R., 1980a: Wave propagation and transport in the middle atmosphere, *Phil. Trans. R. Soc. Lond.*, *A296*, 73-85.

Holton, J.R., 1980b: The dynamics of sudden stratospheric warmings, *Annual Review of Earth and Planetary Science, Vol. 8*, Annual Reviews, Inc., 169-190.

Junge, C.E., C.W. Chagnon, and J.E. Manson, 1961: Stratospheric aerosols, *J. Meteorol.*, *18*, 81-108.

Kawahira, K., 1982: A quasi-one-dimensional model of the ozone transport by planetary waves in the winter stratosphere, *J. Meteorol. Soc., Japan*, *60*, 831-848.

Kessel, R.G. and A.W. Castleman, Jr., 1982: The chemical kinetics of aerosol formation, *The Stratospheric Aerosol Layer*, 69-92 (Topics in current physics, Vol. 28, Springer-Verlag, Berlin, Heidelberg, NY).

Labitzke, K., 1981: The amplification of height-wave 1 in January 1979: A characteristic precondition for a major warming in February, *Mon. Wea. Rev.*, *109*, 983-989.

Labitzke, K., B. Naujokat, and M.P. McCormick, 1983: Temperature Effects on the Stratosphere of the April 4, 1982 Eruption of El Chichon, Mexico, *Geophys. Res. Lett.*, *10*, 24-26.

Lindzen, R. S., and R. M. Goody, 1965: Radiative and photochemical processes in mesospheric dynamics, I, models for radiative and photochemical processes, *J. Atmos. Sci.*, *22*, 341-348.

Mahlman, J.D., and W.J. Moxim, 1978: Tracer simulation using a global general circulation model: Results from a midlatitude instantaneous source experiment, *J. Atmos. Sci.*, *35*, 1340-1374.

Mahlman, J. E., 1979: Heat balance and mean meridonal circulation in the polar stratosphere during the sudden warming of January 1958, *Mon. Wea. Rev.*, *97*, 534-540.

Mahlman, J. D., H. Levy II, and W. J. Moxim, 1980: Three dimensional tracer structure and behavior as simulated in two ozone processor experiments, *J. Atmos. Sci.*, *37*, 655-685.

Matsuno, T., 1971: A dynamical model of the stratospheric sudden warming, *J. Atmos. Sci.*, *28*, 1479-1494.

McCormick, M.P., T.J. Pepin, W.P. Chu, T.J. Swissler, and L.R. McMaster, 1979: Satellite studies of the stratospheric aerosol, *Bull. Amer. Meteor. Soc.*, *60*, 1038-1046.

McCormick, M.P., W.P. Chu, G.W. Grams, P. Hamill, B.M. Herman, L.R. McMaster, T.J. Pepin, P.B. Russell, H.M. Steele, and T.J. Swissler, 1981: High-latitude tropospheric aerosols measured by the SAM II satellite system in 1978 and 1978, *Science*, *214*, 328-331.

McCormick, M.P., H.M. Steele, P. Hamill, W.P. Chu, T.J. Swissler, 1982: Polar stratospheric cloud sightings by SAM II, *J. Atmos. Sci.*, *39*, 1387-1397.

McCormick, M. P., T. J. Swissler, E. Hilsenrath, A. J. Krueger, and M. T. Osborn, 1984: Satellite and correlative measurements of stratospheric ozone: Comparison of measurements made by SAGE, ECC balloons, chemiluminescent, and optical rocketsondes, *J. Geophys. Res.*, *89*, 5315-5320.

McInturff, R.M., ed., 1978: *Stratospheric Warmings: Synoptic, Dynamic and General-Circulation Aspects*, NASA Ref. Publ. 1017, 174 pp.

Newell, R.E., 1964: Further ozone transport calculations and the spring maximum in ozone amount, *Pure Appl. Geophys.*, *59*, 191-206.

Newell, R.E., 1970: Modification of stratospheric properties by trace constituent changes, *Nature, 227,* 697-699.

Newell, R.E., and B.C. Weare, 1976: Factors governing tropospheric mean temperature, *Science, 194,* 1413-1414.

Newell, R. E., and A. Deepak, eds., 1982: Mount St. Helens Eruptions of 1980: Atmospheric Effects and Potential Climatic Impact. NASA SP-458.

Prabhakara, C.P., 1963: Effects of non-photochemical processes on the meridional distribution and total amount of ozone in the atmosphere, *Mon. Wea. Rev., 91,* 411-431.

Quiroz, R.S., Tropospheric-stratospheric interaction in the major warming event of January-February 1979, *Geophys. Res. Lett., 6,* 645-648.

Ramanathan, V., 1976: Radiative transfer within the earth's troposphere and stratosphere: A simplified radiative-convective model, *J. Atmos. Sci., 33,* 1330-1346.

Reiter, R. M., M. P. McCormick, and D. E. Miller, 1982: SAGE-European ozonesonde comparison, *Nature, 300,* 337-339.

Rodgers, C.D., and C. D. Walshaw, 1966: The computation of infrared cooling rate in planetary atmosphere, *Quart. J. Roy. Meteor. Sci., 92,* 67-92.

Rosen, J.M., 1971: The boiling point of stratospheric aerosol, *J. Appl. Meteorol., 10,* 1044-1046.

Sasamori, T., and J. London, 1966: The decay of small temperature perturbations by thermal radiation in the atmosphere, *J. Atmos. Sci., 23,* 543-554.

Schoeberl, M.R., 1978: Stratospheric warmings: Observation and theory, *Rev. Geophys. Space Phys., 16,* 521-538.

Schoeberl, M. R., D. F. Strobel, and J. P. Apruzesel, 1983: A numerical model of gravity wave breaking and stress in the mesosphere, *J. Geophys. Res., 88,* 5249-5259.

Stommel, H., and E. Stommel, 1979: The year without a summer, *Sci. Am., June 1979,* 176-202.

Stroble, D. F., 1977: Photochemical-radiative damping and instability in the stratosphere, *Geophys. Res. Lett., 4,* 424-426.

Toon, O.B., and J.B. Pollack, 1976: A global average model of atmospheric aerosols for radiative transfer calculations, *J. Appl. Meteorol., 15,* 225-246.

Turco, R.P., P. Hamill, O.B. Toon, R.C. Whitten, and C.S. Kiang, 1979: A one-dimensional model describing aerosol formation and evolution in the stratosphere. 1. Physical processes and numerical analogs, *J. Atmos. Sci.*, *36*, 699-717.

Turco, R.P., 1982: Models of stratospheric aerosols and dust, *The Stratospheric Aerosol Layer*, 13-120 (Topics in Current Physics, Vol. 28, Springer-Verlag, Berlin, Heidelberg, NY).

Wang, P. -H., M. P. McCormick, and W. P. Chu, 1983: A study on the planetary wave transport of ozone during the late February 1979 stratospheric warming using the SAGE ozone observation and meteorological information, *J. Atmos. Sci.*, *40*, 2419-2431.

Yue, G.K., 1981: The formation and growth of sulfate aerosols in the stratosphere, *Atmos. Environ.*, *15*, 549-556.

Yue, G.K. and A. Deepak, 1981: Modeling of growth and evaporation effects on the extinction of 1.0 μm solar radiation traversing stratospheric sulfuric acid aerosols, *Appl. Opt.*, *20*, 3669-3675.

Yue, G.K., and A. Deepak, 1982: Temperature dependence of the formation of sulfate aerosols in the stratosphere, *J. Geophys. Res.*, *87*, 3128-3134.

1. Report No.	2. Government Accession No.	3. Recipient's Catalog No.
NASA CR-172540		

4. Title and Subtitle	5. Report Date
Development of Algorithms for Using Satellite and Meteorological Data Sets to Study Global Transport of Stratospheric Aerosols and Ozong	March 1985
	6. Performing Organization Code
7. Author(s)	8. Performing Organization Report No.
Pi-Huan Wang and Adarsh Deepak	2017
	10. Work Unit No.
9. Performing Organization Name and Address	
Science and Technology Corporation P.O. Box 7390 Hampton, VA 23666	11. Contract or Grant No. NAS1-16362
	13. Type of Report and Period Covered Contractor Report
12. Sponsoring Agency Name and Address	
National Aeronautics and Space Administration Washington, DC 20546	14. Sponsoring Agency Code 619-12-20-21

15. Supplementary Notes

Langley Research Center Technical Monitor: Mr. L.R. McMaster

Final Report

16. Abstract

A study was conducted to utilize stratospheric aerosol and ozone measurements obtained from the NASA developed SAM II and SAGE satellite instruments to investigate their global scale transports. In the case of stratospheric aerosols, the analyses showed that, during the stratospheric warming of the winter 1978-1979, the distribution of the zonal mean aerosol extinction ratio in the northern high latitude (~75N) exhibited distinct changes. In addition, dynamical processes might have played an important role in maintenance of this zonal mean distribution. As to the stratospheric ozone, large poleward ozone transports were shown to occur in the altitude region from 24 km to 38 km near 55N during this warming. This altitude region was shown to be a transition region of the phase relationship between ozone and temperature waves from an in-phase one above 38 km. This investigation also showed that the ozone solar heating in the upper stratosphere might lead to enhancement of the damping rate of the planetary waves due to infrared radiation alone in agreement with theoretical analyses and an earlier observational study.

17. Key Words (Suggested by Author(s))	18. Distribution Statement
Transport of Stratospheric Aerosols and Ozone Satellite measurements	Unclassified -- Unlimited Subject Category 46

19. Security Classif. (of this report)	20. Security Classif. (of this page)	21. No. of Pages	22. Price
Unclassified	Unclassified	121	A06

For sale by the National Technical Information Service, Springfield, Virginia 22161